Spectral purity transfer through optical injection using highly coherent, wavelength selectable sources

Amith Karuvath

COLLEGE MATHS, TELECOMS
DOCTORAL INFORMATIQUE, SIGNAL
BRETAGNE SYSTEMES, ELECTRONIQUE

Université de Rennes

THESE DE DOCTORAT DE

L'UNIVERSITE DE RENNES

ECOLE DOCTORALE N° 601
Mathématiques, Télécommunications, Informatique, Signal, Systèmes, Electronique
Spécialité : *Photonique*

Par
Amith KARUVATH

« Spectral purity transfer through optical injection using highly coherent, wavelength-selectable sources »

Thèse présentée et soutenue à Lannion, le 21 novembre 2023
Unité de recherche : INSTITUT FOTON (UMR 6082)
Thèse N° :

Rapporteurs avant soutenance :

Fabien Bretenaker	Directeur de recherche CNRS, Laboratoire LuMin, ENS Paris/Saclay, École Polytechnique
Marc Sciamanna	Professeur, Centrale Supélec, Laboratoire LMOPS

Composition du Jury :

Président :	Mehdi Alouini	Professeur, Université de Rennes, Institut Foton
Examinateurs :		
	Anne Amy-Klein	Professeur, Université Sorbonne Paris Nord / Institut Galilée, Laboratoire de Physique des Lasers
	Ghaya Baili	Ingénieur, THALES TRT
	Vincent Roncin	Maitre de conférences, Université Sorbonne Paris Nord, Laboratoire de Physique des Lasers
Dir. de thèse :	Pascal Besnard	Professeur, ENSSAT (Université de Rennes) / Institut Foton

COLLEGE DOCTORAL BRETAGNE
MATHS, TELECOMS
INFORMATIQUE, SIGNAL
SYSTEMES, ELECTRONIQUE

Université de Rennes

Titre : Transfert de pureté spectrale par injection optique à l'aide de sources hautement cohérentes et sélectionnables en longueur d'onde

Mots clés : laser, Brillouin, fibre, cohérence, injection optique, bruit de fréquence

Résumé : Cette thèse est consacrée à l'étude du transfert de pureté spectrale par injection optique avec la variation de la cohérence du signal injecté. L'idée principale est de distribuer cette forte cohérence à d'autres sources. L'injection optique peut-être défini comme le couplage unidirectionnel entre deux lasers : l'un, appelé maître, alimente en photons la cavité d'un second laser, appelé esclave. Cette technique de synchronisation en fréquence et en phase est couramment analysée à partir des spectres optiques, du comportement temporel ou du bruit d'intensité relatif du laser injecté. Notre analyse est faite grâce à la densité spectrale de puissance du bruit de fréquence, afin de comparer l'influence d'une source externe à la source spontanée interne.

Différents lasers accordables sont utilisés pour un contrôle de la cohérence. Un étage de laser à fibre Brillouin (BFL) est ajouté pour former une source plus cohérente (< kHz ou au Hz), avec une longueur d'onde sélectionnable sur la bande C. Un deuxième étage BFL permet d'atteindre 3 mHz.
Notre étude se concentre sur le seuil d'accrochage en fréquence, ou la puissance optique minimale requise pour un transfert total de pureté. Lorsque l'on diminue la largeur de raie (30 kHz) d'un facteur 10, le seuil augmente du même facteur; mais seulement de +4 dB pour passer de 3 kHz à 1 Hz. Ceci ouvre la possibilité d'un transfert de grande pureté par injection optique sans pénalité sur la puissance optique.

Title: Spectral purity transfer through optical injection using highly coherent, wavelength-selectable sources

Keywords: laser, Brillouin, fiber, coherence, optical injection, frequency noise

Abstract: This thesis is devoted to the study or spectral-purity transfer through optical injection when the coherency of the seeded light is varied. The main idea is to spread this strong coherency and to share it with other sources. Optical injection is the unidirectional coupling between two lasers: one, called the master, feeds photons into the cavity of a second laser, called the slave. This technique of frequency and phase synchronization is commonly analyzed from the optical spectra, the temporal behavior or the relative intensity noise of the injected laser. Our analysis is made thanks to the frequency noise power spectral density, in order to compare the influence of an external source to the internal spontaneous source.

To have a direct control on coherency, tunable lasers with different linewidths are used. To get sub-kHz one (or Hz one), a Brillouin-fiber-laser (BFL) stage is added to form a highly coherent source with selectable wavelength over the C-band. 3 mHz linewidth is obtained by a second BFL stage.
Our study focuses on the frequency-locking threshold, or the minimum required optical power for a complete purity transfer. When decreasing the linewidth from 30 kHz by a factor of 10, the locking threshold is increased by the same factor. However, decreasing from 3 kHz to thinner linewidth (~1 Hz), the power required is not so different (+4 dB) opening the possibility of transfer of high purity through optical injection without penalty on optical power.

ACKNOWLEDGEMENT

I would like to extend my sincere gratitude to my supervisor, Pascal Besnard for his support and guidance throughout my doctoral research. His mentorship has been instrumental in my work. He found time for me to discuss physics during his busy administrative schedule. His support and encouragement helped me to push through the challenges encountered during my thesis. I would like to thank Stephane Trebaol for his extended support and guidance throughout my academic journey.

I would like to thank my jury members Fabien Bretenaker and Marc Sciamanna for agreeing to be the reporters of my manuscript. I extend my appreciation to Mehdi Alouini, Anne Amy-Klein, Ghaya Baili and Vincent Roncin for their constructive feedback during the defense.

I would like to express gratitude to Institut FOTON for giving me an opportunity to pursue my doctoral thesis. Also, for providing the necessary resources and research environment that facilitated the completion of my thesis. I would also like to thank all the academic and support staff of Institut FOTON and ENSSAT. To my colleagues, Ananthu Sebastian, Rasool Saleem, Nessim Jebali, Louis Ruel, Georges Perin, Joseph Slim, Antoine Congar and Dominique Mammez, I am grateful for your support, knowledge sharing and encouragement during my time at Institut FOTON.

Special thanks to my parents, sister and my friends for believing in my abilities, for encouraging me and being my pillars of strength.

Finally, I would like to thank my partner Meenu Thampi for her unwavering support, encouragement and being a driving force behind my achievements.

Amith Karuvath

LIST OF TABLES

LIST OF FIGURES

Figure 1.9:(a) Transfer function of unbalanced interferometer with $\tau_d = 1 \times 10^{-6}$ (for $L_d = 200\ m$) (b) Cutoff frequency and gain conversion of measurement bench as function of delay length L_d.

Figure 1.10: (a)Tunics-PR phase noise and the noise floor of measurement bench with 10 m delay length. (b) Frequency noise measurement of Tunics-PR and linewidth estimation using β-line approximation. The shaded region denotes area under the curve, which helps to determine the integrated linewidth.

Figure 1.11: The principle of laser frequency stabilization. The sensor converts optical frequency fluctuations into voltage fluctuations and generates an error signal. The corrector amplifies the generated error signal and provides the correction signal. The electrical correction signal is converted into optical frequency fluctuations by the actuator and applied to the laser to compensate for the frequency fluctuations.

Figure 1.12: Experimental setup for the stabilization of pump-laser frequency onto a resonance of MZI. OC: Optical coupler, PC: Polarization controller, L_d*=10 m*: Delay length, PD: Photodetector, TIA: Transimpedance amplifier, EC: Electrical coupler, PID: Proportional-integral differential corrector, FG: Function Generator, FN: Frequency noise measurement.

Figure 1.13: Frequency noise measurement of stabilized Tunics-PR tunable laser.

Figure 1.14: Frequency noise measurement of stabilized Tunics-OM tunable laser.

Figure 1.15: Sub-kHz linewidth Tunics-PR, source tunable in C-band.

Figure 1.16 Pump power versus Stokes power of 20-meter and 14-meter BFL cavities.

Figure 1.17: Frequency noise performance of sub-kHz linewidth Tunics-PR tunable laser in C-band.

Figure 1.18: Cascaded mHz linewidth Tunics-PR tunable laser in C-band. EDFA: Erbium-doped fiber amplifier, VOA: Variable optical attenuator, OC: Optical coupler, Pin: Optical power of the input pump, PS1: Power from the Stokes wave of the first stage, Ptrans: optical power of the transmitted pump, PS2: optical power of the second first-order Stokes wave with mHz linewidth.

Figure 1.19: The frequency noise performance of the two cascaded non-resonant Brillouin lasers using Tunics-PR laser tunable in C-band (a) log scale (b) linear scale.

Figure 3.3: Schematic illustration of the variation of the master linewidth. When it is decreased, the contribution of the slave line increases.

Figure A.1: Frequency noise of tunable lasers used as master lasers in optical injection.

Figure A.2: Frequency noise measurements using Tunics OM and estimation of $h_{-\alpha}$ and α by linear regression.

LIST OF ABBREVIATIONS

DFB Distributed Feedback Laser

BFL Brillouin Fiber Laser

PDH Pound-Drever-Hall

RIN Relative Intensity Noise

CRDM Cavity Ring Down Method

EDFA Erbium Doped Fiber Amplifier

PM Polarization Maintaining

VOA Variable Optical Attenuator

OC Optical Coupler

VC Variable Coupler

PZT Piezoelectric Transducer

PID Proportional Integral Differential amplifier

HV High Voltage amplifier

CW Continuous Wave

PSD Power Spectral Density

PC Polarization Controller

PD Photodetector

TIA Transimpedance Amplifier

SSA Signal Source Analyzer

AOM Acousto Optic Modulator

MZI Mach Zehnder Interferometer

EC Electrical coupler

FG Function Generator

FN Frequency Noise measurement

FSR Free Spectral Range

SL Slave Laser

ML Master Laser

VCSEL Vertical Cavity Surface Emitting Laser

DWDM Dense Wavelength Division Multiplexing

CIR Optical Circulator

TABLE OF CONTENTS

INTRODUCTION

The first observation of injection locking was made in 1665 by Huygens, who was unwell and resting in his room. He then noticed the synchronization of two pendulum clocks that were built on a heavily weighted stand, to always have a working clock. This experiment was done to provide explorers with a precise tool to measure time and to correctly determine longitude.

In optics one illustration of synchronization is optical injection, which is the unidirectional coupling between two lasers (named slave (the injected laser) and master laser (the external source)). After the first realization of a laser by Theodore Maiman in 1960 [103], S. H. Stover and W. H. Steier [104] optically injected the signal from a gas laser into a different laser via an optical isolator in 1960. When the master and slave frequencies are close altogether and for an appropriate injected power, the slave laser synchronizes with the master laser and inherits the spectral properties of the master laser in terms of frequency and linewidth.

The development of highly coherent sources is a hot topic that various groups around the world are working on to address a wide variety of applications. They are of major interest because of their ability to improve systems thanks to their high spectral purity.

The main objective of this thesis is to study the purity transfer of a highly coherent source by optical injection. To achieve this goal, I have developed a sub-kHz intrinsic linewidth source with C-band selectable wavelength. It allows us to study the role of the master laser coherence in triggering the optical injection locking when the injected power is varied.

The first chapter of this manuscript focuses on the development and performances characterization of a sub-kHz C-band wavelength selectable source using a non-resonant Brillouin cavity. The properties of Brillouin laser and its different architectures are presented as well as the linewidth narrowing phenomena in a Brillouin fiber laser. Then, I will explain the process of measuring the coherence of a laser using frequency-noise measurement technique. Laser frequency stabilization and some associated experimental techniques to achieve this are also presented. The last part of this chapter is devoted to the development of a C-band wavelength selectable laser with an intrinsic linewidth of the order mHz, by cascading two non-resonant Brillouin cavities, establishing, to our knowledge, a record. Note that using a more coherent pump laser (Koheras^{TM} Adjustik), the linewidth cannot be measured and is under our limit detection (700 µHz).

The main objective of the second chapter is to examine the role of the coherence of the master laser in triggering optical injection locking when the injected power is varied. After a brief introduction on the general properties of optical injection, the theoretical framework is described for this study. It is a generalized transfer function (Airy) for a laser and its variant for an optically injected laser. Then the experimental setup of optical injection is described. Master lasers with different coherencies enable us to show that opposite conclusions in the estimation of the threshold of the frequency locking are drawn when using signal to noise ratio or frequency noise. To have a schematic view, when the coherence of the master laser is increased, the minimum injected power needed to state an injection locking (that can be called locking threshold) lowers, if the estimation parameter is the signal to noise ratio, while it increases, if the estimation parameter is the frequency noise.

The final chapter of this thesis is devoted to discussions, conclusions and perspectives. In particular, we show from experiment and theory that optical injection in an amplification regime may be compared to mixing two signals with different coherencies. This study gives a simple perception of the noise properties of an optically injected system. It opens the way to the realization of sources working in the quantum Schalow-Townes limit and to their use in various applications ranging from quantum optics to highly sensitive sensors.

CHAPTER 1: Sub-kHz C-band selectable wavelength source

1.1 Introduction

Highly coherent lasers are of major interest currently as it is essential for various laser applications since it improves the system drastically due to its high spectral purity. In this chapter, I will describe one of the main objectives of the thesis that is to develop a sub-kHz linewidth laser emitting at a wavelength selectable in the C-band.

Several groups are working all over the world to develop highly coherent lasers to meet a wide variety of applications. It should be noted that commercially available coherent sources (RIO's ORION™ Laser Source from LUNA™ company, OEWAVE™ laser source, which is based on a high-quality factor Whispering Gallery Mode (WGM) micro-resonator, KOHERAS™ Adjustik from NKT Photonics™...), can be, for some, very weakly tunable, typically on one nanometer (RIO™, KOHERAS™ Adjustik, ...). More coherent single frequency sources have been studied, [1-5] or even proposed recently [6,7]. Concerning coherent tunable lasers, different approaches were proposed to develop them. Kotaki *et al.* [8] developed a distributed feedback laser (DFB) with a linewidth of 1 MHz. They obtained an output power of 40 mW and a tuning range of 2.2 nm. Okai *et al.* [9] in 1994 developed a 100 kHz linewidth DFB laser with an output power of 10 mW and a tunability of 1.3 nm. In 2008, Yoffe *et al.* [10] developed a tunable laser based on DFB array with a linewidth of 500 kHz with 30 mW output power in the C-band. Ishii *et al.* [11], designed an L-band tunable distributed feedback laser array in 2009 with a wavelength tuning range of 40 nm and an output power of 20 mW. They reported a narrow linewidth of less than 580 kHz over the entire tuning range. A wavelength-tunable laser diode with

an external optical cavity of Si wire waveguide ring resonators was fabricated by the group of Nemoto [12]. This source had a 44 nm wavelength tuning range covering the entire L-band and reported a spectral linewidth narrower than 100 kHz. In 2013, Faugeron *et al.* [13] developed a 1 mm long DFB laser using an asymmetrical cladding based on the dilute waveguide technique with an output power of 180 mW. This laser source had an optical linewidth better than 300 kHz and a tuning range of 9.7 nm. Hulme *et al.* [14] designed and fabricated a hybrid silicon tunable Vernier ring laser with a tuning range of 40 nm and a linewidth of 338 kHz. In the same year 2013, Keyvaninia *et al.* [15] developed a heterogeneously integrated III-V on silicon laser with a linewidth of 1.7 MHz and a tuning range of 8 nm. A thermally tuned super-structure distributed Bragg reflector laser was developed by Larson *et al.* [16]. It had a spectral linewidth of 300 kHz and 40 nm wavelength tuning across the C-band. Mizrahi *et al* [17] developed an integrated tunable C- band laser embedded in a silicon chip with a linewidth narrower than 200 kHz. In 2014, Sasahata *et al.* [18], demonstrated a tunable 16 DFB laser array with a linewidth of 350 kHz. It had a tuning range of 37 nm in the L-band. Komljenovic *et al.* [19] developed, in 2015, a fully integrated tunable single mode hybrid silicon laser with a linewidth of 260 kHz and a tuning range of 29 nm from 1553 nm to 1582 nm. Komljenovic *et al.* [20] also developed a widely tunable narrow linewidth monolithically integrated external cavity semiconductor laser with a linewidth below 100 kHz with a tuning range of 54 nm in O-band. In 2015, Kobayashi *et al.* [21] demonstrated a Si-photonic hybrid ring external cavity wavelength C-band tunable laser with a linewidth narrower than 15 kHz. In 2017, Lipson *et al.* [22] designed and demonstrated a compact narrow linewidth integrated laser based on low-loss silicon nitride waveguides coupled to a III-V gain chip. They observed a

linewidth of 13 kHz with 1.7 mW output power around 1550 nm. Fan *et al.* [23] presented an integrated chip based InP-Si_3N_4 hybrid laser with a fundamental laser linewidth of 290 Hz linewidth with a tunable range of 81 nm at 1550 nm. In 2019, Huang Morton *et al.* [24] in 2021 developed a silicon photonics foundry based integrated coherent tunable laser with a tuning range of 118 nm. They reported a Lorentzian linewidth below 100 Hz for their laser source.

This chapter will cover the development of sub-kHz source with wavelength selectable on the C-band using a non-resonant Brillouin cavity. Brillouin laser and its different architectures will also be discussed. Then, I will explain how to measure the coherency of a laser, using frequency-noise measurement technique. This chapter will also give a few words about laser frequency stabilization. The latter part of this chapter will also contain the development of a mHz-(intrinsic) linewidth C-band wavelength-selectable laser using non-resonant Brillouin cavities.

1.2 Brillouin Laser

Several techniques have been developed to reduce the linewidth of a laser to sub-kHz level such as high finesse cavity [25], filter [7], or delay line [26]. Increasing the coherency may require suppressing the frequency fluctuations of the laser line, which is named stability. Note that lasers with long-term stability do not require these lasers to be very coherent. This stability may be wanted for a beating frequency [27] or a unique frequency [28,29], which could be obtained by controlling the laser frequency by a servo-lock onto a reference (optical cavity, another laser). One of the most promising approaches

to develop a compact and narrow linewidth laser is based on stimulated Brillouin scattering [30]. Brillouin fiber lasers (BFL), using stimulated Brillouin scattering in fibers, produce intrinsic narrow sub-kHz linewidths [1-6,31-49], which are several orders of magnitude narrower than the incident pump beam.

Brillouin scattering may occur at low optical powers spontaneously due to presence of thermally excited acoustic vibrations at room temperature in the fiber. A photon from an incident wave disappears to generate a scattered photon and a phonon [51]. The back scattered wave is downshifted in frequency and is called a Stokes wave, named after George Stokes [52], who proposed wavelength upshift in the process of fluorescence (luminescence) in the 19^{th} century. This process is spontaneous Brillouin scattering.

The pump and Stokes wave beat together leading to the formation of an interference pattern. At higher pump intensity, the amplitude of this beating increases and creates a modification of the matter density along the spatial pattern. This phenomenon known as electrostriction [53] is the ability of a material to be compressed in the presence of an electric field. The electrostriction phenomenon induces the formation of a large number of phonons, which will amplify the Stokes wave generation through a nonlinear process similar to a third order nonlinear optical interaction. The generated Stokes wave and pump interacts to reinforce the generation of Stokes wave. This reinforcing process amplifies the Stokes wave generation. This cyclic process is the stimulated Brillouin scattering.

The Brillouin lasers are of two types based on the method of pumping, non-resonant and resonant BFL. In non-resonant pumping BFL, the pump laser travels only once inside the cavity, whereas in a resonant pumping BFL, the pump laser continuously circulates inside

the cavity. This continuous circulation will lower the threshold of resonant BFL compared to non-resonant BFL.

The first concept of Brillouin laser was demonstrated by Hill *et al.* [54] in 1976. They reported a cascaded process of up to 14 laser lines in the spectrum. In 1982, Stokes *et al.* [55] exhibited an all-fibered Brillouin laser using a single-mode optical fiber and a directional coupler, which helped them to reduce the cavity losses, thereby bringing the Brillouin laser threshold down to 0.56 mW for the 4 μm-core fiber. Smith *et al.* [30] developed, in 1991, a BFL with a spectral linewidth of 2 kHz and an intrinsic linewidth of less than 30 Hz. In 2000, a theoretical analysis was performed by Debut *et al.* [31]. Moreover, they showed that the Brillouin laser linewidth might be reduced and smoothed, with respect to the pump linewidth, under the combined action of acoustic damping and cavity losses. They also demonstrated a 10-dB linewidth reduction experimentally with a 12-meters-long BFL [32]. The process of linewidth narrowing in BFL will be explained in this chapter. In 2006, Geng *et al.* [33] demonstrated a highly stabilized low-noise BFL with ultra-narrow spectral linewidth using Pound-Drever-Hall (PDH) frequency locking method [56]. They reported a linewidth reduction of 20 dB at 1550 nm. A hybrid Brillouin/erbium fiber laser that uses both Brillouin gain and gain in erbium-doped fiber [34] was demonstrated in 1996. Similarly, BFLs based on Bragg grating [35], Mach-Zehnder interferometer [36] and self-injection locking [57] were also reported. A non-resonant pumping based BFL was reported by Mihelic [58] in his PhD thesis. Vahala *et al.* [37] developed a Brillouin laser, in 2012, based on chemically etched ultrahigh-Q wedge resonator on a silicon chip. In this work, they tried to generate a beating signal at microwave frequency [38]. They characterized this Brillouin laser and showed a cascading

effect at 1550 nm [39]. In 2014, Vahala *et al.* [40] demonstrated a narrow linewidth Brillouin laser at 1064 nm from ultra-high Q silica wedge disk resonator on silicon. They claimed to reach the fundamental Schawlow-Townes limit with a frequency noise of the order of 0.1 Hz^2/Hz (300 mHz). A 10 dB linewidth reduction compared to the pump laser was observed by Kabakova *et al.* [41] in 2013, using a Brillouin laser based on chalcogenide photonics chip. In 2014, Gundavarapu *et al.* [42] demonstrated a 0.7 Hz fundamental linewidth Brillouin laser in an integrated Si_3N_4 waveguide. But the drawback of this system is that the central frequency of the laser line has high fluctuations (flicker noise and low frequency noise will be introduced in the following).

In 2019, Loh *et al.* [43] used a large mode volume optical resonator with 2 meter optical fiber to suppress the resonator's fast thermal fluctuations and demonstrated an integrated linewidth of 20 Hz.

A detailed description about laser linewidths and the measurement technique will be explained in this chapter.

Non-resonant and resonant BFL were also studied in the team "photonics systems" at Institut FOTON as well. Kenny Hey Tow, in his thesis [44], developed in 2012 a non-resonant BFL with suspended core and micro-structured chalcogenide fiber [1,45,46]. The non-resonant BFL with suspended core $As_{38}Se_{62}$ chalcogenide fiber exhibited a low threshold power of 22 mW. He used a $Ge_{10}As_{22}Se_{68}$ micro-structured chalcogenide fiber to develop a compact second-order Stokes BFL. He observed the first order lasing at 6 mW and a second order lasing at 22 mW with non-resonant pumping. The second order Stokes was observed at high pumping power due to Fresnel reflections at the facets of

chalcogenide fiber. The linewidth of the pump laser was 4 MHz. The linewidths of first and second order Stokes were respectively measured to be 270 kHz and 20 kHz respectively, providing a reduction ratio of 400 (26 dB**)**.

Schadrac Fresnel developed a non-resonant BFL in his thesis [47]. The non-resonant cavity was made using a 20 meter long silica fiber. The Stokes wave was observed at a lasing threshold of 60 mW with a reduction factor of 40 dB when the Stokes frequency noise is compared to that of the pump laser. He also demonstrated a resonant BFL using a 20 meter fiber ring cavity and studied the relative intensity noise and frequency noise of the Stokes orders, showing the possibility of reducing the RIN as well.

The main objective of Ananthu Sebastian's [48] thesis was to study the noise dynamics of multi-Stokes Brillouin laser and to explore the associated physics as part of it. He proposed a technique for the characterisation of Brillouin gain cofficient directly from probing the laser cavity using cavity ring-down method (CRDM) [49]. This method also enabled him to extract the material gain, optical cavity parameters and lasing properties. He investigated the relative intensity noise (RIN) properties of a multi-Stokes BFL by analysing the intensity noise of each Stokes wave and studied the noise dynamics of cascaded Brillouin scattering process. He reported a 20 dB/Hz intensity noise reduction compared to that of the RIN input pump laser [50]. He also explored the fundamental limitations of frequency noise reduction for non-resonant and resonant cavities. A collaborative work, which was done with Ananthu, is also a part of this thesis. It consists in cascading two non-resonant BFL and explore the limitation in frequency noise reduction. This experiment quickly reached the noise floor of our bench and prevented us from exploring further the noise

reduction. I improved the noise floor in the last part of my thesis as well as the overall performances of the Brillouin coherent source.

This chapter will be focused on the development of sub-kHz C-band wavelength-selectable source using non-resonant Brillouin cavity. The chapter will begin with the linewidth narrowing effect in BFL based on the study of Debut *et al.* [31] in section 1.2. Pre-stabilization of the pump laser to reduce its flicker noise using an unbalanced Mach-Zehnder cavity will also be explained. After that, the architecture of sub-kHz tunable laser source in the C-band will be introduced and the method to measure the coherency of the source will be discussed using frequency noise analysis. The final part of this chapter will emphasize on the cascading of two non-resonant cavities to realise a mHz intrinsic-linewidth BFL with a wavelength that can be fixed at a wavelength in the C-band when the pump source is a tunable laser.

1.2.1 Brillouin laser

Spontaneous Brillouin scattering is generated from thermally excited acoustic vibrations [135] at room temperature. It is produced from diffraction of an incident optical wave by a volume index grating formed by the acoustic wave, moving at the acoustic wave velocity (V_A). In a single-mode optical fiber, it results in the formation of a Stokes wave (of lower frequency) by a pump wave as illustrated in figure 1.1. An anti-Stokes wave (with a gain spectrum symmetric, with respect to the pump, to that of the Stokes but at a higher frequency) is also produced when the acoustic wave has an opposite direction to the incident wave.

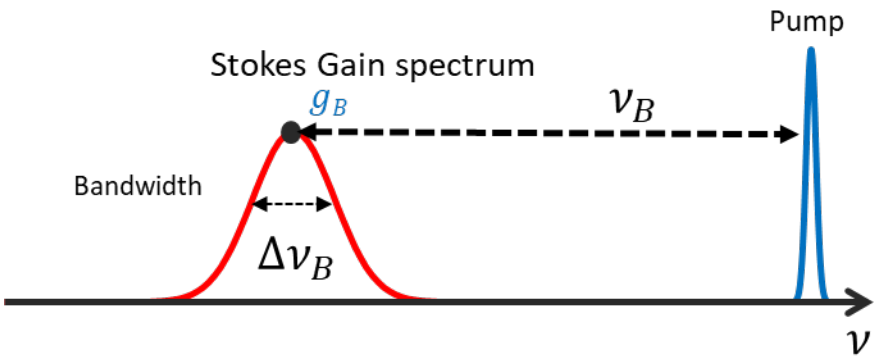

Figure 1.1: Stokes process in the spontaneous regime. A pump signal produces a Brillouin response. The horizontal axis is the axis for frequency.

The Brillouin frequency shift ν_B has been measured at 10.87 GHz and g_B at 1.95 10^{-11} m/W [49] for standard SMF28 optical fibers. The gain bandwidth at half maximum $\Delta\nu_B$ is 27.5 MHz. The pump and Stokes wave beat together at the frequency ν_B, giving rise to an interference. When the pump power is increased, the beating power also increases and the pattern modifies the matter density following a phenomenon called electrostriction, showing the capacity of an electrical field to compress a material. This index grating is moving at the speed of sound in the medium. This electrostriction process reinforces the Stokes Wave generation. The whole process is called Stimulated Brillouin Scattering (SBS). As a matter of fact, the electrostriction process creates phonons. The phonons propagating in the same direction as that of the pump are favored with respect to the contra-propagating phonons. It implies that the Stokes wave and anti-Stokes have unequal power contrary to the case of spontaneous scattering.

As the pump is increased, the Brillouin gain bandwidth is decreasing to a lower limit, 6.5 MHz.

If this Brillouin amplification is associated to a cavity, a process equivalent to a laser may occur if the amplification compensates for the losses after a roundtrip inside the cavity (when considering a Fabry-Perot cavity). The cavity has a filtering effect and imposes its modal conditions through a transfer function, by defining longitudinal modes separated by a Free Spectral Range ($\Delta\nu_{FSR}$) as shown in figure 1.2. To get a single-mode Brillouin laser with an optimized gain, we need to fulfill two necessary conditions: $\nu_B = N\,\Delta\nu_{FSR}$ (N being an integer) and $\Delta\nu_B < \Delta\nu_{FSR}$. Mode-hopping may occur for longer cavity length, that has the advantage to reduce the laser threshold (as the gain $e^{g_B L_{eff} I_{pump}}$ will increase with the fiber length (L_{eff} is the effective length, I_{pump} the optical intensity of the incident pump)).

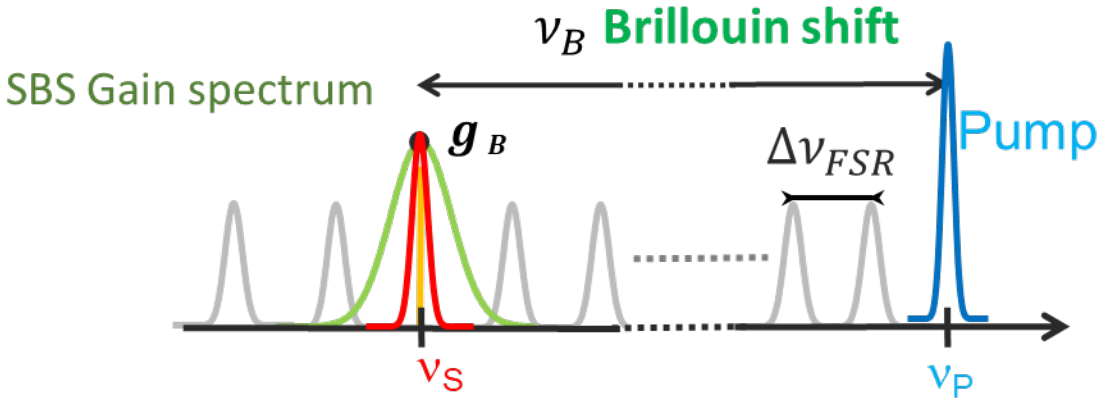

Figure 1.2: SBS gain spectrum (green profile) associated to the transfer function of the cavity (grey line). The Brillouin bandwith is lower than the FSR ($\Delta\nu_{FSR}$), which can be obtained by acting on the fiber length constituting the cavity. In this figure, the Brillouin shift (ν_B) is a multiple of the FSR ($\nu_B = N\,\Delta\nu_{FSR}$) so that the Brillouin gain associated to the Stoke frequency (ν_S) is g_B.

Note that the resonances associated to the fiber cavity will be temperature dependent as well as the Brillouin frequency shift. At a frequency of 193.6 THz, the resonance frequency shift is 1.5 GHz for a variation of one Celsius degree [48] while the Brillouin frequency coefficient is 1 MHz/K. The Brillouin frequency is also dependent on the pump wavelength $\left(\nu_B = \frac{2nV_A}{\lambda_{Pump}}, n\ is\ the\ refractive\ index\right)$ with a ratio of 7 MHz/nm. If the temperature is stabilized, one can easily adjust the Brillouin curve by changing the pump wavelength, in order to make the Brillouin-gain maximum corresponding to a resonance of a Stokes wave, getting a selectable wavelength for the Stokes wave.

In the next two subsections, ring cavity configuration will be described.

1.2.2 Resonant Brillouin laser architecture

This section will cover the architecture of a resonant Brillouin laser [48]. Figure 1.3 shows the architecture of resonant BFL. The output of the pump laser is amplified using an EDFA and injected inside the cavity thanks to a circulator and a coupler. A variable optical attenuator helps to control the input pump inside the cavity. 1 % of the pump signal is collected for monitoring the power. In resonant Brillouin laser, the pump and Stoke waves are resonant inside the cavity. It can develop several Stokes orders. The counter propagating Stokes 1 wave acts as a pump for counter propagating Stokes 2 wave at higher pumping power.

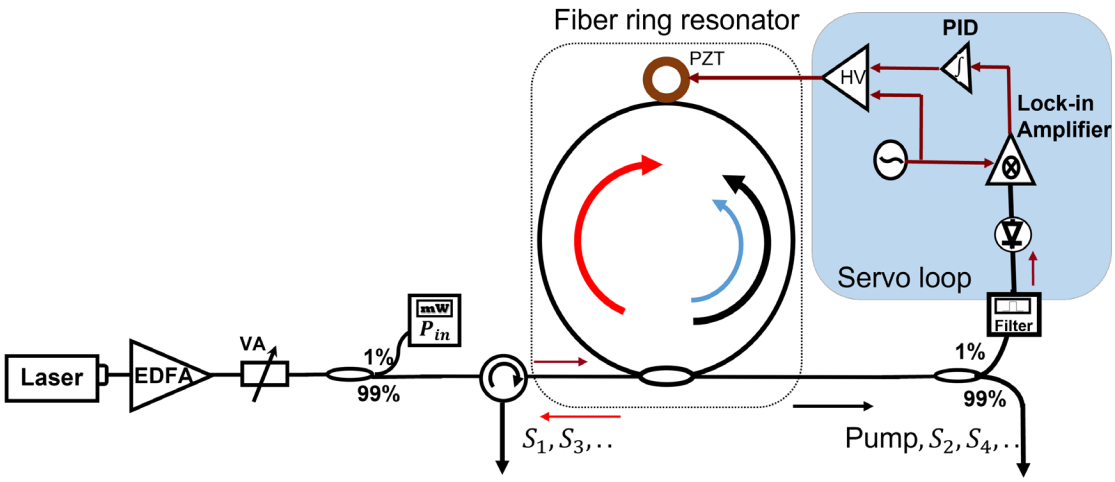

Figure 1.3: Architecture of resonant pumped multi-Stokes BFL. EDFA: Erbium doped fiber amplifier, VA: Variable attenuator, VC: Variable coupler, PZT: Piezoelectric transducer, Filter: Yenista optical filter, PID: Proportional-integral differential amplifier, HV: High-voltage amplifier. Blackline: Pump laser, red line: Stokes 1 wave, blue line: Stokes 2 wave.

The black arrow inside the fiber ring resonator indicates the pump propagation inside the cavity. The circulating pump initiates Brillouin amplification enabling the generation of Stokes 1 wave (red arrow) in the opposite direction of the pump wave. For pump power above the threshold of Stokes 1 wave, Brillouin lasing threshold is reached giving rise to its efficient emission. When the optical power of the wave Stokes 1 is increased, it plays the role of pump for the emission of Stokes 2 wave (blue arrow), and then the cascading process is activated. The laser threshold for various Stokes waves can be drastically reduced when the pump signal is resonantly coupled to the cavity. It can be achieved by locking a cavity resonance to the wavelength of the CW pump laser. Applying the voltage on a piezoelectric will modify the cavity length and will then control the frequency position of the cavity resonances. The output signals like the transmitted pump, Stokes 1, Stokes 2 etc. can be extracted from the couplers for analysis.

The resonant cavity has the advantage of having lower threshold [43], [48] when compared to non-resonant BFL.

1.2.3 Non-resonant Brillouin laser architecture

A schematic sketch of non-resonant Brillouin laser is shown in Figure 1.4. Different pump lasers will be used in the following, including commercially available tunable C-band lasers. An Erbium Doped Fiber Amplifier (EDFA) amplifies the pump laser output. This amplified beam is considered as the input pump with constant intensity and frequency noise parameters. A variable optical attenuator (VOA) controls the injected power inside the BFL cavity. A 99/1 % coupler is used to monitor the input pump power inside the cavity.

The cavity consists of 20 m polarization-maintaining (PM) fiber. It was designed by us and built by the company IDIL. Even lower lengths may be used at the price of higher Brillouin laser threshold. A 95/5 % coupler and a 3-port coupler form a fiber ring cavity with a Q-factor 5.6 x10^8 and total round-trip losses of 0.83 (ratio of the intensity after one single trip and of the incident intensity). The non-resonant BFL cavity is passively stabilized by gluing the fiber onto a metallic plate (operation realized by IDIL).

The optical output of the pump laser (black arrow) is injected inside the cavity from port 1 to port 2 of the circulator.

The transmission of pump from port 3 to port 2 is not allowed (or at least optically isolated with a coefficient superior to 35 dB) so that the pump circulates on a single roundtrip, only in one direction from port 2 to port 3. The pump's single passage from port 2 to port 3 causes stimulated Brillouin scattering inside cavity. Once it satisfies the Brillouin laser

condition (gain overcomes the cavity losses), the laser is running. The Stokes wave (in red) is generated in the opposite direction of that of the pump and will circulate from port 3 to port 2 with multiple roundtrips. The Stokes wave and transmitted pump are collected through the output of a 95 % / 5 % coupler and monitored using a power-meter.

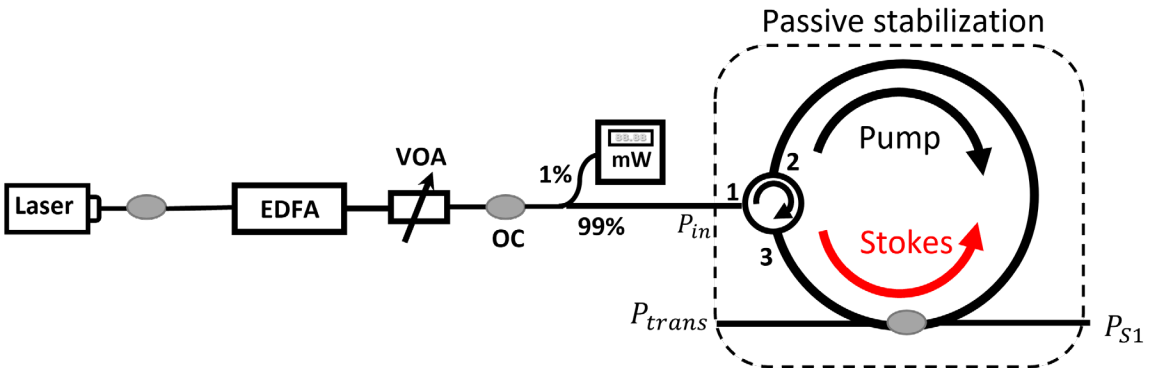

Figure 1.4: Architecture of non-resonant Brillouin fiber laser cavity. EDFA: Erbium-doped fiber amplifier, VOA: Variable optical attenuator, OC: Optical coupler, Pin: optical power of the input pump, P_{S1}: optical power of the Stokes wave of first order, P_{trans}: optical power of the transmitted pump.

The Brillouin shift is 10.87 GHz. The laser threshold is at 61.8 mW of pump power with around 25 % of slope efficiency.

In this thesis, two cavities will be used. They were designed by us and built by the company IDIL. The second one consists of 14-m polarization-maintaining (PM) fiber.

1.2.4 Linewidth narrowing in non-resonant Brillouin fiber laser.

Brillouin fiber lasers are highly coherent light sources, which are useful in various applications as mentioned in section 1.1. The linewidth of the Stokes wave generated is several orders of magnitude narrower than that of the pump laser. For conventional laser

sources, the population inversion provides the amplification of light. In such sources, spontaneous emission occurring in the gain medium acts as a fundamental noise limitation of its monochromatic nature as given by Schawlow-Townes [59]. It is of the order of tens of kHz for semiconductor lasers and in the sub-hertz level for gas lasers. The spontaneous emission gives rise to what we will call intrinsic (or natural) linewidth. However, it is not the only source of noise in conventional lasers. Their linewidth also depends on pump fluctuations, or/and different external noise fluctuations (thermal, acoustical, …) that broadens the laser linewidth. In the case of BFLs, the fundamental noise limitation is due to spontaneous scattering. It turns out that the noise level in BFL due to spontaneous scattering is very low, when compared to other noise contributions such as the noise from pump laser. As a matter of fact, a strong coupling exists between the phase of the pump laser and that of the emitted Stokes wave so that the frequency noise of the BFL is intensely linked to the frequency noise of the pump laser. A low noise pump laser could be used to induce an even lower noise BFL. The noise due to cavity is another source of noise in BFL. It is due to variations in cavity length and feedback efficiency caused by thermal and mechanical fluctuations. It implies laser intensity variations and slow drifts of the emitted Stokes frequency. The fluctuations in the fiber can be controlled by stabilizing the laser cavity, which will reduce the drift in Stokes frequency. Nevertheless, they do not contribute to the intrinsic linewidth of the Stokes wave as we will see in the following.

As mentioned in the introduction of this section, Smith *et al.* [30] observed in 1991 the linewidth narrowing of a BFL experimentally. Later in 2000, Debut *et al.* [31] theoretically explained it. They studied the linewidth narrowing based on the framework of a three-wave model of stimulated Brillouin scattering. There is an interaction between the three waves

via electrostriction process. The pump and acoustic wave interact to generate a Stokes wave. Then, the intensity and phase noises of these waves are coupled together. It was shown that the phase noise of pump laser is transferred to the Stokes wave after being strongly reduced and smoothed under the combined influence of acoustic damping and cavity feedback [31,32]. The phase noise transfer of the BFL is given as:

$$S_{\phi}^{Stokes} = \frac{-lnR}{\beta_A - lnR + i2\pi f} \frac{e^{i\pi f} sin\pi f}{\pi f} S_{\phi}^{pump} \quad 1.1$$

S_{ϕ}^{pump} and S_{ϕ}^{stokes} denotes the power spectral density (PSD) of phase noises of Stokes wave and input pump. The PSD will be introduced in the following. *R* represents the cavity feedback rate and β_A is the acoustic damping rate. The equation 1.1 can be factorized into two parts:

$$H_1(f) = \frac{-lnR}{\beta_A - lnR + i2\pi f} \quad 1.2$$

$$H_2(f) = \frac{e^{i\pi f} sin\pi f}{\pi f} \quad 1.3$$

In the first part of the equation 1.1, H_1 shows that phase fluctuations of the pump laser are filtered and reduced before being transferred to the Stokes wave as $|H_1|<1$. The second part, H_2, corresponds to a smoothing effect during phase noise transfer, due to the cavity. *K* represents the phase noise reduction between the pump and emitted Stokes wave. From equation 1.2, it is expressed as:

$$K = \left(1 - \frac{\beta_A}{lnR}\right)^2 \qquad 1.4$$

A Brillouin laser with a 20-meters fiber length cavity and having feedback rate of R = 0.78 and an acoustic damping rate of β_A = 17.27 provides a frequency noise reduction of 37$\pm$1 dB. A frequency noise reduction of up to 40 dB may be easily reached, as observed in [47], [48] and [44].

1.3 Technique for measuring the coherency of a laser.

A brief idea about the noise in a conventional laser and Brillouin fiber laser was given in section 1.2. The theoretical and experimental concepts of laser noises are presented in numerous sources [44], [47],[48], [60-64].

In conventional lasers, spontaneous emission initiates the amplification by stimulated emission. The origin of fundamental fluctuations of laser parameters, namely the intensity and phase, are due to spontaneous emission. The technical noise such as, acoustic and mechanical vibrations, temperature fluctuations and the influence from pump noise also degrades the laser linewidth (we will see that it is in a low-frequency range that we will precise). All these contributions lead to amplitude and phase noises.

In the subsequent subsections, the relationship between the phase noise, frequency noise and the laser linewidth will be discussed. An experimental method to determine the frequency noise using self-heterodyne technique will also be put forward.

1.3.1 Frequency noise in laser

At an optical frequency of ν_0, the scalar electric field of a light wave emitted by a single frequency laser with noise is given as:

$$E(t) = [E_0 + \delta E(t)]e^{i[2\pi\nu_0 t + \Phi(t)]} \quad 1.5$$

Where $\delta E(t)$ and $\Phi(t)$ are random processes that expresses fluctuations in amplitude and phase respectively. The instantaneous frequency of a laser $\nu(t)$ is:

$$\nu(t) = \nu_0 + \delta\nu(t) \quad 1.6$$

Where ν_0 is the central laser frequency or the mean frequency. The relation between phase and frequency fluctuations is expressed as a derivative:

$$\delta\nu(t) = \frac{1}{2\pi}\frac{d\Phi(t)}{dt} \quad 1.7$$

Equation 1.7 can be rewritten to give the instantaneous frequency:

$$\nu(t) = \frac{1}{2\pi}\frac{d}{dt}[2\pi\nu_0 t + \Phi(t)] = \nu_0 + \frac{d\Phi(t)}{dt} = \nu_0 + \delta\nu(t) \quad 1.8$$

The principal property is the stationarity of the derivative of the phase, which doesn't imply the stationarity of the phase. However, this last condition is considered at least during the time of observation. It enables to use the autocorrelation function of the phase and the PSD. The PSD of the frequency fluctuations $\delta\nu(t)$ is the Fourier transform of the autocorrelation function of $\delta\nu(t)$.

$$S_\nu(f) = \int_{-\infty}^{+\infty} R_{\delta\nu(t)}(\tau) e^{-i2\pi f} d\tau \qquad 1.9$$

Where $R_{\delta\nu(t)}(\tau)$, is the autocorrelation function of the frequency fluctuations $\delta\nu(t)$:

$$R_\nu(\tau) = < \delta\nu(t)\delta\nu(t-\tau) > = \lim_{T\to\infty} \frac{1}{T} \int_{-T/2}^{+T/2} dt \delta\nu(t)\delta\nu(t-\tau) \qquad 1.10$$

The relation between phase and frequency noise can be easily deduced:

$$S_\nu(f) = f^2 S_\Phi(f) \qquad 1.11$$

Where the PSD of $S_\nu(f)$ and $S_\Phi(f)$ are simply related through f^2, the square of the frequency.

$S_\Phi(f)$ is expressed in radian/Hz $S_\nu(f)$ in Hz^2/Hz.

The PSD is then measured in the electrical domain in a frequency-range going typically up to 1 MHz. (Note that this measurement could be made above the GHz range for semi-conductor lasers in order to include the relaxation oscillation frequency).

It has been established (references in [61]) that the PSD of a laser frequency-noise has mainly two contributions:

$$S_\nu(f) = \frac{h_{-1}}{f} + h_0 \qquad 1.12$$

A first contribution is a white noise corresponding to a constant value h_0 over the frequency ranger under consideration. The associated phase noise is proportional to $1/f^2$. It is due to the spontaneous emission, and it corresponds to a Lorentzian line shape for the laser line. The linewidth linked to the white noise is called the "intrinsic"[1] linewidth. The general notion attached to this noise is coherency.

A second contribution $\frac{h_{-1}}{f}$ is a low frequency component, the flicker noise; the phase noise has then a $1/f^3$ dependency. It includes different contributions from fundamental to technical causes. The flicker noise component provides a Gaussian shape to the laser line. The general property associated to this contribution is the stability of the laser frequency, which is major subject of metrology [65-68].

In the more general case, the flicker noise or 1/f term $\frac{h_{-1}}{f}$ may be replaced by:

$$\frac{h_{-\alpha}}{f^{\alpha}} \quad \text{with } 1<\alpha<2 \qquad 1.13$$

$\frac{h_{-2}}{f^2}$ is linked to the random walk frequency noise. The phase-noise PSD is then proportional to $\frac{1}{f^4}$.

Note that h_1 corresponds to phase flicker noise; the frequency noise PSD is then proportional to f (the phase-noise PSD is proportional to $\frac{1}{f}$). And h_2 corresponds to white

[1] We prefer to use the qualifier "intrinsic" rather than "natural".

phase noise; the frequency noise PSD is then proportional to f² ; the phase noise PSD is constant.

1.3.2 Relation between the electrical domain and the optical domain

The relation between the laser line in the optical domain and the laser frequency-noise PSD in the electrical domain is well described in [61-63]. *Elliot et al.* [63] gave in 1982 a detailed calculation from the laser field expressed in 1.5 to the linewidth of the laser line. It is also possible to get the relation between the auto-correlation function of the laser field and the frequency-noise PSD.

Assuming relations 1.5 to 1.9, the autocorrelation of the laser field, $R_E(\tau) =< E^*(t)E(t+\tau) >$, is then given by an expression of the frequency-noise PSD $S_\nu(f)$:

$$R_E(\tau) = E_0^2 e^{i2\pi\nu_0\tau} e^{-2\int_0^{+\infty} S_\nu(f)\frac{sin^2(\pi f\tau)}{f^2}df} \qquad 1.14$$

The laser spectrum in the optical domain is obtained by taking the Fourier transform of the auto-correlation function given by (from Wiener-Khintchine theorem):

$$S_E(\nu) = 2\int_{-\infty}^{+\infty} e^{-i2\pi\nu\tau} R_E(\tau)d\tau \qquad 1.15$$

The PSD of laser frequency-noise may include white, flicker and random walk noise or any type of noise. The influence of white and flicker noise will be presented separately.

1.3.2.1 White noise

When the frequency noise of a laser only consists of white noise, $h_{-1} = 0$ and its PSD is written in the electrical domain:

$$S_\nu(f) = h_0 \tag{1.16}$$

The laser spectrum has a Lorentzian shape. From equations 1.14 and 1.15, the laser spectrum is given by:

$$S_E(\nu) = E_0^2 \frac{h_0}{(\nu - \nu_0)^2 + \left(\frac{\pi h_0}{2}\right)^2} \tag{1.17}$$

The intrinsic laser linewidth is given by:

$$\Delta\nu_L = \pi h_0 \tag{1.18}$$

This relation will be used to determine the intrinsic linewidth.

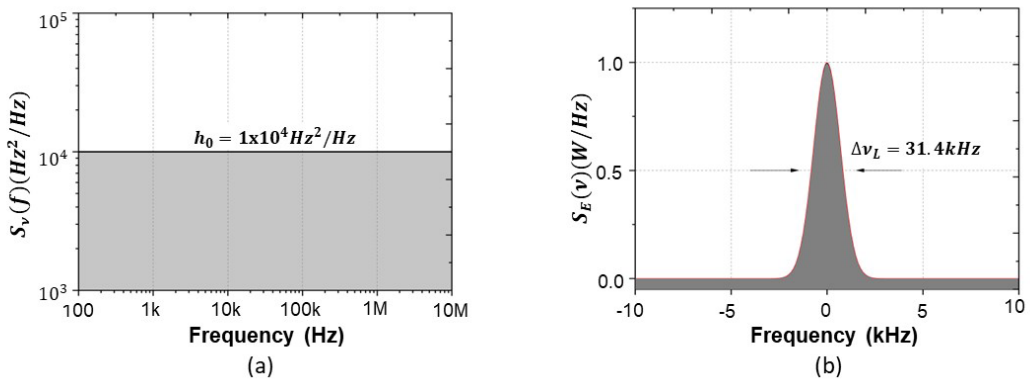

Figure 1.5: (a) Frequency noise plotted for $S_\nu(f) = h_0 = 10^4\ Hz^2/Hz$; (b) Optical spectrum of the laser line with an intrinsic linewidth of $\Delta\nu_L = 31.4\ kHz\ (= \pi h_0)$.

The white frequency noise for $h_0 = 10^4 Hz^2/Hz$ is plotted in Figure 1.5a. The equivalent optical spectrum of the laser line with an intrinsic linewidth of $\Delta\nu_L = 31.4\ kHz$ is also shown in Figure 1.5b.

1.3.2.2 Flicker Noise

In the case of flicker noise or 1/f noise, the laser frequency noise PSD is written in the electrical domain:

$$S_\nu(f) = \frac{h_{-1}}{f} \qquad 1.19$$

By substituting this expression in equation 1.14, we obtain:

$$R_E(\tau) = E_0^2 e^{i2\pi\nu_0\tau} e^{-2\int_0^{+\infty} h_{-1}\frac{sin^2(\pi f\tau)}{f^3}df} \quad 1.20$$

In the above equation 1.20, the integral $J = \int_0^{+\infty} h_{-1}\frac{sin^2(\pi f\tau)}{f^3}df$ is undefined at $f = 0$. Taking as the lower bound of integration the inverse of the time of observation, which may be confused with τ [61], J becomes a finite integral and has an analytic expression.

Thus, the optical spectrum of flicker noise $\left(\frac{h_{-1}}{f}\right)$ is then a Gaussian function given by [61]:

$$S_E(\nu) = E_0^2\frac{\sqrt{\pi}}{\sigma}e^{-(\nu_0-\nu)^2/\sigma^2} \quad 1.21$$

σ^2 is directly related to the width of the laser line: $\sigma^2 = 3.56h_{-1}$. It corresponds to frequency drifts of the central optical frequency ν_0. In this case, we will call the associated width of the line, the integrated linewidth of a laser. As we will see in the following, in presence of spontaneous emission, the whole Lorentzian spectrum will drift at low frequencies. The function given in equation 1.21 may be considered as a probability density of the fluctuations of the central frequency.

In the next section, we will use the β-line method to estimate the integrated linewidth and we will explain also how to measure the intrinsic linewidth.

1.3.2.3 General case with flicker and white noise

The frequency noise of a laser includes both white and flicker noise. In the electrical domain, the PSD of the frequency noise of a laser contains h_0 and h_{-1}. In the optical domain, the resulted laser line is the convolution product of both Lorentzian $(h_0\ part)$ and

Gaussian function $\left(\frac{h_{-1}}{f}\ part\right)$. It is called a Voigt function [61]. The Lorentzian has a stable linewidth and for the Gaussian case the linewidth depends on the observation time (T_{obs}) of the frequency noise spectrum. Hence, the Voigt function linewidth will also depend on the observation time (T_{obs}).

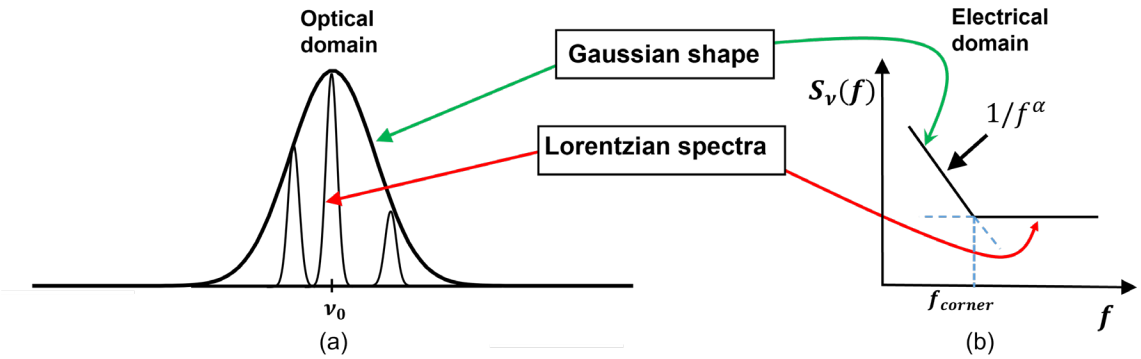

Figure 1.6: (a) The laser line fluctuations expressed in the optical domain, showing drifts of the laser line; the Lorentzian amplitude is linked to the drift probability; (b) the frequency noise PSD in the electrical domain; f_{corner} separates regions of white noise contribution and $1/f^{\alpha}$ contribution.

Figure 1.6(b) shows, in the electrical domain, two contributions. At low frequencies, noise has a $1/f^{\alpha}$ behavior. At higher frequencies, the white noise (h_0) due to spontaneous emission only prevails. These two regions are separated by the intersection of the two noise contributions at a frequency, called the corner frequency (f_{corner}). Above this frequency, the spontaneous emission is only contributing to the laser line. Considering a frequency band of observation [f_1, f_2] is equivalent to consider a temporal interval of observation $\left[T_{bandwidth} = {}^{1}/_{f_2}, T_{obs} = {}^{1}/_{f_1}\right]$. T_{obs} is the duration of observation corresponding to f_1

while f_2 is linked to the electrical bandwidth B_{det} of detection, corresponding to the smallest time of observation, $1/B_{det}$.

Usually, one has to choose a detection bandwidth slightly above f_{corner} in order to integrate all the noise contributions, especially the whole low-frequency components (or $1/f^{\alpha}$ contribution) and the white noise. Assuming that this is the case, varying the observation time (or $f_1=f_{obs}=1/T_{obs}$) will affect the linewidth measurement. Thus, if $T_{obs}<1/f_{corner}$ or $f_{corner} < 1/T_{obs}$, then during the time of observation T_{obs}, only the white noise will contribute to the laser line, which has a Lorentzian shape and is centered at the laser frequency ν_0, fixed by the cavity or/and the laser transition. Increasing the observation time will make $f_1=1/T_{obs}$ closer to the corner frequency. When $T_{obs}>1/f_{corner}$ or $1/T_{obs}< f_{corner}$, the $1/f^{\alpha}$ low-frequency contribution starts to play a role, which becomes more important as the observation time T_{obs}, is increased.

As shown in Figure 1.6(a), in the optical domain, the influence of this contribution is to temporally drift the laser line. This laser-frequency shift follows a gaussian statistical law given by the low frequency components.

In the case of flicker noise, the estimation of the integrated linewidth is directly linked to a Voigt profile, the convolution of a Lorentzian function and a Gaussian profile, for which an approximate linewidth is known (equation 1.18, $\sigma^2 = 3.56\, h_{-1}$).

In the more general case, the flicker noise is replaced by a low frequency component as explained before in equation 1.13.

The lecture of figure like 1.6 is enough to have all the required information in laser physics. However, some research groups in photonics are only used to laser line measurements in the optical domain. In order to image the influence of the low-frequency components, one gives the linewidth for a definite time of observation. In order to get an estimated value that is called integrated linewidth, we will introduce, in the next section, a general method to give the linewidth from frequency-noise measurements.

1.3.2.4 Estimation of the laser linewidth using β-line approximation

In this section, a technique to estimate the integrated linewidth will be explained.

The lasers used in this thesis have both white noise and low-frequency-noise components.

The technique of β-line approximation was proposed by Di Domenico *et al.* [62]. The idea is to have a simple procedure to estimate the integrated linewidth. As explained in the last section, the frequency noise PSD of a laser can be separated into 2 regions based on the corner frequency. The β-line is a way to have a rough estimation of the maximum frequency f_2, which is sufficient to get a good estimation of the integrated linewidth. The β-line separates the frequency noise PSD into two regions by drawing a simple line:

$$S_{\beta-\text{line}}(f) = \frac{8\ln(2)}{\pi^2} f \qquad 1.22$$

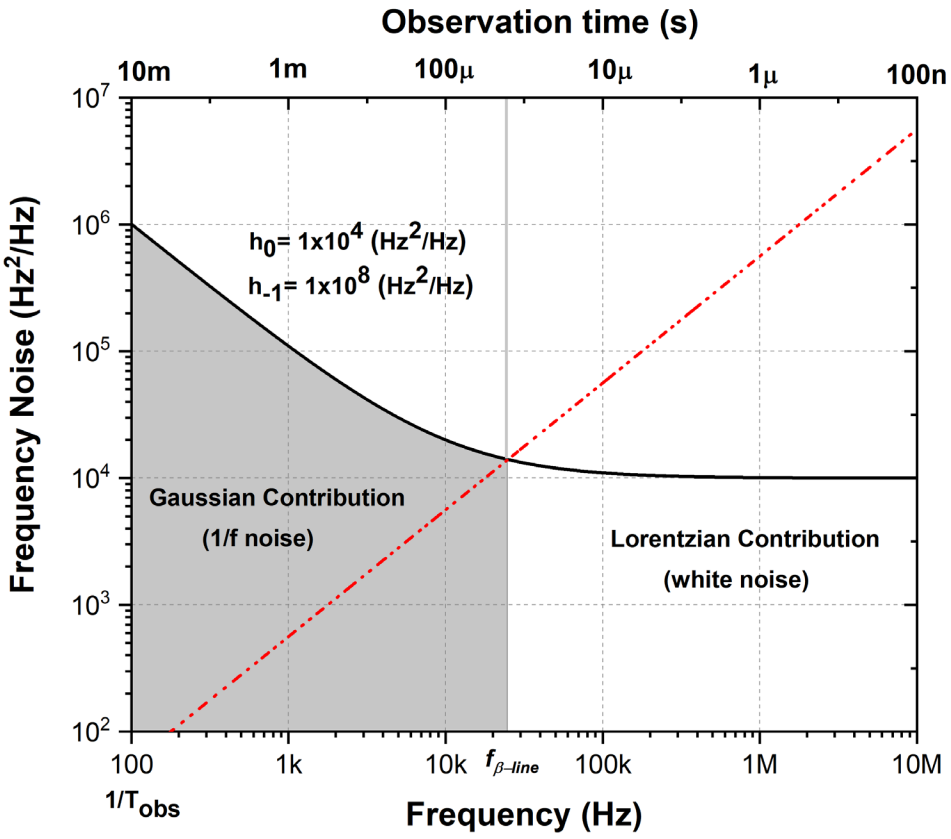

Figure 1.7: Laser frequency-noise PSD including flicker noise and white noise. The red dotted line (β-line) separates the frequency noise in two regions. Above $f_{\beta\text{-line}}$, the noise contribution is a white noise, implying in the optical domain a Lorentzian line shape that gives the intrinsic linewidth. Below $f_{\beta\text{-line}}$, the frequency noise has an additional contribution, which causes a line with a Voigt profile in the optical domain that gives the integrated linewidth.

The β-line $S_{\beta-\text{line}}$ intersects the frequency-noise PSD at a frequency $f_{\beta\text{-line}}$. It separates the frequency noise spectrum into two separate regions as shown in Figure 1.7, according to what has been explained in the previous section. In the β-line approximation method [62], the frequency noise located above $f_{\beta\text{-line}}$ corresponds to white noise. It implies a Lorentzian

laser line-shape in the optical domain. The frequency noise located below $f_{\beta\text{-line}}$ contributes the technical noise (grey-shaded region) as shown in the Figure 1.7. The integrated line depends on the observation time T_{obs}. The corresponding "integrated linewidth" of the optical spectrum can be calculated with an error of 10 % by the equation:

$$\Delta\nu_g = \sqrt{8\ln(2)\,A} \tag{1.23}$$

Where A is the area under the curve given by the integral from $1/T_{obs}$ to $f_{\beta\text{-line}}$:

$$A = \int_{\frac{1}{T_{obs}}}^{f_{\beta-\text{line}}} S_\nu(f)df \tag{1.24}$$

Note that with this formula $1/T_{obs}$ must be lower than $f_{\beta\text{-line}}$ (if $f_{\beta\text{-line}} = 1/T_{obs}$, A =0 leading to a null linewidth, which is nonsense as the lower limit must be the intrinsic linewidth). The idea is to find the upper bound that enables to have an invariance in the calculation of equation 1.24. T_{obs} being fixed, the result A of the integral 1.24 remains unchanged if we increase the upper bound of integral 1.24 with values above $f_{\beta\text{-line}}$.

The Figure 1.7 is plotted as a function of frequency with $h_{-1} = 1 \times 10^8 Hz^2$ and $h_0 = 1 \times 10^4 Hz^2/Hz$. The red dotted line ($\beta$-line) separates the frequency noise into 2 regions at the intersection frequency $f_{\beta\text{-line}}$. The intrinsic linewidth measured from the Figure 1.5 is $\pi h_0 = 31.4\,kHz$. The integrated linewidth for an observation time of 10 *ms* (100 *Hz*) is 66.75 *kHz*. The β-line approximation gives a good estimation of the integrated linewidth from the laser frequency-noise PSD. An exact value could be also calculated using relations 1.14 and 1.15.

In the next section, the experimental setup to measure the laser frequency-noise will be detailed by introducing the correlated delayed self-heterodyne method.

1.3.3 Experimental measurement of frequency noise

In this section, I present the frequency noise measurement technique used during my thesis. This technique was used to characterize the frequency noise measurement of the sub-kHz laser emitting in the C-band, which is a core tool of this thesis.

1.3.3.1 Radio-frequency source analyzer method: correlated delayed self-heterodyne technique

A correlated delayed self-heterodyne technique, or radio-frequency source analyzer method, was used for this measurement [64]. In this delayed self-heterodyne technique, the delay time of the signal is shorter than the coherence time of the laser to maintain the statistical dependence of the interacting fields, which includes information regarding the phase (frequency) noise of the laser under test. The phase noise is measured in the electrical domain thanks to a signal source analyzer (SSA), which includes an internal radio-frequency source (local oscillator). If the delay time is longer than laser coherence time, the corresponding delayed self-heterodyne technique is called uncorrelated technique. It measures the autocorrelation of the laser line shape. The uncorrelated self-heterodyne technique gives an estimation of the laser integrated linewidth (equation 1.24).

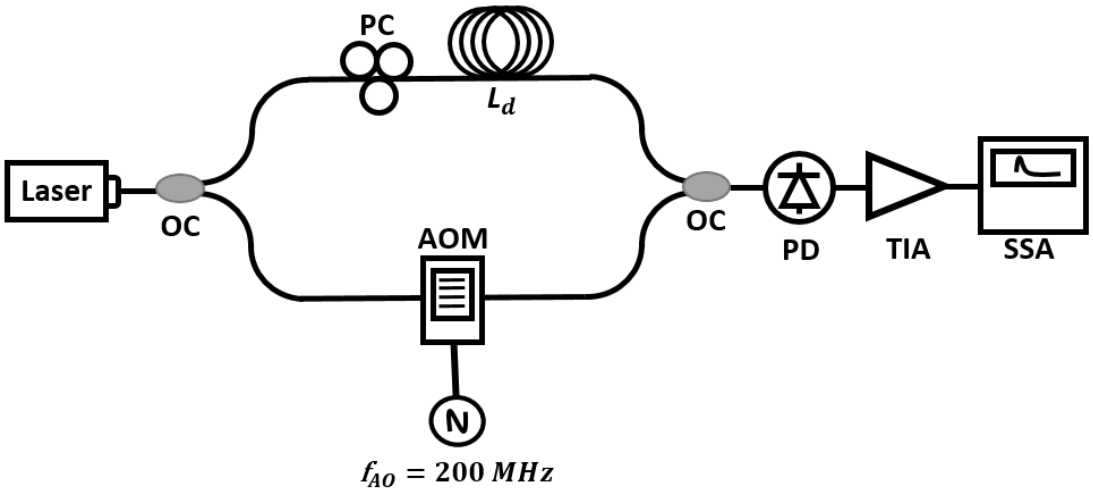

Figure 1.8: Correlated self-heterodyne frequency noise measurement setup. OC: Optical coupler, PC: Polarization controller, PD: Photodetector, TIA: Transimpedance amplifier, SSA: Signal source analyzer, AOM: Acousto-optic modulator, L_d: delay fiber length.

The correlated self-heterodyne frequency noise measurement setup is shown in Figure 1.8. As can be seen in Figure 1.8, the input signal of the laser is divided following two arms of the measurement setup. This interferometer enables access to the laser field phase at a shifted frequency f_{AO}. One arm includes a delay fiber (L_d). L_d is a short delay length (from 1 meter to a few hundred meters). The corresponding time delay (τ_d) is given by:

$$\tau_d = \frac{nL_d}{c} \tag{1.25}$$

Where c is the speed of light and n is the refractive index of the fiber medium. The delay time τ_d is much shorter than the coherence time τ_{coh} of the laser ($\tau_d \sim 1\ \mu s \ll \tau_{coh} \sim 100\ \mu s\ or\ more\ in\ our\ study$). The coherence time of the laser τ_{coh} is given by:

$$\tau_{coh} = \frac{1}{\Delta\nu_L} \tag{1.26}$$

An acousto-optic modulator shifts the optical signal in the other arm by a frequency $f_{AO} = 200\ MHz$. This is why the method is referred to as heterodyne technique.

At the output of the interferometer, after a coupler, the photodetector (PD) detects the radio frequency signal of the two interacting fields at a frequency of f_{AO}. The photocurrent is then amplified by a transimpedance amplifier (TIA). The phase noise PSD of the interacting fields is measured by using a signal source analyzer (SSA). The polarization controller (PC) ensures that the signal detected at SSA is maximum. The SSA is a ROHDE&SCHWARZ FSWP signal source analyzer (13 GHz bandwidth). In our case, the phase noise is detected at f_{AO}. The phase noise measurement provided by the SSA uses a phase locked loop with an internal reference oscillator and an internal phase detector.

To summarize, the correlated delayed self-heterodyne technique consists in using an interferometer to get access to the optical phase of the field. The phase noise of the detected electrical signal amplified by a TIA is analyzed by a dedicated equipment, an SSA.

In the following, we will establish how to get the laser frequency noise from this experimental measurement.

Then we will discuss the noise floor of such an experimental technique.

1.3.3.2 Measurement of Frequency Noise

The electric field of a laser is given by:

$$E(t) = E_0 e^{i[2\pi\nu_0 t + \Phi(t)]} \quad 1.27$$

Where E_0 is the amplitude, $\Phi(t)$ is the phase of the signal and the central laser frequency is ν_0. It is assumed that the laser has negligible intensity noise. The detected intensity by the photodetector is proportional to:

$$I_d(t) = 2E_0^2\left[1 + cos[2\pi f_{AO} t - 2\pi\nu_0\tau_d + \Delta\Phi(t,\tau_d)]\right] \quad 1.28$$

The phase difference between 2 interacting waves, or phase jitter between t and t + τ_d, is given by:

$$\Delta\Phi(t,\tau_d) = \Phi(t) - \Phi(t+\tau_d) \quad 1.29$$

The interferometer enables us to get the phase difference. The SSA measures at a frequency f_{AO} the phase noise $S_{\Delta\Phi,SSA}(f)$ provided by the TIA and proportional to I_d; the photocurrent at the SSA is $\Re$ g_{LNA} I_d where $\Re$ is the photodetector responsivity and g_{LNA} the electric amplifier gain. The equation 1.28 does not consider phase noise introduced by any other component in the measurement setup, especially by the frequency shifter. In our case the measured phase noise is higher than the noise generated by the acousto-optic component, and more precisely its electrical oscillator in the frequency shifter.

From this measurement, one can easily deduce the phase noise PSD of the detected signal (laser phase) from equation 1.29 by a Fourier transform $\left(\Delta\Phi(f) = \Phi(f)\left(1 - e^{-i2\pi f\tau_d}\right)\right)$:

$$S_{\phi,laser}(f) = \frac{1}{4sin^2(\pi f\tau_d)} S_{\Delta\Phi,SSA}(f) \quad 1.30$$

The frequency noise PSD is linked to the phase noise PSD by equation 1.11. The expression of the laser frequency noise PSD can then be related to the measured phase noise PSD:

$$S_{\nu,laser}(f) = \left(\frac{1}{2\pi\tau_d sinc(\pi f\tau_d)}\right)^2 S_{\Delta\Phi,\ SSA}(f) \qquad 1.31$$

With $sinc(x) = \frac{sinx}{x}$.

1.3.3.3 Role of the interferometer: gain and detection bandwidth

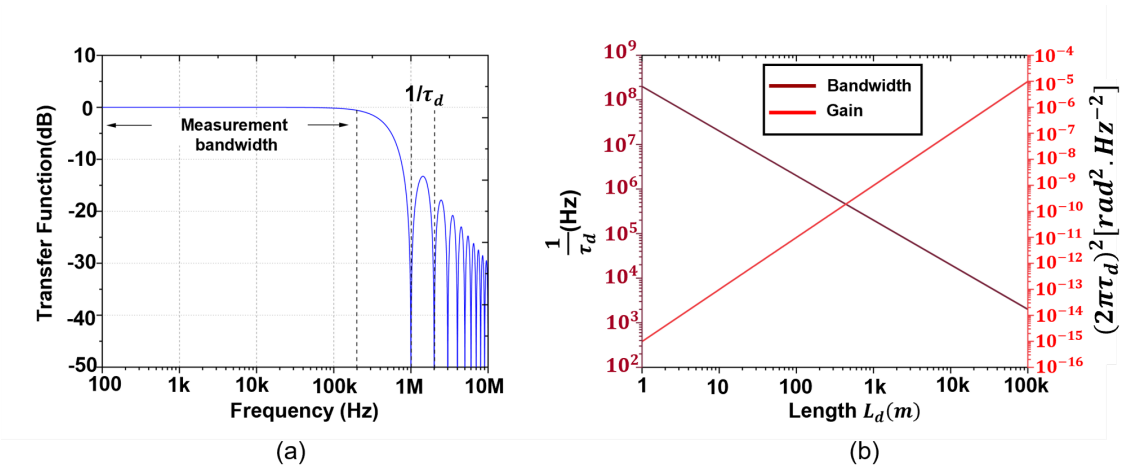

Figure 1.9:(a) Transfer function of unbalanced interferometer with $\tau_d = 1 \times 10^{-6}$ (for $L_d = 200\ m$) (b) Cutoff frequency and gain conversion of measurement bench as function of delay length L_d.

The SSA detects a phase noise PSD from the interferometer. The laser frequency-noise PSD is obtained by dividing the measured noise PSD by the term $(2\pi\tau_d sinc(\pi f\tau_d))^2$. This transfer function is linked to the transmission function of the interferometer, which is

a sine function, and to the Fourier transform of a derivative. The interferometer behaves as a low-pass filter. The measurement bandwidth is inversely proportional to the delay time τ_d of the interferometer (or the length). The Figure 1.9a shows the transfer function of an unbalanced interferometer with a delay of 200 meters ($\tau_d = 1\ \mu s$). The cut-off frequency for a delay of 200 meters is 1 MHz as seen from the figure. It provides a measurement bandwidth: for instance, if it is defined by a transfer function at -3 dB, then the bandwidth is 442 kHz, which is obtained by solving $\text{sinc}^2(x)=0.5$. In our study we use different delay lengths from a few meters (4 meters correspond to a FSR of 50 MHz) to 400 meters (FSR = 0.5 MHZ).

The conversion gain of the interferometer in the measurement bandwidth is $(2\pi\tau_d)^2$ for frequencies well below $1/\tau_d$. The Figure 1.9b illustrates the variation of conversion gain and measurement bandwidth with respect to the delay lengths. Upon increasing the delay lengths, the measurement bandwidth will decrease as seen from the Figure 1.9b. To increase the measurement bandwidth, it is necessary to decrease the delay lengths. Thus, very different delays should be used for characterizing lasers with very different linewidths. The measurement bandwidth should be greater than the laser linewidth. Otherwise, the laser line will be modulated by the transfer function of the interferometer. Increasing delay lengths will lead to a reduction of the measurement bandwidth but also to an increase of the conversion gain as observed from the Figure 1.9b.

One important property of the phase noise $S_{\Delta\Phi,\,SSA}$ measured by the SSA can be caught from equation 1.30. Assuming a detection in the measurement bandwidth or in other words $sinc(\pi\tau_d) \approx 1$, then increasing the delay fiber length increases τ_d as well as the conversion

gain $(2\pi\tau_d)^2$; it follows that the measured phase noise $S_{\Delta\Phi,SSA}(f)$ is also increasing exactly in the proportion of the conversion gain as the laser frequency (or phase) noise $S_{\nu,laser}$ is the external value to be measured and is not dependent on the delay fiber length.

This last property is well-known [148] as the mean-squared phase jitter is proportional to τ (if only the spontaneous contribution is considered):

$$\langle \Delta\phi^2(\tau_d)\rangle = 2\pi\Delta\nu_L\tau_d = 2\pi^2 h_0\tau_d \qquad 1.32$$

This last property is calculated from the general formula (directly extracted from the relation between Fourier transforms of the phase and of the phase jitter, and from the fact that the autocorrelation function of the phase jitter $R_{\Delta\phi}(\tau_d = 0)$ is equal to the mean-squared phase jitter at $\tau_d = 0$):

$$\langle \Delta\phi^2(\tau_d)\rangle = 2\int_0^{+\infty} S_{\Delta\phi}(f)\,df = 4\int_0^{+\infty} S_\nu(f)\frac{sin^2(\pi f\tau_d)}{f^2}df \qquad 1.33$$

The phase difference between 2 interacting waves or the phase jitter given by equation 1.29 is a zero-mean stationary Gaussian random process having a probability density function between t and t + τ_d: $\frac{1}{\sqrt{2\pi\langle\Delta\phi^2(\tau_d)\rangle}}exp\left(-\frac{\Delta\phi^2(\tau_d)}{2\langle\Delta\phi^2(\tau_d)\rangle}\right)$.

This last property implies that the optical-field autocorrelation function of equation 1.14 is then given by (considering that the signal is at f_{AO}):

$$R_E(\tau_d) =< E^*(t)E(t+\tau) >= \langle E_0^2 e^{i2\pi\nu_0\tau_d}e^{-i\Delta\phi(t,\tau_d)}\rangle \qquad 1.34$$

As $\langle e^{-i\Delta\phi(t,\tau_d)}\rangle = e^{-\frac{1}{2}\langle\Delta\phi^2(\tau_d)\rangle}$ for a zero-mean stationary Gaussian random process:

$$R_E(\tau_d) = E_0^2 e^{i2\pi\nu_0\tau_d} e^{-\frac{1}{2}\langle\Delta\phi^2(\tau_d)\rangle} = E_0^2 e^{i2\pi\nu_0\tau_d} e^{-\pi\Delta\nu_L\tau_d} = E_0^2 e^{i2\pi\nu_0\tau_d} e^{-\pi\Delta\nu_L\tau_d}$$

The Fourier transform of the normalized autocorrelation function $\left(g_E^{(1)}(\tau_d) = Re\left(\frac{R_E(\tau_d)}{R_E(0)}\right) = Re\left(e^{i2\pi\nu_0\tau_d}\langle e^{-i\Delta\phi(\tau_d)}\rangle\right) = e^{-\frac{1}{2}\langle\Delta\phi^2(\tau_d)\rangle} cos(2\pi\nu_0\tau_d)\right)$ is obviously a Lorentzian with a full width at half maximum $\Delta\nu_L$.

In summary, increasing the delay fiber length increases τ_d and thus the phase jitter (or its mean-squared value) as well as the conversion gain $(2\pi\tau_d)^2$. As the mean-squared phase jitter is proportional to $\Delta\nu_L\tau_d$ $(= \pi h_0\tau_d)$, decreasing the linewidth that has to be measured can be compensated by a longer fiber delay or conversion gain $(\propto \tau_d^2)$ at the price of a lower detection-bandwidth.

Hence, a compromise should be found between the two parameters, detection bandwidth and conversion gain, to keep them high to have enough detection bandwidth and enough signal strength above the noise floor of the measurement bench. An example of frequency noise measurement of Tunics-PR is shown in the next section.

1.3.3.4 Noise floor of the frequency-noise characterization bench

The noise floor of the bench will be caused by any noise other than that of the laser. Any noise arising from the measurement bench is considered as a contribution to the noise floor other than that of the laser under test. Mechanical and acoustic vibrations, thermal fluctuations, delay fiber length variations, SSA noise, noise emerging from the AOM, photodetector and TIA contribute to the noise floor of the bench. The main contribution of the noise will be that of the interferometer, SSA and the frequency shifter as far as we

assume to have enough signal to ignore the shot noise of the photodetector. This last assumption is reached by selecting conveniently the conversion gain or the delay fiber length. The frequency noise can be limited by the laser relative intensity noise. It corresponds to in equation 1.28 or more exactly to the noise of the product $E(t)E(t+\tau_d)$ resulting from the beating of the two fields coming from the two arms of the interferometer. It reveals the capacity of the SSA to track the frequency f_{AO} from $cos[2\pi f_{AO}t - 2\pi\nu_0\tau_d + \Delta\Phi(t,\tau_d)]$ when there are field-amplitude fluctuations. The intensity noise influence is negligible in our study.

The SSA has typical values of phase noise sensitivity at a frequency 200 MHz (f_{AO}) are in dBc (in a bandwidth of 1 Hz):

Frequency offset	1 Hz	10 Hz	100 Hz	1 kHz	10 kHz	100 kHz
Phase noise sensitivity (dBc)	-85	- 105	- 130	- 150	- 160	-170
Frequency noise floor (Hz^2/Hz)	-85	- 85	- 90	- 90	- 80	-70
Minimal linewidth (nHz)	10	10	3	3	30	300

Depending on the electrical frequency f considered, the minimal linewidth that can be measured is between 3 nHz and 300 nHz.

However, the driver used for the frequency shifter has a contribution. It is estimated by measuring the phase noise without any delay in both fibre arms so that it certainly overestimates the exact value.

Frequency	100 Hz	1 kHz	10 kHz	100 kHz
Phase noise sensitivity (dBc)	- 105	- 115	- 120	-140
Frequency noise floor (Hz^2/Hz)	- 65	- 55	- 40	-40
Minimal linewidth (µHz)	1	10	314	314

The AO driver brings a limitation around 315 µHz for the noise floor of the frequency-noise PSD. The performance of this driver can be improved even if the driver in use is not that of the manufacturer.

The main limitations are brought by the interferometer itself.

We used a method proposed in [147] to evaluate the overall phase noise of the experimental bench. It consists in inserting two identical fiber spools in each arm of the interferometer (Figure 1.8). In this configuration, the delay and the phase jitter are null so that in equation 1.28 the beating term becomes $cos\left[2\pi f_{AO}t + \Phi_{system}(t)\right]$ with $\Phi_{system}(t)$ the stochastic phase due to the different environmental perturbations. The beating between the different frequency components of the lines of the two signals from the two arms is coherent. It generates a DC component and is negligible at other frequencies. The measured phase noise may be attributed to the environment and principally to the interferometer, which acts as a sensor, that will reveal different perturbations (thermal, acoustical…). This method is systematically used to characterize different delay lengths. A longer length will improve the gain conversion in the unbalanced interferometer as well as the noise floor. The noise floor for 200 meters is for frequency noise measurements 3 mHz. I have

improved this noise floor down to 700 μHz by using two ultra-stable fiber spools of 400 meters, kindly donated by Exail (formerly IxBlue). The packaging of the device, that brings mechanical insulation and thermal stability, is extremely important in achieving the lowest possible noise floor. Thus, in a first try to improve the noise floor, we used 400-meters fiber spool from a company, for which it results in catastrophic noise floor.

In conclusion, the balance interferometer method is used to characterize the noise of our set-up with an ability to reach 700 μHz.

1.3.4 Frequency noise measurement of a commercial source (Tunics-PR)

In this section, we detail the frequency noise measurements of *Tunics-PR* tunable laser (Photonetics, EXFO photonics). The integrated (for 10 ms observation time) and intrinsic linewidth are measured using the β-line approximation technique [62].

Before measuring the frequency noise, it is important to estimate the noise floor of the measurement bench. The phase noise of *Tunics- PR* tunable laser and the noise floor are shown in the figure 1.10a. The noise floor is obtained by inserting the same length (here 10 meters) of delay fiber in both arms of the Mach-Zehnder interferometer (MZI). The delay length is the one used for the unbalanced interferometer (Figure 1.8).

Frequency noise of the laser under test is obtained with the help of the equation 1.31. The frequency noise measurement of *Tunics-PR* laser is shown in Figure 1.10b. The red curve illustrates the frequency noise. The β-line (blue) separates the spectrum into 2 regions. The grey shaded region helps to calculate the integrated linewidth of *Tunics-PR.*

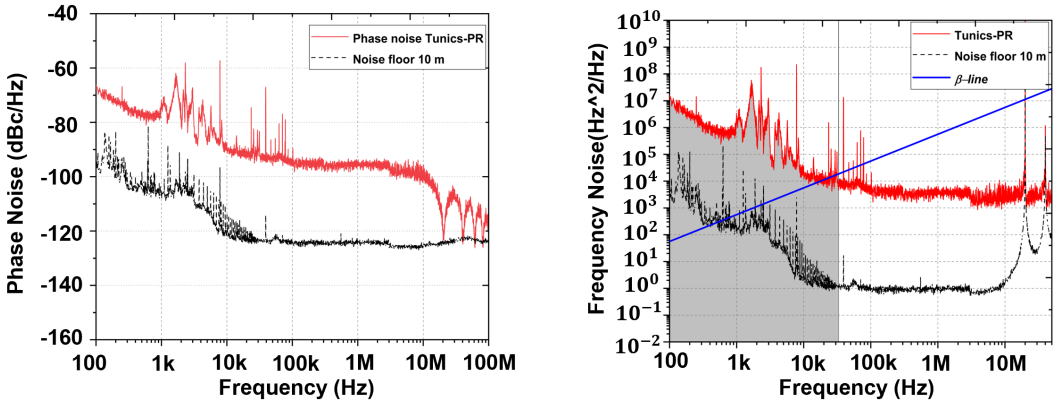

(a) (b)

Figure 1.10: (a)Tunics-PR phase noise and the noise floor of measurement bench with 10 m delay length. (b) Frequency noise measurement of Tunics-PR and linewidth estimation using β-line approximation. The shaded region denotes area under the curve, which helps to determine the integrated linewidth.

The intrinsic linewidth calculated from Figure 1.10b is 31.4 *kHz* that can be compared to the free spectral range of the interferometer (FSR = 20 MHz) as L_d = 10 m (τ_d = 50 ns). The integrated linewidth for an observation time of 10 *ms* is 337 ± 33 *kHz*. The integrated linewidth measurement using β-line method has approximately an error factor of 10 %. Hence, a ten-percentage error is added to all the integrated linewidth measurements in this thesis. The peaks in the curve Figure 1.10b is due to thermal and mechanical fluctuations. The noise floor is at a level of approximately 1 Hz. As already said, insertion of 400 meters fiber spool enables to reach a noise floor of 700 µHz. This allowed us to measure the accurate intrinsic linewidth of the sub-Hz linewidth cascaded non-resonant BFL laser that is presented in the section 1.6.

The following section will explain the technique to reduce the technical noise of the laser and how to improve its frequency stability. *Tunics- PR* tunable laser will be used in this thesis to realize a sub-kHz laser with a selectable wavelength in the C-band. Note that

different sources have been used with success (see Annex.3). It will also be used to cascade two Brillouin lasers to obtain mHz linewidth.

1.4 Laser frequency stabilization

This section will address the technique for the stabilization of laser frequency on an unbalanced fiber interferometer. The stabilization of laser frequency onto a resonance of an unbalanced Mach-Zehnder interferometer will reduce the low-frequency noise of the laser [68]. The cavity, which is more stable than the laser, will transfer its stability to the laser leading to a reduction of the flicker noise. Several articles discussing the laser linewidth reduction using a servo-control could be found in [26,27,69]. The commonly used optical frequency discriminators also include the use of resonance of atomic or molecular transitions [70,71], of resonance of optical cavity [72-74]. Ultra-high finesse optical cavities could be also used to stabilize the laser frequency to reduce fast fluctuations and can even diminish the intrinsic linewidth [75-77].

1.4.1 Servo loop control

The block diagram of the servo-control is shown in the Figure 1.11. The principle of laser frequency stabilization involves measuring the laser frequency fluctuations by comparing them to a reference frequency. The difference in frequency between reference and laser frequency fluctuations is called the error signal. Here, the reference is a resonance of the MZI. The corrector amplifies the generated error signal. The actuator converts the electrical

correction signal to optical frequency fluctuations and acts on the laser to stabilize it. The sensor in this work consists of a MZI (frequency discriminator) followed by an electrical photodetection chain. The MZI converts the frequency fluctuations into intensity fluctuations.

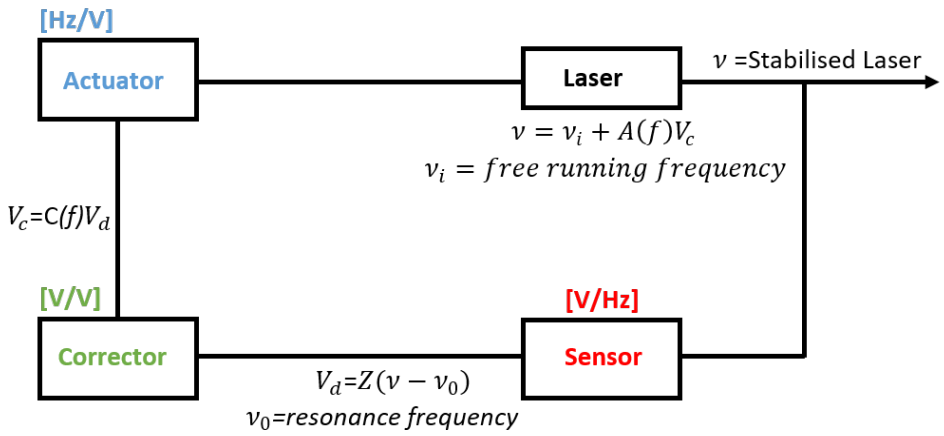

Figure 1.11: The principle of laser frequency stabilization. The sensor converts optical frequency fluctuations into voltage fluctuations and generates an error signal. The corrector amplifies the generated error signal and provides the correction signal. The electrical correction signal is converted into optical frequency fluctuations by the actuator and applied to the laser to compensate for the frequency fluctuations.

The photo-detection chain involving the photodiode and transimpedance amplifier measures the optical intensity fluctuations in the electrical domain. A proportion integrator corrector (PID) is used to generate the amplified correction signal and to stabilize the system. The actuator corrects the frequency fluctuations of the laser by modulating a parameter, which is in direct relation with the optical frequency. Here, it is the driving current.

Let us consider the transfer function of the sensor, corrector and actuator to be *Z(f), C(f)* and *A(f).* Let the frequency fluctuations of the laser at the input of the system be ν_i and the stabilized frequency of the laser, ν. The reference frequency is assumed to be ν_0. The voltage at the output of sensor is given by V_d:

$$V_d = Z(f)\delta\nu \tag{1.33}$$

Where $\delta\nu = \nu - \nu_0$ is the frequency deviation from the reference frequency ν_0 of the stabilized laser. The PID then amplifies the output voltage of the sensor. The output voltage of the corrector is given by V_c:

$$V_c = C(f)V_d \tag{1.34}$$

Where $C(f)$ is the transfer function of the corrector. The stabilized laser frequency, ν is given by:

$$\nu = \nu_i + A(f)V_c \tag{1.35}$$

On substituting equations 1.35 and 1.36 in 1.37 becomes:

$$\nu = \nu_i + A(f)C(f)Z(f)\delta\nu \tag{1.36}$$

The difference in frequency between the free running and stabilized laser is $\Delta\nu = \nu_i - \nu_0$. The transfer function of the closed loop servo, $H^{CL}(f)$ is:

$$H^{CL}(f) = \frac{\delta\nu}{\Delta\nu} = \frac{1}{1 + G(f)} \quad 1.37$$

Where $G(f) = A(f)C(f)Z(f)$ is the gain of the open servo loop. The close-loop gain is a measure of how well the change in reference cavity frequency is tracked by the laser frequency. It is the ratio of ν to ν_0 . The servo loop decreases the frequency deviation $\Delta\nu$ of the free running laser by the factor of open-loop gain.

$$Closed\ loop\ gain = \frac{G(f)}{1 + G(f)} \quad 1.40$$

The PSD at the output of the system, $S_{\nu,OUT}(f)$ is given by [78]:

$$S_{\nu,OUT}(f) = \frac{S_{\nu_i,IN}(f)}{1 + |G(f)|^2} \quad 1.41$$

Where $S_{\nu_i,IN}(f)$ is the PSD related to frequency fluctuations at the input of the system. To improve the frequency stabilization, the gain of the open-loop has to be as high as possible over the spectral range on which stabilization is required. In the next section, I explain the experimental setup for laser frequency stabilization using an unbalanced Mach-Zehnder Interferometer (MZI).

1.4.2 Stabilization of pump frequency

Tunics-PR tunable source is the laser to stabilize. The frequency noise measurement of *Tunics-PR* is shown in Figure 1.10. The objectives are to stabilize the laser frequency or in

other terms to decrease the low-frequency noise (flicker, random walk and other noise given by the equation 1.13). Figure 1.12 gives a sketch of the experimental set-up.

The interferometer cavity, being more stable than the pump laser, transfers its stability to the laser. The *Tunics-PR* tunable laser signal is split into two arms through an optical coupler. One arm is used for characterization of stabilized-laser frequency-noise. The other arm is used for stabilization through the MZI interferometer. A time delay is introduced between the two arms by adding extra fiber length with L_d=*10 m*.

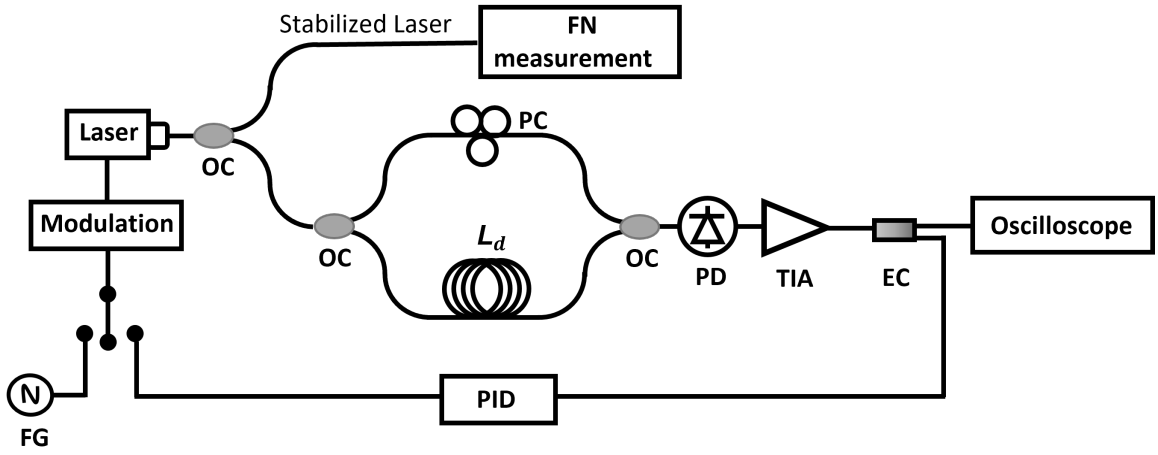

Figure 1.12: Experimental setup for the stabilization of pump-laser frequency onto a resonance of MZI. OC: Optical coupler, PC: Polarization controller, L_d=*10 m*: Delay length, PD: Photodetector, TIA: Transimpedance amplifier, EC: Electrical coupler, PID: Proportional-integral differential corrector, FG: Function Generator, FN: Frequency noise measurement.

The MZI cavity, being more stable than the pump laser, will transfer its frequency stability to the laser frequency through a servo-loop control on the driving current to correct the frequency fluctuations of the laser. The MZI along with photodetector and transimpedance

amplifier constitutes the sensor of the stabilization system. The output signal from the interferometer is detected using a photodetector and amplified using a TIA. The function generator is used to identify the voltage corresponding to the quadrature of the interferometer. The electrical coupler splits the signal into two. 50 % is used for observation through an oscilloscope. The other 50 % is sent to a PID module. A correction signal is generated via a proportional-integrator corrector. The generated correction signal is used to modulate the bias current of the source via its current controller to correct the fluctuations of pump laser as explained in the Figure 1.11. The frequency noise measurement of the stabilized *Tunics-PR* pump laser showed significant improvement in the integrated linewidth due to the suppression of its flicker noise. Thanks to the MZI cavity setup. The experimental results will be presented in the next section.

1.4.2.1 Tunics-PR

The free running of *Tunics-PR* laser line is illustrated by the red line in the Figure 1.13. The stabilized *Tunics-PR* is shown by the green line.

We can observe the suppression of the flicker noise of free running *Tunics-PR* starting from 40 kHz. The maximum noise suppression is observed in the frequency range of 1 kHz to 10 kHz. The bump observed at a frequency of 80 kHz is due to the high integrator gain of the PID used for the stabilization. The flicker noise of the free running *Tunics-PR* at 10 *ms* was observed to be 337 ± 33 kHz. The flicker noise of the stabilized *Tunics-PR* reduced to 4.75 ±0.47 kHz.

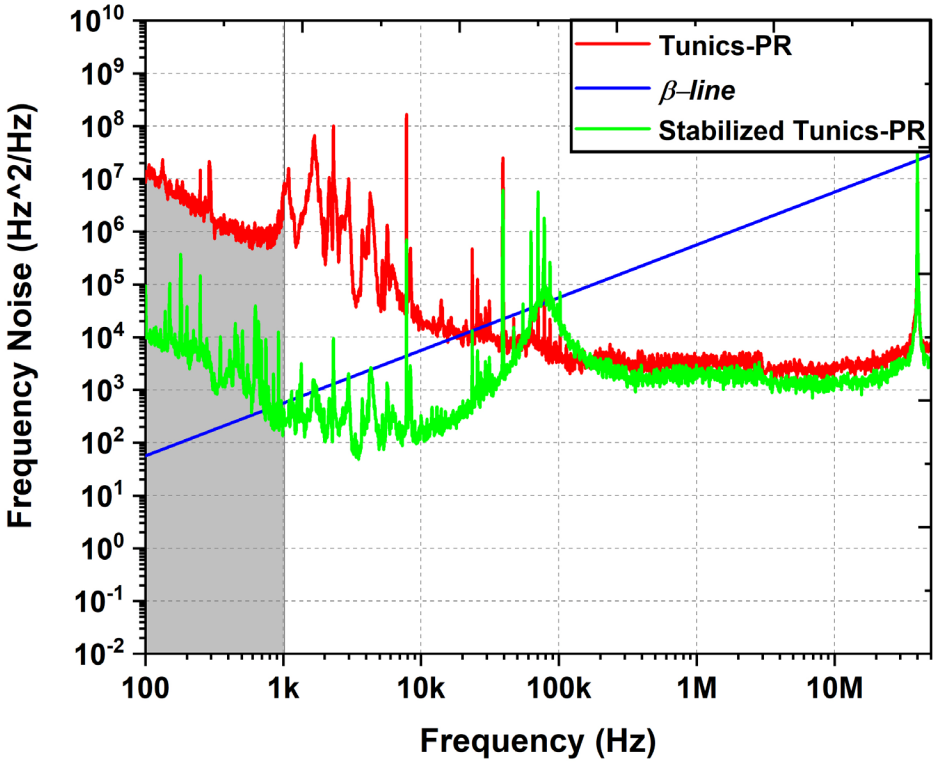

Figure 1.9: Frequency noise measurement of stabilized Tunics-PR tunable laser.

1.4.2.2 Tunics-OM

The frequency noise measurement of *Tunics-OM* tunable laser subjected to stabilization is shown in the Figure 1.14. The stabilized *Tunics-OM* tunable laser is shown by magenta line. The black line illustrates the free running *Tunics-OM* laser line.

Flicker noise suppression is observed beginning from 50 kHz to the lower frequency range. The integrated linewidth of free running *Tunics-OM* is 106.77 ± 10 kHz at 10 *ms*. The

flicker noise of the stabilized Tunics-OM was reduced to 3.44 ± 0.34 kHz at 10 *ms*. The maximum noise reduction is observed between the frequency range of 1 kHz to 10 kHz.

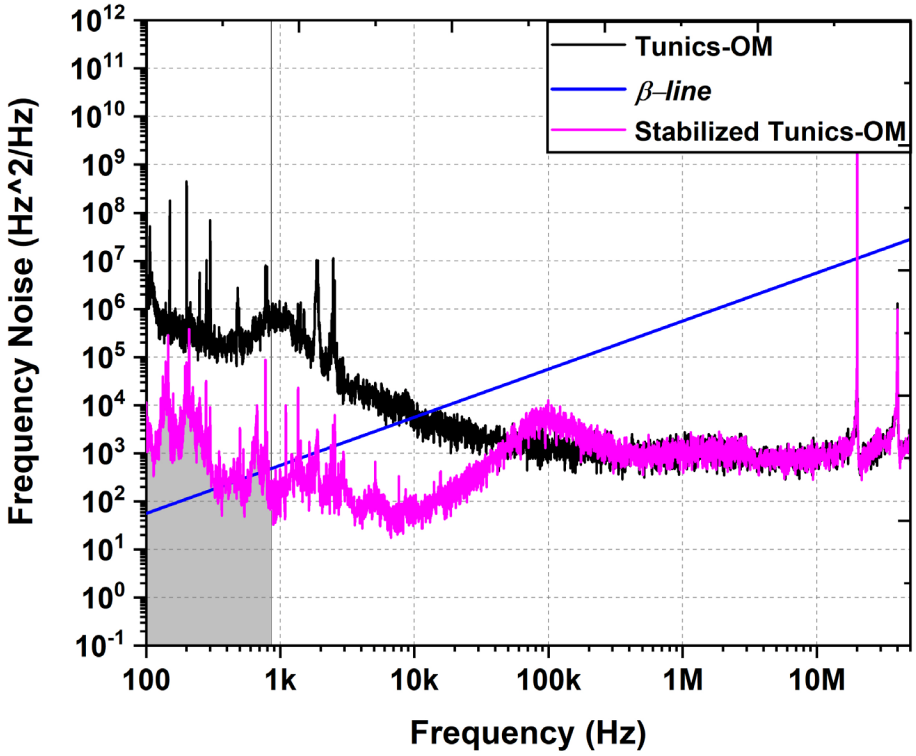

Figure 1.10: Frequency noise measurement of stabilized Tunics-OM tunable laser.

In the low frequency range of 100 Hz to 1 kHz, the noise increases due to the limitation in the correction of servo-loop. A noise bump is observed at 100 kHz, like the one observed in Figure 1.13.

In the beginning of this work, our belief was that a locking method would be necessary to compensate for the strong jitter of the tunable source. All first measurements were made using that locking. However, it turns out that good results were obtained without this locking on the pump wavelength. As we will be interested in the following intrinsic linewidth, we choose to get results without any locking or servo-loop.

Tunics-OM has better frequency noise performances compared to *Tunics-PR,* but the tuning resolution is higher than that of *Tunics-PR*. Tunics-OM has a tuning resolution of 10 picometer; that of *Tunics-PR* is 1 picometer. Hence, *Tunics-PR* is chosen as the pump source to develop sub-kHz linewidth laser with a wavelength selectable in the C-band. Note that the set-up enables to operate at any wavelength over the C-band. The performances of the developed sub-kHz linewidth laser will be the object of the next section.

1.5 Performances of sub-kHz linewidth laser with selectable wavelength in the C-band

The frequency noise performance of a laser, with sub-kHz linewidth, with selectable wavelength in the C-band, is discussed in this section. A detailed description of the architecture of this source is already presented in section 1.2. *Tunics-PR* tunable laser operating in C-band is chosen as the pump source to develop a highly coherent tunable laser source. A 14-meter long Brillouin cavity (FSR =14.3 MHz) is used for this purpose. The amplified *Tunics-PR* pump laser is injected inside the cavity from port 1 to port 2 of the circulator. The input pump makes a single pass inside the cavity via port 2 to port 3. The narrow linewidth Stokes wave circulates in the opposite direction of the *Tunics-PR*

pump source, and it is collected at the output of the coupler, P_{S1}. The experimental setup of sub-kHz linewidth *Tunics-PR* is shown in Figure 1.15. As discussed in section 1.2.1 (**Figure 1.2**), the match between a resonance of the laser cavity (the Stokes wavelength ν_S) and the frequency at gain maximum $(\nu_{Pump} + \nu_B)$ may be adjusted by different ways. It could be bringing by changing the fiber length of the laser cavity through a servo-loop [47] controlling the output power. We didn't choose this solution as we want a very simple set-up. As the Brillouin frequency is also dependent on the pump wavelength with a ratio of 7 MHz/nm, ν_B could be adjusted to correspond to multiple of the free-spectral range ($\nu_B = N\,\Delta\nu_{FSR}$) so that the Brillouin gain associated to the Stoke frequency ν_S is g_B. In practice, by tuning the pump wavelength over the nanometer range, one can adjust the gain so that its maximum is at a resonance frequency of the cavity. Thus, the wavelength of the coherent source can be selected over the C-band with a resolution around the nanometer. The temperature and mechanical stability were enough to ensure reproducible and constant measurements.

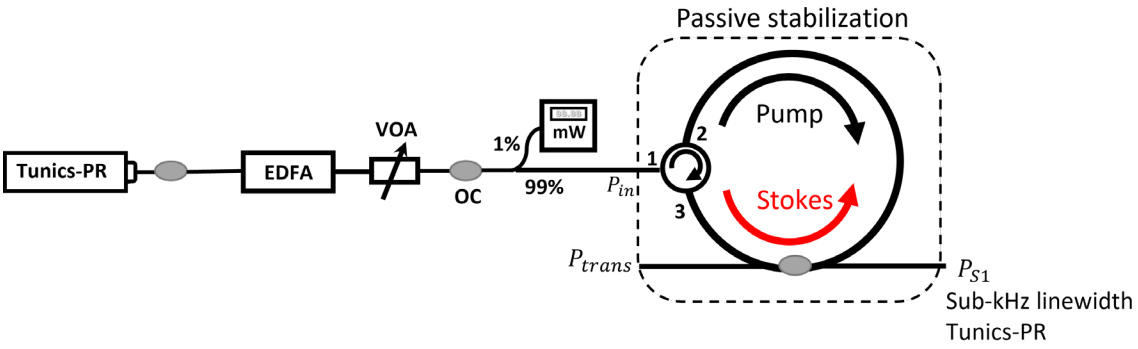

Figure 1.11: Sub-kHz linewidth Tunics-PR, source tunable in C-band.

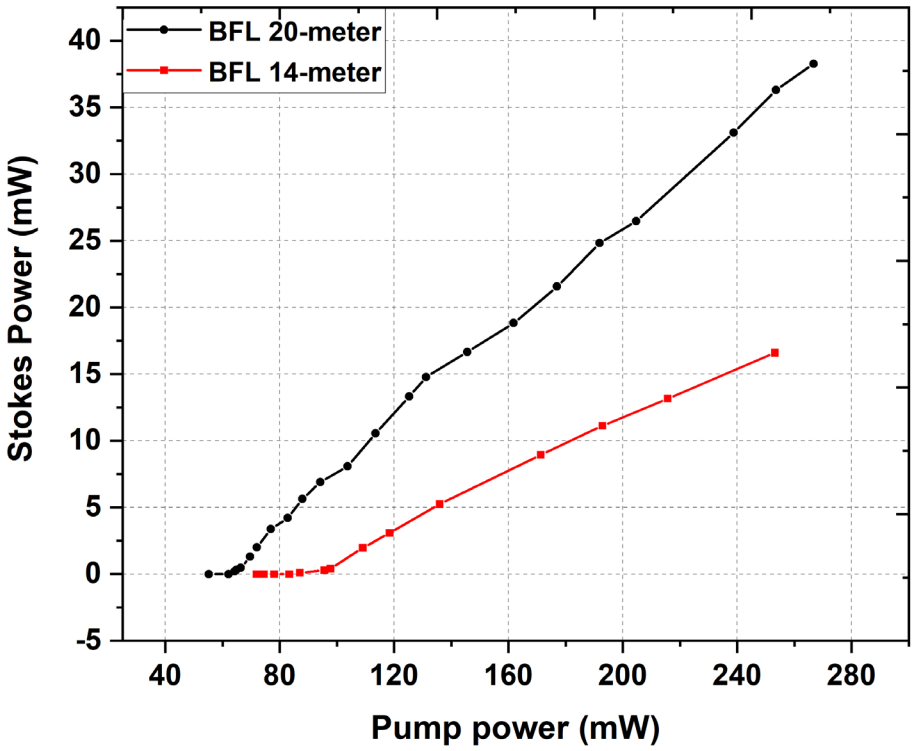

Figure 12 Pump power versus Stokes power of 20-meter and 14-meter BFL cavities.

The pump power versus Stokes power of the 20-meter and 14-meter Brillouin cavities are shown in the Figure 1.16. The measured threshold of 20-meter Brillouin cavity (black) is 58.5 mW and the slope efficiency is 18.5%. The 14-meter Brillouin cavity (red) has a threshold of 86 mW and slope efficiency of 10.3%.

The frequency noise performance of sub-kHz linewidth *Tunics-PR* laser is shown in the Figure 1.17. The *Tunics-PR* pump laser used to generate the sub-kHz linewidth laser has an intrinsic linewidth of 31 kHz.

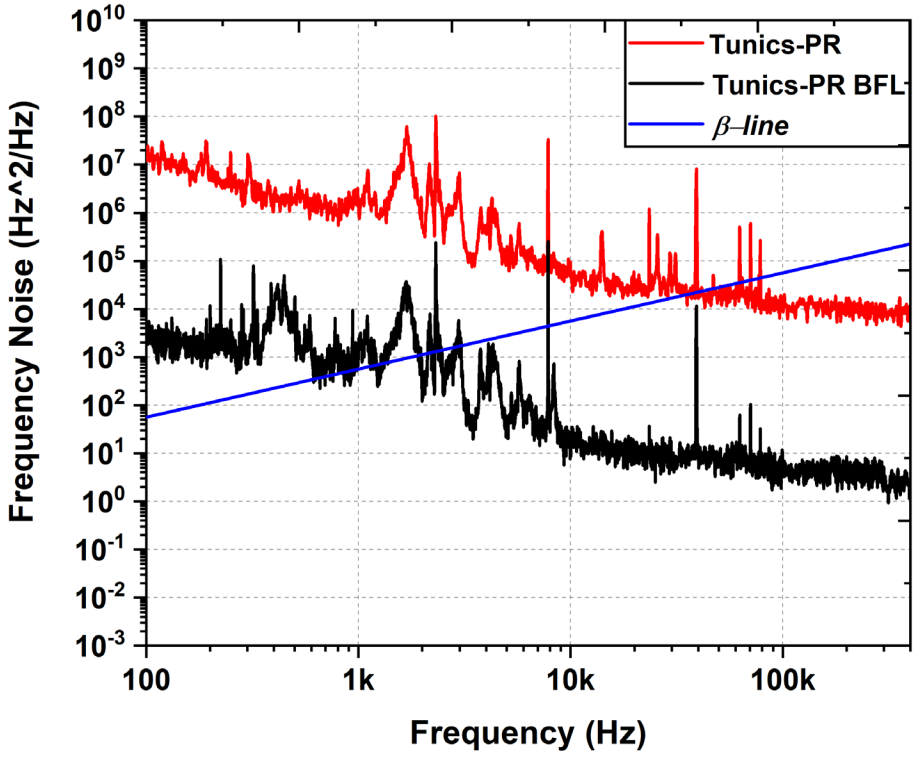

Figure 1.13: Frequency noise performance of sub-kHz linewidth Tunics-PR tunable laser in C-band.

The integrated linewidth estimated according to the β-line approximation is 337±33 kHz for an observation time of 10 *ms*. The generated narrow linewidth Tunics-PR BFL has an

intrinsic linewidth of 12 Hz. The observed integrated linewidth at 10 *ms* is 6.2 ± 0.62 kHz. The intrinsic linewidth of the tunable pump laser is reduced by a factor of 33.9 dB. It is due to the linewidth narrowing effect of the Brillouin cavity as explained in section 1.2.3, thanks to the 14-meter length Brillouin cavity. A disadvantage of this type of architecture is the occurrence of mode hopping. Mode hopping could be suppressed by stabilization of cavity length on the pump wavelength [79]. The linewidth estimation of two cascaded BFL is also studied in this thesis. It is presented in the next section 1.6.

1.6 mHz linewidth cascaded non-resonant tunable BFL

Two non-resonant BFL are cascaded together to generate mHz linewidth tunable laser in C-band. *Tunics-PR* tunable laser is used as the pump laser in this experiment. Two Brillouin cavities with lengths of 20 meters and 14 meters are chosen for this setup. Both the cavities are passively stabilized by gluing the fiber on to a metallic plate. The architecture of cascaded non-resonant tunable laser in the C-band is illustrated in the Figure 1.18.

P_{S1} is the Stokes wave of the first stage generated using 20-meter length fiber cavity using *Tunics-PR* tunable laser. The P_{S1} output is then amplified using an EDFA and injected into the 14-meter length fiber cavity. P_{S1} output acts as the pump laser and it is controlled using a variable optical attenuator after amplification before coupling via a circulator into the BFL cavity. 1 % of the pump power is collected for monitoring.

P_{S1} will induce stimulated Brillouin scattering again inside the second non-resonant cavity once it satisfies the Brillouin laser condition and overcomes the cavity losses. It finally

gives the emission of a first-order Stokes wave of the second stage with mHz linewidth at P_{S2} output. The frequency noise measurement is done by extracting this P_{S2} output.

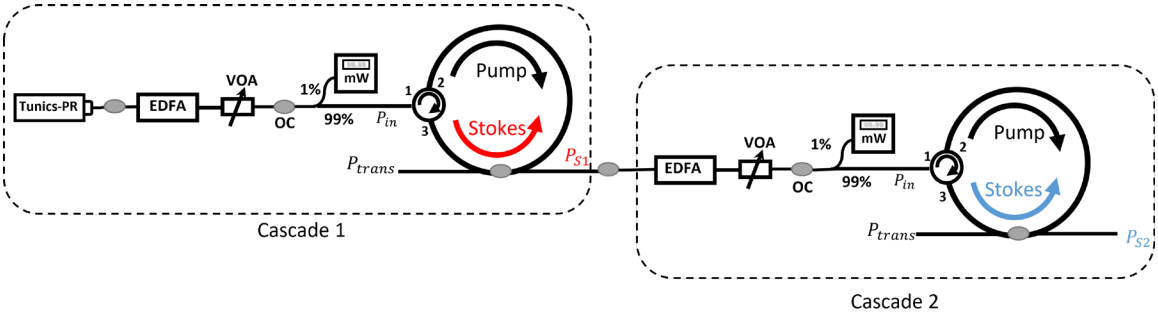

Figure 1.14: Cascaded mHz linewidth Tunics-PR tunable laser in C-band. EDFA: Erbium-doped fiber amplifier, VOA: Variable optical attenuator, OC: Optical coupler, P_{in}: Optical power of the input pump, P_{S1}: Power from the Stokes wave of the first stage, P_{trans}: optical power of the transmitted pump, P_{S2}: optical power of the second first-order Stokes wave with mHz linewidth.

The frequency noise measurement is done by extracting this P_{S2} output. A frequency noise reduction of 40 ± 1 dB is expected from the 20-meter fiber cavity and a reduction of up to 33 ± 1 is expected from the 14-meter fiber cavity used as the second cascade. A reduction factor close to 73 dB could be expected when compared to the frequency noise of the pump laser used. The frequency noise performance of the two cascaded non-resonant *Tunics-PR* tunable laser is presented in the Figure 1.19. A noise reduction of 70 dB is observed experimentally. The cascaded *Tunics-PR* tunable laser contributes an intrinsic linewidth of 3.14 mHz. The measured integrated linewidth at 10 ms is 9.5±0.95 kHz. The grey spectrum shows the noise floor of the bench measured. Initially, at the beginning of my Ph.D. work, the noise of our bench was above the PSD of laser frequency noise signal. This bench was improved at the end of this Ph.D. work by replacing the former fiber spools by ultra-stable fiber from iXBlue. We thank Benoit Cadier (Exail formerly IxBlue). Obviously, the low

frequency noise could be reduced as presented in the section 1.4.1 for Tunics-PR and Tunics-OM tunable lasers [68].

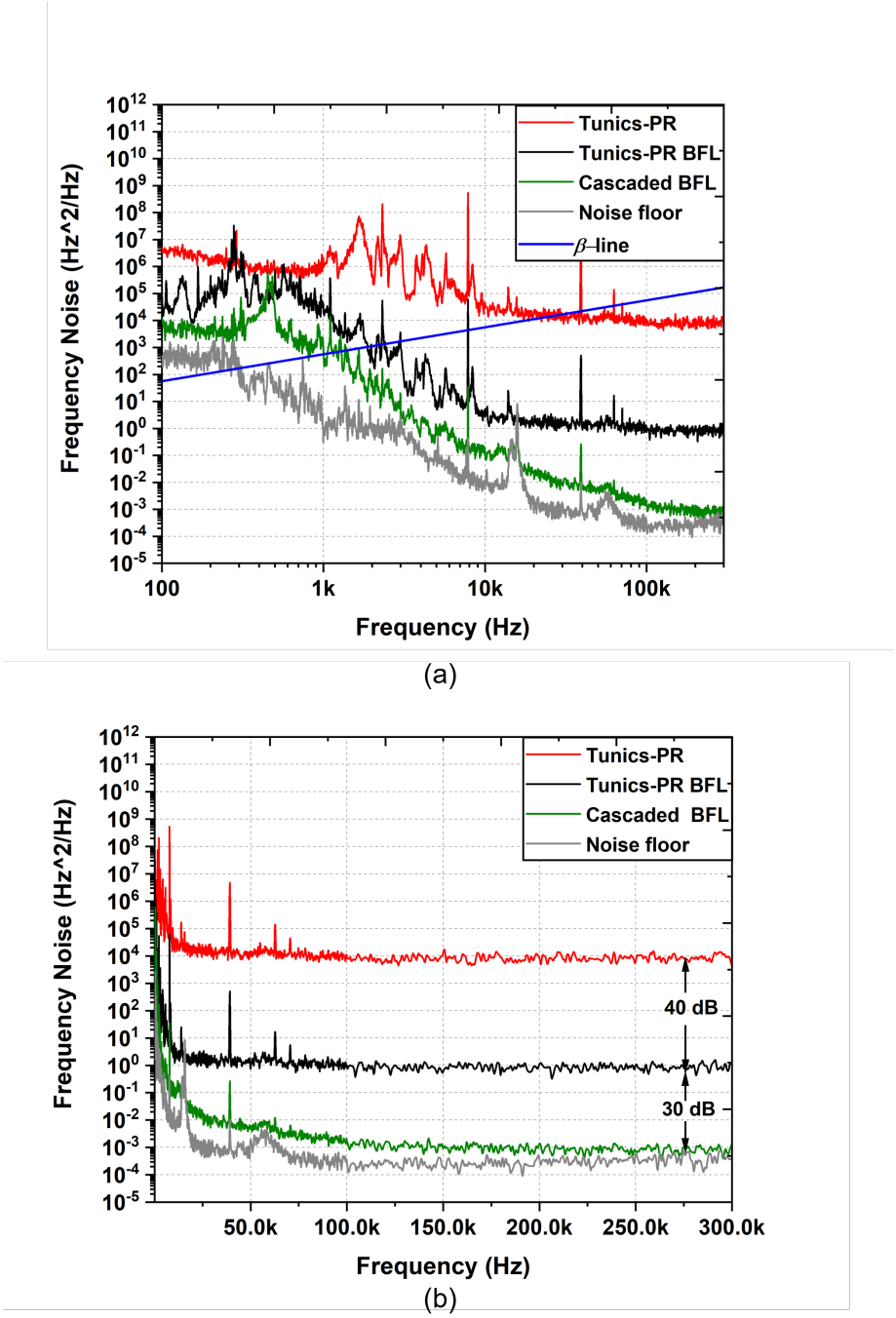

Figure 1.15: The frequency noise performance of the two cascaded non-resonant Brillouin lasers using Tunics-PR laser tunable in C-band (a) log scale (b) linear scale.

No servo loop was used to obtain Figure 1.19 . It shows clearly a 16-dB reduction of the low frequency noise of the Tunics-PR pump laser by cascading two Brillouin cavities. In other terms the Brillouin effect stabilizes laser emission. However, it should be noted if we want to reach a low frequency noise at the order of the white noise, or in other terms if we want to have fluctuations of central laser frequency of the order of the laser linewidth (3 mHz), it means a relative stability ($\Delta\nu/\nu_0$) of $1.55\text{x}10^{-17}$, which is by far under the scope of this thesis. A stabilized and ultra-coherent C-band tunable laser would require a reference signal [80-82] or for cheaper version of stabilization, a simple interferometer [68].

In the rest of the manuscript, servo-loop to reduce the low frequency noise will not be used either for the pump or the Brillouin cavity. The absence of stabilization is justified by the fact that we can clearly distinguish the different contributions in studying the coherency transfer through optical injection. It involves the study of noise transfer between the master and slave laser.

1.7 Conclusion

In this chapter, a basic introduction about sources with narrow linewidth was given. The architecture of non-resonant BFL and the associated linewidth narrowing was also discussed. The phase noise, frequency noise and β-line approximation for linewidth measurement were also explained.

Laser frequency stabilization using an unbalanced MZI and an experimental demonstration of the same was performed on *Tunics-PR* and *Tunics-OM* tunable lasers. The flicker noise of *Tunics-PR* decreased down to 4.75 ± 0.47 kHz from a free running flicker noise of 337 ± 33 kHz at 10 *ms*. The flicker noise of the stabilized *Tunics-OM* got reduced to 3.44 ± 0.34 kHz from 106.77 ± 10 kHz at 10 *ms.*

We demonstrated Brillouin laser with intrinsic linewidth of the order mHz and selectable wavelength over the C-band. We should mention that using a single-frequency DFB fiber laser (Koheras Adjustik, NKT Photonics) with an intrinsic linewidth of 100 Hz ($h_0 = 30$ Hz^2/Hz) and an integrated linewidth of 3.9 kHz ± 0.9 kHz, the frequency noise of the Brillouin laser is below the noise floor at the sub-mHz level.

CHAPTER 2. FREQUENCY LOCKING WITH ULTRA-COHERENT SOURCES

2.1 Introduction

2.1.1 A very brief description of optical injection

Optical injection is the unidirectional coupling between two lasers (named slave (the injected laser) and master laser (the external source)). A main property of optical injection is frequency locking. It consists in a technique of optical frequency and phase synchronization when an external light is seeded inside a laser cavity [83]. When the master (ν_M) and slave (ν_S) frequencies are close altogether and for an appropriate injected power (in the μW range), the slave laser synchronizes with the master laser and inherits the spectral properties of the master laser in terms of frequency and linewidth [84-88].

The locking range is defined as the values of the detuning $\Delta\nu$ ($= \nu_M - \nu_S$) for which the frequency locking exists. It has been identified since Adler and is written for semiconductor lasers [89]:

$$-\sqrt{1+\alpha_H^2}\frac{\sqrt{1+r_2^2}}{r_2}\sqrt{f_c}\sqrt{\frac{P_{Master}}{P_{Slave}}}FSR < \Delta\nu < \frac{\sqrt{1+r_2^2}}{r_2}\sqrt{f_c}\sqrt{\frac{P_{Master}}{P_{Slave}}}FSR \qquad 2.1$$

FSR stands for Free Spectral Range; it is the inverse of the roundtrip time of light (energy) τ_{cav} inside the cavity; its value is easily defined for a Fabry Perot cavity of length L and group-index n_g by $\tau_{cav} = \frac{2n_gL}{c}$. The locking range is proportional to the FSR and the square

root of the injected power P_{Master}. More precisely, it is proportional to the ratio of the injected power P_{Master} over the injected Slave optical power P_{Slave}. Note that the properties of optical injection may be strongly dependent on the injected Slave optical power, which can be varied through the slave-laser pumping-rate. Thus, as the properties of the optically injected laser may be very different for the same r_p $\left(=\frac{P_{Slave}}{P_{Master}}\right)$, it is better to have the knowledge of both P_{Slave} and P_{Master}. It is why we will not use r_P in this manuscript.

The precise injected power should consider the transmission $\sqrt{1+r_2^2}$ through the coupling face of the laser cavity and a coupling factor f_c that includes different losses (coupling optics, optical isolator...) or unwanted or desired attenuation. The division by r_2 is due to a normalization, linked to the expression of the differential equation (Annex.1). α_H is the amplitude-phase coupling parameter [90]. It creates a dissymmetry in the response of the injected laser with respect to the sign of the detuning [91]. The term $\sqrt{1+\alpha_H^2}$ is coming from the standard linear analysis in order to obtain the stationary phase (or frequency of the injected slave laser) [92].

In fact, the analysis is more complex as two stationary phase (or frequency) solutions are co-existing [89] for the same injected-slave optical power (or photon number). One is stable, the other one unstable. Figure 2.1 from [89] shows the areas of locking regime in the phase space [frequency detuning - injection ratio]. The solid curves show the boundaries between optical injection locking and non-locking regions. Within the region of optical injection locking, stable and unstable locking areas exist, and the dotted line gives their boundary. Various dynamics such as wave-mixing, chaotic oscillations, period doubling may take place in the non-locking region [93-95].

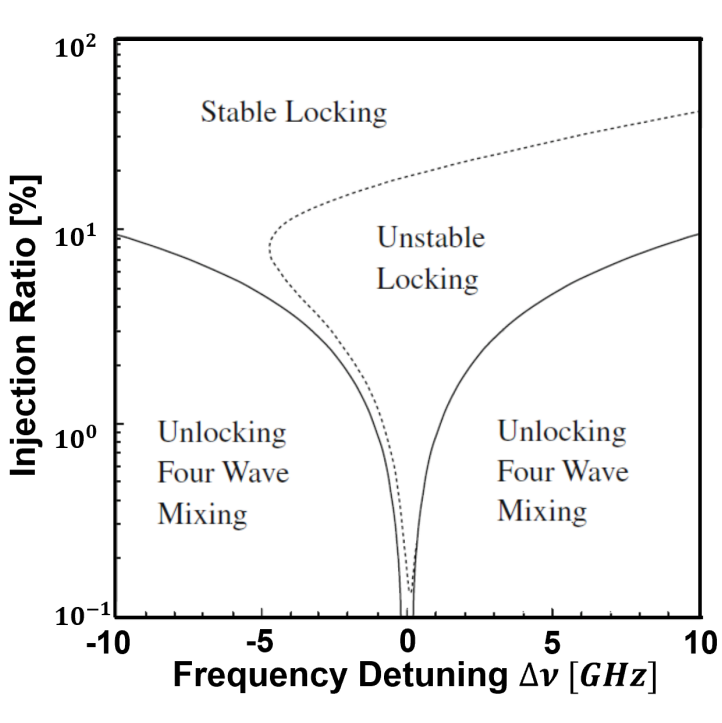

Figure 2. 1: Locking and unlocking regions in phase space of frequency detuning and injection field from (Ohtsubo [89]).

An analysis in terms of bifurcation reveals a more complex dynamic [95-97]. The experimental results [98] are in good agreement with simulations [93,94]. Figure 2. 2 shows a comparison between experiment and theory from [94]. Among the knowledge brought from the dynamics of optically injected lasers, there is a different behavior when crossing the boundary locking-unlocking or unlocking-locking. At negative detuning, the transition from locking to unlocking is abrupt. It is due to saddle-node bifurcation. While at positive detuning, there is a smooth transition from wave mixing operation to frequency locking.

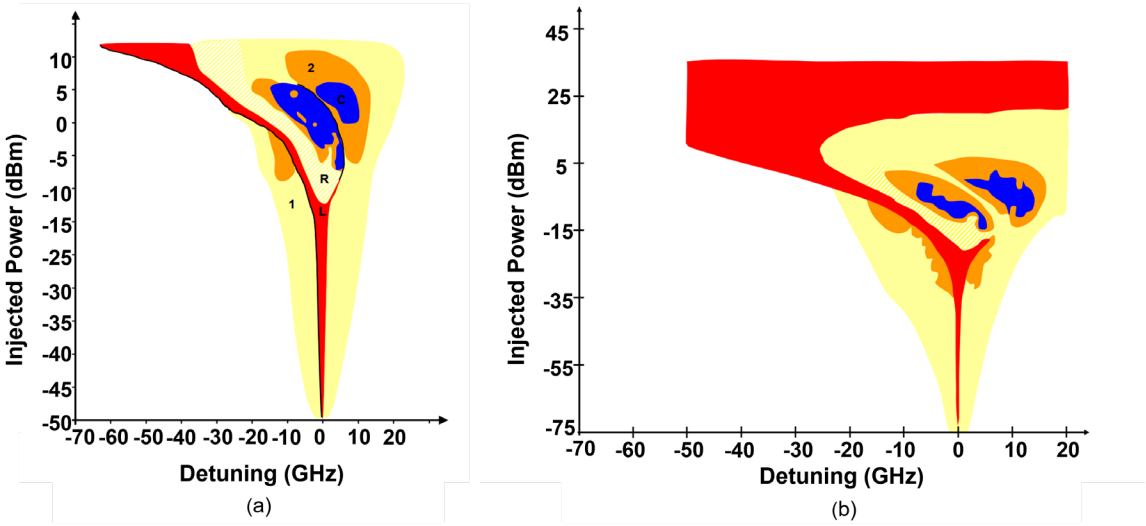

Figure 2. 2: (a)The experimental and (b) numerical simulation of an injected slave laser. The *x*-axis represents the detuning between the master and slave laser and *y*-axis represents the injected power. 'L' represents the locking region, '1' stands for single wave mixing, '2' for period-doubling wave mixing, '4' is period-doubling quadrupling wave mixing, 'C' and 'R' represents chaos and undamped relaxation oscillation.

It is due to a hopf bifurcation. When the detuning is decreased from positive values, the slave component and, if any, other frequencies, which originate from wave mixing, decrease continuously so that the injected (and amplified) master line remains the unique frequency of the injected slave laser, which finally corresponds to the frequency locking.

2.1.2 Short review of optical injection using semiconductor lasers

Huygens made the first observation of injection locking in 1665. As it was mentioned in the introduction, he noticed that his bedroom clock synchronized to another one. He concluded that weak vibrations transmitted was sufficient to lock the frequency of one

pendulum onto the other one [99]. Vincent *et al.* first reported the evolution of injection locking of electronic oscillators in 1919 [100], where an electronic oscillator was disturbed and synchronized to a weak oscillator input connected to a feedback circuit. Alder *et al.* described, in 1946, the dynamics of injection locking for oscillators [101]. Paciorek *et al.* extended the theory considering strong signal injection [102]. Since the invention of lasers by Mainman [103] in 1960, Stover and Steier optically injected the signal from a gas laser into another laser via an optical isolator in 1966 [104]. Kobayashi and Kimura reported the first optical injection experiment using semiconductor lasers in 1980[105]. In 1982, Lang modified the classical theory and added the linewidth enhancement factor into the optical injection locking laser rate equation[106]. In 1985, Mogensen *et al.* presented a thorough theoretical and experimental investigation of locking conditions and stability properties for a semiconductor laser with external light injection[92]. Petitbon *et al.* performed a detailed study of locking bandwidth and position in 1988 [107]. The development of semiconductor lasers motivated the researchers to explore the applications of optical injection locking in optical communications [108]. In 1990s, the researchers made efforts in advancing the theory and applications like the research on strong optical injection locking [109] and demonstration of optical injection phase lock loops [110]. Due to the increasing demand of high bandwidth lasers for radio frequency and high-speed telecommunication applications, more than 10 times bandwidth enhancement was demonstrated using strong optical injection locking to standard DFB lasers and VCSELs [111-113]. Optical injection locking can isolate and amplify single frequency tone signal for application in DWDM optical communication. It provides high gain filtering and low noise. When the slave laser is injection locked to a selected channel, it amplifies the selected channel within its locking

range and attenuates signals out of the range [114,115]. Optical injection locking is an ideal amplifier of signal carrying a precise and specific frequency. It provides a very high amplification and can be designed to amplify signals within a limited locking range [116]. Kim *et al.* in 2016 showed that optical injection can be used for wavelength conversion of a CW laser that carries information about precise frequency [117]. Optical injection locking was exploited to recover optical carriers in optical domain to enable low complexity and low latency homodyne coherent communications [118,119]. It can be used to isolate and manipulate individual comb tones for arbitrary waveform generation [120], sensing and terahertz signal generation [121]. In 2013, Schneider *et al.* presented radiofrequency signal-generation system with over seven octaves of continuous tuning using optical injection [122].

One topic of research at Institut Foton is optical injection for over 25 years. Several Ph.D. students from Institut Foton have worked on optical injection [86,87,93,123-126]. Annex.2 gives a short summary of these works. The main properties that I will use will be detailed in the next sections of this manuscript.

In this chapter, we will first begin by giving a general idea about the properties of optical injection. The next section will focus on theoretical study about the transfer function of a laser and transfer function of an injected laser. The experimental setup of optical injection will be presented in the subsequent section. The main focus of this chapter is to study the role of the master-laser coherence in triggering the optical-injection locking when the injected power is varied. The homemade *Tunics-OM BFL* laser with selectable wevelength in the C-band will be used as one among different master lasers for this study. Master lasers

of different coherencies like *Tunics-PR*, *Tunics-OM* and *Agilent* tunable lasers will also be used for this experiment.

2.2 General properties of optical injection

To sketch optical injection, the photons of master laser are seeded inside the cavity of a slave laser. An optical circulator or isolator ensures the unidirectionality to avoid any disturbance of the master laser by the optical field of the slave laser as shown in the Figure 2. 3. When the frequencies of both the master and slave lasers are close together and for an appropriate injected power, optical injection allows the transfer of the spectral properties of the master laser to the slave laser.

Figure 2. 3: The principle of optical injection.

The slave laser is said to be locked when all the spectral properties are transferred to the slave laser. Hence, the slave laser is synchronized to the master laser. In this condition, the slave laser operates at it's own power whereas the spectral properties (frequency, linewidth, intensity noise) are given by the master laser [84]. The master lasers have generally a

narrower linewidth than the slave laser, but have less output power than the slave laser. Using the technique of optical injection, narrow linewidth lasers with high output powers can be developed. The parameters affecting optical injection are, the power (P_{inj}) injected by the master laser inside the cavity of the slave laser, the detuning ($\Delta\nu = \nu_m - \nu_s$) between the optical frequencies of the master (ν_m) and the slave (ν_s) lasers and the pumping rate $\left(r = \frac{I}{I_{th}}\right)$. The pumping rate is the ratio of the pump current (I) of the slave laser and the laser-threshold current (I_{th}). The injected slave may exhibit different behaviors like frequency locking, wave mixing, relaxation, excitability, period doubling and chaos when the control parameters are varied. The different regimes observed are mapped onto a chart, whose axes are the injected power and the detuning [127,128]. Under frequency-locking conditions, slave laser has the same linewidth as that of master laser. If the master line is thiner than that of the free slave, frequency locking is known as spectral 'purity' transfer; spectral 'impurity' transfer corresponds to a master line larger than that of the free-slave laser [129].

2.3 Spectral properties of an injected laser

In this section, I will introduce the theoretical tools that I will use to explain the observations that have been done in this thesis. I will use a transfer function that was introduced by G.M Stéphan in 1998 [85]. The transmission function or transfer function is an Airy function for a cold cavity. A laser consists of a source of photons, a cavity and an amplifying medium. The source of photons is provided by spontaneous emission. It is required to have photons to amplify by an amplifying medium through stimulated emission.

The cavity is the resonator. Its transfer function can thus be generalized when it is filled by an amplifying medium (or in other words, when considering gain). The slave laser is then considered as a narrow band amplifier of noise. In [85], this generalized transfer function describes how a master laser imposes its spectral properties to a slave laser.

2.3.1 Objectives

The last chapter focused on the realization of a tunable laser with an integrated linewidth below 10 kHz. The main objective was to develop a homemade narrow-linewidth tunable source whose linewidth is controllable. The interest in such highly coherent sources is described in the following. If the synchronization of oscillators [101,130,131] and transfer of purity is known for decades [132], the native properties of optical injection locking, using a highly coherent source, have not been explored so far [116], mainly because of the difficulty to make the laser linewidth an easily controllable parameter. The main idea in this chapter is to study the possibility to distribute the coherency to other lasers using highly coherent lasers with an order of kHz integrated linewidth and Hz intrinsic linewidth. In order to study the influence of optical coherency on the transfer of purity when using optical injection, frequency noise measurement of the optically injected laser with tunable lasers having different linewidths will be analyzed in this chapter.

2.3.2 The transfer function generalized to a laser.

The transfer function (generalized Airy function) used in this chapter corresponds to that presented in optics in context of multiple-waves interferences [133]. We consider a Fabry-

Perot interferometer with two plane mirrors of reflectivity R, separated by a medium of index *n* and length *d.* It is then illuminated at normal incidence by a beam of intensity I_0. The transmitted intensity *I* is a function of λ and it is expressed under Airy function as [134]:

$$I(\lambda) = I_0 \frac{1}{1 + \frac{4R}{(1-R)^2} \sin^2\left(\frac{2\pi nd}{\lambda}\right)} \qquad 2.2$$

2.3.3 The Airy function of a passive cavity

The schematic diagram of a passive cavity subjected to an external signal is shown in the Figure 2. 4. The passive Fabry-Perot cavity consists of two plane mirrors M_1 and M_2 separated by a passive medium of refractive index *n* and length *d.* The complex reflectivity of mirror M_1 is r_1 and M_2 is r_2.

The complex transmission is denoted by t_1 and t_2. The internal response of this cavity to a continuous external monochromatic exciting field arriving on the cavity at normal incidence will be discussed here. The transverse profile of the incoming field will not be considered here. The plane waves inside the interferometer are therefore considered.

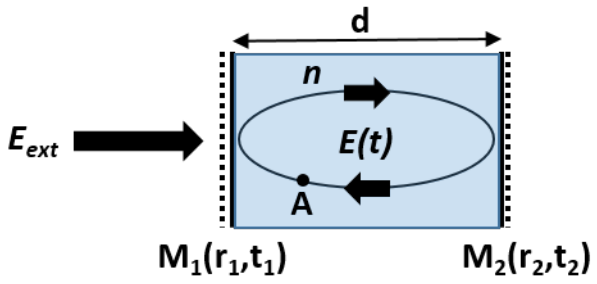

Figure 2. 4: The schematic diagram of a passive Fabry-Perot cavity.

The external electrical field E_{ext} is expressed in the time domain as:

$$E_{ext}(t) = E_{ext}e^{i\omega t} \qquad 2.3$$

We will call I'_{ext} $|E_{ext}|^2$, which is proportional to the optical intensity associated to the external field through the Poynting theorem[2]. Here, we are interested in the internal response of the cavity by observing the complex field *E* at point A of the cavity. We study the stationary solution of this system, such that the amplitude of the field at point A is invariant after one round trip inside the cavity. By introducing its duration $\tau_{AR} = \frac{2nd}{c}$ and its corresponding phase shift $\Phi = \omega\tau_{AR} = 2\pi\nu\tau_{AR}$, this field becomes:

$$E(t + \tau_{AR}) = E(t) \qquad 2.4$$

$$E(t + \tau_{AR}) = r_1 r_2 e^{i\omega\tau_{AR}} E(t) + t_1 E_{ext} \qquad 2.5$$

From the equations 2.4 and 2.5, the stationary internal field is given by:

[2] The optical intensity (W/m²) is related to E: $I = 2nc\varepsilon_0|E|^2 = 2nc\varepsilon_0 I'$[135].

$$E = \frac{t_1 E_{ext}}{1 - r_1 r_2 e^{i\omega\tau_{AR}}} \qquad 2.6$$

By multiplying the equation 2.6 by its complex conjugate, we get I, which results of the multiplication of I_{ext} by the well-known Airy function of the Fabry-Perot interferometer:

$$I = \frac{T_1}{(1 - r_1 r_2)^2 + 4 r_1 r_2 \sin^2\left(\frac{\Phi}{2}\right)} I_{ext} = T(\Phi) I_{ext} \qquad 2.7$$

Where,$\Phi = \frac{4\pi\nu n d}{c}$ is the phase accumulated by the wave propagating during one round trip. T_1 represents the intensity transmission of mirror M_1. At normal incidence, T_1 is given by the product of t_1 and its complex conjugate t_1^*. I is the optical intensity inside the cavity as the equation 2.7 relates the transfer function T (Φ) to the ratio of the output I and input (I_{ext}) intensities:

$$T(\Phi) = \frac{I'}{I'_{ext}} = \frac{I}{I_{ext}} \qquad 2.8$$

2.3.4 The Airy function of an active cavity

The generalized Airy function of the laser will be obtained from the transfer function of a passive cavity. Spontaneous emission is now the internal excitation field, which comes from the response of medium to an external pumping. The gain of the active medium should be considered from now. The useful quantities for the description of the generalized Airy function of a single frequency laser with central frequency ν_0 are normalized frequency x,

power spectral density *y,* normalized power *Y,* saturated gain g, spontaneous emission *S* and losses *L*.

The normalized frequency *x* relative to the FSR of an empty cavity is defined as:

$$x = \frac{2\pi\nu d}{c} \qquad 2.9$$

The total power *Y*, inside the cavity, is the power normalized by the saturation power. Y is the sum of power spectral densities over all the normalized frequencies given by:

$$Y = \int_{-\infty}^{+\infty} y(x)dx \qquad 2.10$$

As y and Y are normalized quantities, they are proportional to both optical power and optical intensity.

The concept of saturated gain *g* is introduced for this active medium. It is expressed in an exponential form e^g, so that the cumulative gain over a round trip in the cavity applies to a complex field by multiplying its associated optical intensity by the term e^g. The saturation of gain is expressed by the equation:

$$g = \frac{g_0}{1+Y} \qquad 2.11$$

The maximum gain available is the linear gain g_0 (given in m^{-1} if it is not normalized). The saturated gain *g* decreases when the normalized power *Y* increases in the cavity. *S* is a

normalized spontaneous emission power contained in the laser-operating spectral band. A saturated expression of spontaneous emission *S* is also introduced.

$$S = \frac{S_0}{1+Y} \qquad 2.12$$

The loss term L considers the losses at the mirrors as well as the losses accumulated during the propagation in the medium. It is also expressed in an exponential form e^{-L} as the gain[3]. The cumulative losses over a round trip in the cavity apply to a complex field by multiplying its amplitude by the term e^{-L}. g (G), L, S is all dependent on the frequency x. From the equation 2.7 and other definitions discussed in this section, the Airy function of laser can be expressed as:

$$y = \frac{S}{(1-e^{-L+g})^2 + 4e^{-L+g}\sin^2\left(\frac{\Phi}{2}\right)} = T(\Phi)S \qquad 2.13$$

This expression of the laser Airy function takes into account three fundamental ingredients of a laser, namely the internal source **S** (translated by spontaneous emission, which provides the first photons to start the lasing process), the amplifying medium (by the gain **g**, due to the stimulated emission) and the resonance effect of the cavity translated by the structure of the Airy function T (Φ) (equation 2.7 , 2.13). The internal Source S is transformed by a simple multiplication by the transfer function (equation 2.13 $T(\Phi)S$) to

[3] If α_a are the linear residual losses for the intensity, which are added to the losses due to the atomic transition, by introducing the total losses α_T and the longitudinally spatially-distributed mirror-losses α_M, the expression e^{-L} may be written: $e^{-L} = e^{-\frac{\alpha_T}{2}2d} = r_1 r_2 e^{-\frac{\alpha_a}{2}2d}$, which implies: $\alpha_T = (\alpha_a + \alpha_M) = \left(\alpha_a - \frac{1}{2d}\ln(R_1R_2)\right)$. The photon lifetime in the cavity is then: $\frac{1}{\tau_p} = \mathrm{v}_g\alpha_T = \mathrm{v}_g(\alpha_a + \alpha_M) = \mathrm{v}_g\left(\alpha_a - \frac{1}{2d}\ln(R_1R_2)\right)$.

give the power spectral density of the laser. Bondiou *et al.* studied this function starting from Maxwell's equations [129].

The cumulative phase for a round trip of the field inside the cavity is $\Phi = \frac{4\pi\nu nd}{c}$. It depends on the refractive index n of the medium, which can be frequency dependent and saturated:

$$n(\nu) = n_0(\nu) + \frac{n_1}{1+Y} \tag{2.14}$$

The cumulative phase $\Phi = 2\pi$ at resonance frequency ν_0. For any frequency ν,

$$\Phi(\nu) = 2\pi\nu\frac{2n(\nu)d}{c} - 2\pi\,\nu_0\frac{2n(\,\nu_0)d}{c} \tag{2.15}$$

Upon performing the first-order expansion of refractive index around the central frequency ν_0,

$$n(\nu) = n(\,\nu_0) + n(\nu - \,\nu_0)\frac{\partial n(\nu)}{\partial \nu}|\,\nu_0 \tag{2.16}$$

Equation 2.15 can be written as:

$$\Phi(\nu) = \frac{4\pi d n_g}{c}(\nu - \,\nu_0) \tag{2.17}$$

By expressing the cumulative phase as a function of normalized frequency and by introducing a characteristic quantity of amplifying medium *A* defined as:

$$A = 2n_g \tag{2.18}$$

The expression for cumulative phase over a round trip is written as:

$$\Phi(x) = A(x - x_0) \qquad 2.19$$

By inserting this condensed form of the cumulative phase into the expression for the Airy function given by equation 2.13, the generalized equation for the Airy function for a laser can be expressed as follows:

$$y(x) = \frac{S}{(1 - e^{-L+g})^2 + 4e^{-L+g} \sin^2\left(\frac{A(x - x_0)}{2}\right)} = T(x)S \qquad 2.20$$

Equation 2.20 is complex as y(x) is function of its own integral.

2.3.5 Calculation of the total intensity Y and of the laser linewidth

The Airy function of the laser allows calculating the normalized intensity (or power) Y and the laser linewidth. This last quantity is the frequency-band, over which the laser emits. When the linear gain per round trip is greater than the losses, i.e., $g_0 > L$ ($g = L$ defines threshold). The linewidth of the laser emission is smaller than the width of the emission. The spectral density y is only significative in a narrow spectral band around the resonance frequency x_0 ($\propto \nu_0$). In this small spectral range, a good approximation leaves the quantities gain g, spontaneous source S and dispersion of medium A, independent of frequency x. These quantities will be written for $\nu = \nu_0$ or $x = x_0$. Considering that, the difference $(x - x_0)$ remains, near a mode at x_0, very small in front of 1 (which corresponds to FSR for ν) so that the sine function can be expanded to the first order along $(x - x_0)$.

The equation 2.20 becomes a Lorentzian function (knowing that A, g, S, L are independent of the frequency):

$$y(x) = \frac{S}{(1 - e^{-L+g})^2 + e^{-L+g}A^2(x - x_0)^2} = \frac{S}{e^{-L+g}A^2} \frac{1}{\mathbb{\Gamma}^2(x - x_0)^2} \quad 2.21$$

For this Lorentzian function, the half width at half-maximum $\mathbb{\Gamma}$ is given by:

$$\mathbb{\Gamma} = \frac{1 - e^{-L+g}}{Ae^{\frac{-L+g}{2}}} = \frac{2}{A} sinh \frac{L - g}{2} \quad 2.22$$

Integrating the equation for *y* given by equation 2.21 over the frequency, we get the total intensity, *Y:*

$$Y = \int y dx = \frac{S}{e^{-L+G}A^2} \frac{\pi}{\mathbb{\Gamma}} \quad 2.23$$

The quantities *S, G* and *A* depend on *Y.* Hence, *Y* appears as a solution of the implicit equation 2.23 as $\mathbb{\Gamma}$, A, G, S are dependent on Y (equations 2.11, 2.12, 2.14).

Above the threshold, we know an approximate solution of *Y* called the Lamb's solution denoted by Y_L resulting from the condition gain = losses (at the laser threshold, the number of photons generated by the optical amplification exactly compensates the number of photons lost by absorption and by the mirrors).

$$g = L \quad 2.24$$

$$\frac{g_0}{1+Y} = L \tag{2.25}$$

$$Y_L = r - 1 \tag{2.26}$$

Where, $r = \frac{g_0}{L}$ is the normalized gain at threshold also known as the pump parameter. We then set $Y = Y_L + \delta Y$ and call δY the deviation from Lamb's solution.

In equation 2.21, at resonance when $x = x_0$ i.e.,$\nu = \nu_0$, the denominator vanishes if $g = L$, which is practically not acceptable because the power spectral density *y* should remain finite. Hence, it is essential to keep a distance to Lamb's solution($\delta Y \neq 0$), to keep $G \neq L$. The approximation $Y = Y_L$ in *S* and *A* will turn out to be acceptable without any first order consequence on the value of *y*.

Using the expression of $\mathbb{\Gamma}$ from equation 2.22, the equation 2.23 becomes:

$$Y = \frac{\pi S}{A} \frac{1}{\left[e^{\frac{(-L+g)}{2}} - e^{3\frac{(-L+g)}{2}}\right]} \tag{2.27}$$

The argument from the exponential function can be developed as:

$$-L + \frac{g_0}{1+Y_L+\delta Y} = -L + \frac{g_0}{1+Y_L}\left(1 + \frac{\delta Y}{(1+Y_L)}\right)^{-1} \tag{2.28}$$

$$\approx -L + \frac{g_0}{1+Y_L} - \frac{g_0 \delta Y}{(1+Y_L)^2} \tag{2.29}$$

Where $-L + \frac{g_0}{1+Y_L} = 0$.

Upon substituting this value of exponential function, we can deduce the expression for deviation from Lamb's solution:

$$\delta Y = \frac{\pi S(1+Y_L)^2}{A g_0 Y_L} \qquad 2.30$$

We reintroduce Lamb's solution ($\delta Y = 0$) by cancelling *S*. It would ignore the spontaneous emission and the role it plays in the description of the field of laser line.

On substituting equation 2.30 in equation 2.22 and using the approximation:

$$L - G \approx \frac{g_0 \delta Y}{(1+Y_L)^2} \qquad 2.31$$

$$2\mathbb{\Gamma} = \frac{2}{A} sinh\left[\frac{g_0 \delta Y}{2(1+Y_L)^2}\right] = \frac{2}{A} sinh \frac{\pi S}{4AY_L} \approx 2\frac{\pi S}{A^2 Y_L} \qquad 2.32$$

Hence, the FWHM of the laser is given by:

$$2\mathbb{\Gamma} = \frac{2\pi S}{A^2 Y_L} \qquad 2.33$$

From equation 2.33, we can say that the linewidth of the laser is inversely proportional to the intensity of laser, proportional to the spontaneous emission, depends on the amplifying medium via the term A (i.e., the group index, $A = 2[n(\nu_0 + (\nu - \nu_0)\frac{dn}{d\nu})]$) and is proportional to the losses. This law was established by Schawlow-Townes [59].

2.4 The Airy function of an injected laser

The application of the generalized Airy function to the case of optical injection is detailed in this section. We will consider two lasers: the master laser and the slave laser. With respect to the slave laser, the master laser is another source term, which is added to the spontaneous emission of the slave laser. Its structure is identical to that of the free slave laser. We will write the normalized power spectral densities of master and slave lasers, y_M and y_S respectively. We also introduce a coefficient that indicates the fraction of master power seeded inside the slave cavity. We can therefore write the set of two equations for the master and the free-slave lasers as:

$$y_M(x) = \frac{S_M(x)}{(1 - e^{-L_M+G_M})^2 + 4e^{-L_M+G_M}\sin^2(A_M(x - x_M)/2)} \qquad 2.\ 34$$

$$y_S(x) = \frac{S_S(x)}{(1 - e^{-L_S+G_S})^2 + 4e^{-L_S+G_S}\sin^2(A_S(x - x_S)/2)} \qquad 2.\ 35$$

We will consider optical injection at zero detuning in a first approximation. With this last assumption, the master and slave frequencies are equal ($x_M = x_S = x_0$). We also assume that the terms *S, A* and *G* are independent of the frequency as the emission bandwidth is very narrow. It follows the simplified expressions, in which the optical injection is considered by the term containing η (the external PSD y_M is simply added to the slave spontaneous source S_S):

$$y_M(x) = \frac{S_M}{A_M^2 e^{-L_M+G_M}} \frac{1}{\mathbb{\Gamma}_M^2 + (x - x_0)^2} \qquad 2.\ 36$$

$$y_{IS}(x) = \frac{S_S + \eta y_M(x)}{A_S^2 e^{-L_S+G_S}} \frac{1}{\mathbb{\Gamma}_S^2 + (x - x_0)^2} \quad 2.37$$

$$y_{IS}(x) = \frac{S_S}{A_S^2 e^{-L_S+G_S}} \frac{1}{\mathbb{\Gamma}_S^2 + (x - x_0)^2} \quad 2.38$$

$$+ \frac{1}{A_S^2 e^{-L_S+G_S}} \frac{\eta S_M}{A_M^2 e^{-L_M+G_M}} \frac{1}{\mathbb{\Gamma}_S^2 + (x - x_0)^2} \frac{1}{\mathbb{\Gamma}_M^2 + (x - x_0)^2}$$

By integrating equation 2.38 on the normalized frequencies, we get the total intensity Y_{IS}:

$$Y_{IS} = \frac{S_S}{A_S^2 e^{-L_S+G_S}} \frac{\pi}{\mathbb{\Gamma}_S} + \frac{1}{A_S^2 e^{-L_S+G_S}} \frac{\eta S_M}{A_M^2 e^{-L_M+G_M}} \left[\frac{\pi}{\mathbb{\Gamma}_S \mathbb{\Gamma}_M (\mathbb{\Gamma}_S + \mathbb{\Gamma}_M)} \right] \quad 2.39$$

$$Y_{IS} = \frac{1}{A_S^2 e^{-L_S+G_S}} \frac{1}{\mathbb{\Gamma}_S} \left[\pi S_S + \frac{\eta Y_M}{\mathbb{\Gamma}_S + \mathbb{\Gamma}_M} \right] \quad 2.40$$

The numerical solution of equation 2.40 helps us to determine the saturation intensity of the injected slave Y_{IS} , as well as the PSD y_S of the injected slave. Finally, the spectral linewidth of the injected laser may be deduced, and the injected slave PSD can be plotted for different values of the injection rate η. The evolution of PSD of injected slave with respect to injected power is shown in Figure 2. 5. It turns out that three regimes can be identified:

- The first one corresponds to the fact that injected power is so low (~ 100 pW) that the master laser has no influence on the slave laser line. Nevertheless, the amplified external photons can be identified in a sea of photons [116].

- The second one is an amplifying regime, in which the slave laser behaves as an optical amplifier for the master. It was the first demonstration of the use of a laser an optical amplifier [116].
- The third regime corresponds to the optical injection regime for which a threshold has been reached. Above this threshold, the slave line is the one of the master and a saturation process occurs: any increase of the injected optical power will not be amplified and will be simply added. It defines a threshold for frequency locking.

In this section, we have shown from the generalized transfer function that the influence of optical injection is a modification of the noise source of the transfer function (see equations 2.20, 2.21 and 2.38). The input noise source is the addition of two contributions: the internal field (spontaneous photons from the amplifying medium) and the external field (injected photons from the master laser). They compete for the start-up of the laser [86,123,136].

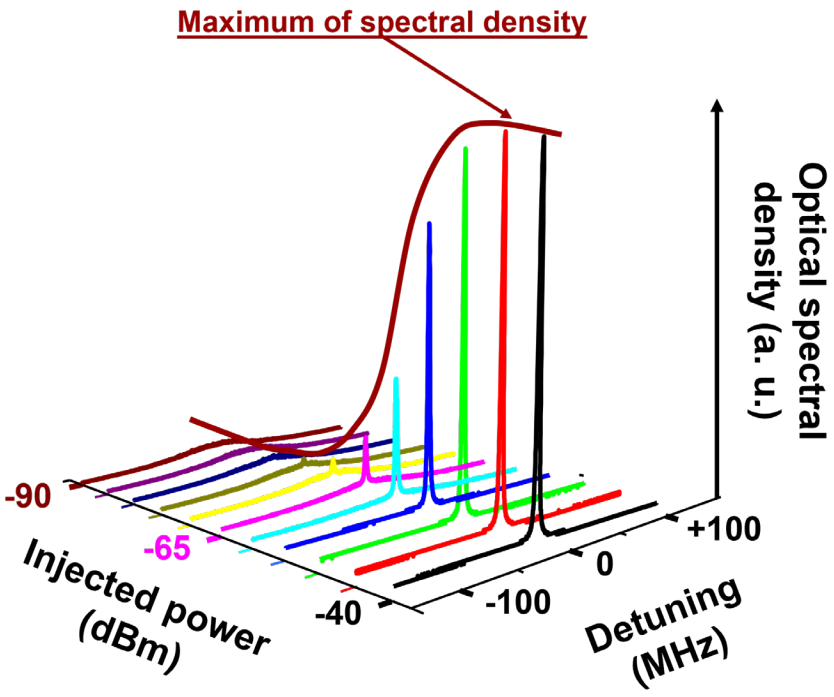

Figure 2. 5: The evolution of PSD of injected slave with respect to injected power measured using a Fabry-Perot interferometer by S. Blin [128].

The analysis of optical injection is commonly done from the optical spectra, the temporal behavior or the relative intensity noise of the injected laser.

In the next section, we will study optical injection by using the frequency noise PSD, which in our case, seems to be to us, the right characterization to compare the influence of an external source to that of the internal spontaneous source.

2.5 Experimental setup of optical injection

We will discuss the experimental setup of optical injection in this section. Optical injection is a unidirectional coupling between a slave laser and a master laser. When the frequencies of both the master and slave laser are closer and for an appropriate injected power, the master laser transfers its spectral properties to the slave laser.

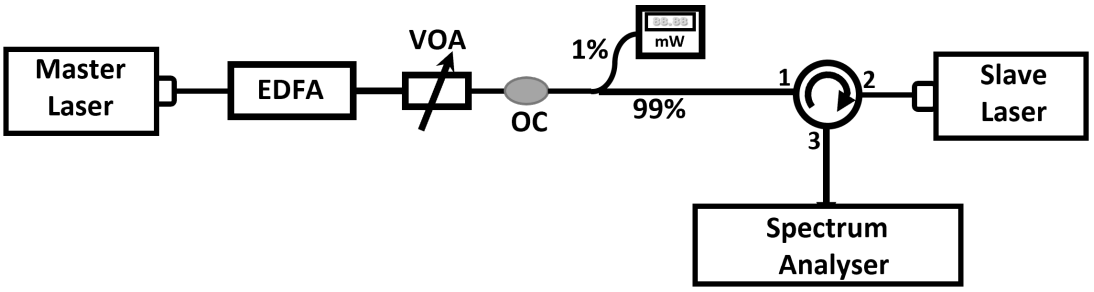

Figure 2. 6: Experimental setup of optical injection. EDFA: Erbium-doped fiber amplifier, VOA: Variable optical attenuator, OC: Optical coupler, CIR: Optical circulator, OI: Optical isolator.

The experimental setup of optical injection is shown in the Figure 2. 6. Several master lasers are used with different linewidths, which is the core parameter that we want to vary. In order to work at zero detuning, the master laser should be tunable (or at least the wavelength should be selectable). The master lasers used are commercially available tunable sources (*Tunics-PR*[4], *Tunic-OM*, *Agilent)* and a Brillouin fiber laser (BFL) using as pump a tunable laser (*Tunics-OM)* that we will call *Tunics-OM BFL*. The different master intrinsic-linewidths are 30 kHz (*Tunics-PR*), 3 kHz (*Tunic-OM*, *Agilent*), 1 Hz (*Tunics-OM BFL*).

[4] Tunics™ are tunable sources from the company Photonetics, which has been bought by YENISTA, recently bought by EXFO.

In a first attempt, we used single frequency lasers from Eblana™ (EP1550-DM-B) with no integrated optical isolator at a wavelength of 1550 nm. Eblana's Discrete-Mode (DM) technology platform enables DFB-like performance. However, the best performances are obtained at a given bias current and temperature. As the wavelength of a semiconductor laser is temperature dependent (- 3 GHz/°C) and bias-current dependent (3 GHz/mA), it is more convenient to slightly tune the temperature and the bias current to reach the null detuning while the master wavelength is roughly adjusted (usually with 1 pm (125 MHz) resolution). As a matter of fact, the operating point was usually such that longitudinally mode hoping could occur so that we prefer not to use these lasers. In a second attempt, DFB lasers at 1550.12 nm specified to be with no isolators from Fujitsu™ (FRL15DCWx-A8) were used. They proved to be fragile and broke easily. For both lasers (Eblana and Fujitsu), we asked for the absence of optical isolator contrary to the commercial product; it was a specific demand. Finally, we choose bulk DFB lasers from Alcatel Optronics™ (A 1954 LC; double heterojunction and buried ribbon). These sources are packaged in a butterfly box containing a temperature sensor and a Peltier element for external temperature control, a photodiode for power output calibration and an optical isolator integrated into a recovery optic for injecting the useful signal into a single-mode optical fiber. This slave laser has an inbuilt optical isolator inside, which is not a problem as we want to study optical injection for small injected power. We have used an *Alcatel* semiconductor laser polarized at 1.1 times its threshold as the slave laser. It is optically isolated by 35 dB (value that we measured). This isolation is not a problem, as we want to look at the influence of optical injection with low injected power. The wavelength of such laser is in the C-band. The *Alcatel* slave laser is operated at 19.8 mA, 1.1 times its threshold.

For all the lasers studied, the threshold current varies between 9 mA and 25 mA, and the efficiency between 1 µW/mA and 6 µW/mA. The maximum powers obtained are of the order of 3 mW, typical SMR are above 10 dB at 1.1 threshold and above 40 dB at 4 times threshold. The relaxation frequency is around 1 GHz at 1.1 threshold and around 7 GHz at 4 times threshold. The optical frequency drift due to bias current is typically -1 GHz/mA. Similarly, the wavelength drift of our diodes with temperature is of the order of +5 GHz/K. These two values give a great flexibility to tune the slave wavelength. In the following, the results are given for a laser emitting at 1556 nm that has an integrated linewidth of 39.8±3.9 MHz and an intrinsic linewidth of 32.73 MHz ($h_0 = 1.04 \times 10^7 Hz^2/Hz$). Note that the intrinsic and integrated linewidth could be modified by the standard driver. Thus, old version of drivers from ILX Lightwave™ (LDC3900) could give typical values of 1 MHz for the linewidth while using low noise laser driver (like Koheron™ CTL101-1-B-100) will give typical values of 0.4 MHz.

The output of the master laser is amplified using an erbium-doped fiber amplifier from Lumibird. This amplified master-laser output is then controlled using a variable optical attenuator. A 99/1 % coupler is used to monitor the power injected inside the slave-laser cavity. The master laser output is injected inside the slave laser cavity via port 1 to port 2 of an optical circulator. The optical circulator protects the master laser setup from back reflected signals (note that used extended-cavity tunable sources have already an optical isolator). The optically injected slave-laser signal is collected outside port 3 of the optical circulator. This signal is then characterized using an optical spectrum analyzer or the frequency-noise bench that has been described in chapter 1. The optical spectrum analyzer gives good indications of the optical-injection regime [93]. The optical spectral of the

injected slave may observed using an optical spectrum analyzer (a Brillouin optical spectrum with 10 MHz resolution, BOSA from Aragon photonics^{TM}) or a Fabry-Perot spectrum analyzer (3 MHz resolution). The different regimes of optical injection could be thus identified by varying the control parameters.

The control parameters in an optical injection experiment are the injected power P_{inj} and the detuning $\Delta\nu = \nu_m - \nu_s$ between the optical frequencies of master (ν_m) and slave (ν_s) lasers. The pump rate r of the slave laser is fixed during experiments. The pumping rate $\left(r = \frac{I}{I_{th}}\right)$ is the ratio between the pumping current (I) of the slave laser and the pump current (I_{th}) at threshold. The experimental results are obtained either by fixing the detuning between the master and slave lasers and then varying the injected power, or by fixing the injected power and then varying the detuning between the lasers.

When a laser is injected by a master that has a narrower optical linewidth [86,129], the injected photons are covering, in frequency, all the optical slave-laser-line.

On the contrary, when a slave laser with wider spectrum is injected by a narrow master laser [116,128,138], the narrow master signal can be separated from the injected laser spectral density. At low injection levels, a narrow signal is seen on the top of the injected laser spectrum as shown in the Figure 2. 7(a).

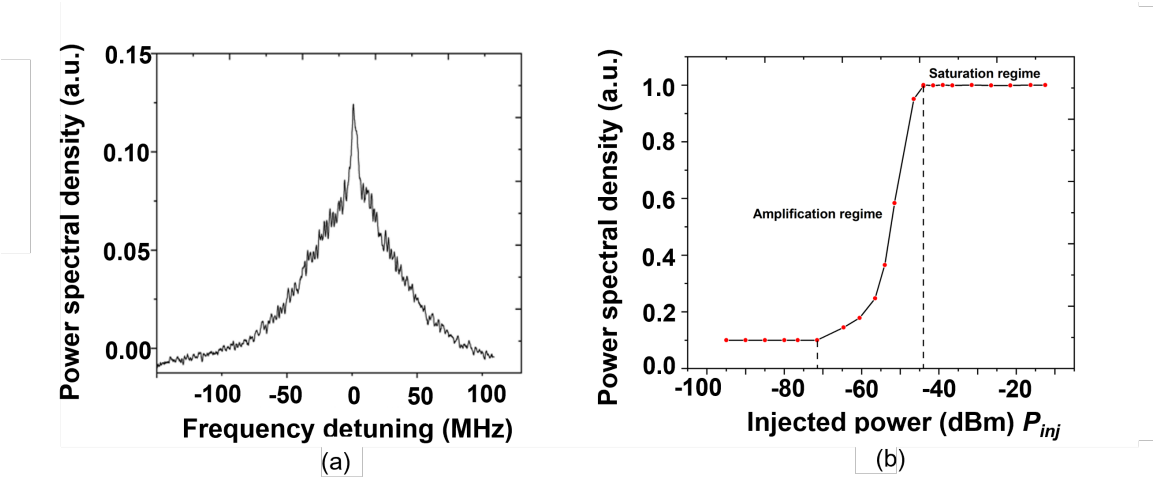

Figure 2. 7: (a) Slave laser injected by a narrow linewidth weak master signal. The narrow peak on top of the injected laser spectrum is the master signal. (b) The Fabry-Perot spectra of the injected slave PSD for increasing injected powers of *Tunics-OM BFL* master laser.

The narrow signal can be easily distinguished from the wide slave spectrum if the slave is injected close to its threshold. When the injected power of the master laser is increased slowly from very weak values (picoWatt), the optical-injection enters in the amplification regime and the slave laser amplifies the narrow master-signal at the expense of its own spectral power as shown in the Figure 2. 7(b). This amplification can be of the order of 50-60 dB [116], which is a common figure in laser amplification[5]. For very low injected power, the maximum power spectral density of the injected slave remains same as free slave laser spectral density since the injected power is too small to cause detectable change in the Fabry-Perot analyzer used. When the injected power is increased, the injected-slave PSD follows a linear increase as the slave is now in the amplification regime. By further increasing the injected power, the injected-slave PSD remains constant and enters a

[5] A single spontaneous photon is generating commonly 100000 photons by stimulating emission in a laser.

saturation regime, which is similar to that encountered when a laser crosses its operating threshold. In this case, the optical power of the injected slave is too important for all photons to be amplified, the gain being finite and allowing the amplification of a finite number of photons. The gain decreases with the photon flux. We can define a frequency locking threshold for the optical injection as for lasers (this applies to the external signal serving as an initiating source for the laser process). Above this threshold, all the power from the slave spectrum is then transferred to the narrow linewidth master signal. I will show in this thesis that transfer is progressive and asymptotic, and that the coherency transfer rate is dependent on the master-laser coherency.

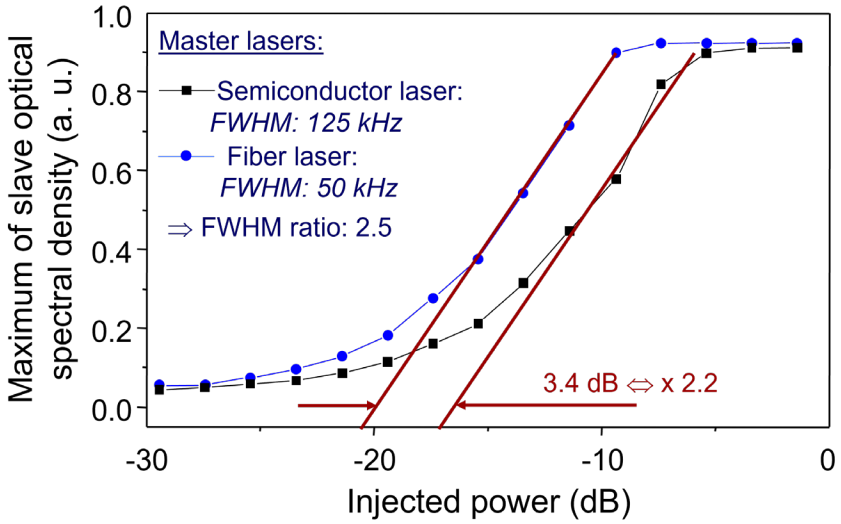

Figure 2. 8: The PSD of 2 optically injected lasers. The blue and black lines represent a slave laser injected by two different coherent master lasers. The blue line is for a master laser of higher coherency than the case shown by the black line. This measurement has been proposed by S. Blin [138] to characterize the spectral linewidth of coherent lasers.

As seen from Figure 2. 8, a coherent master laser completely transfers its PSD to the slave for a lower injected power (blue line) than a master laser with higher linewidth (black line).

In the next section, we will study the frequency noise analysis of the injected slave laser using the sub-kHz linewidth tunable master laser developed during my thesis. For this study, we will also use master lasers of different linewidths. Frequency noise analysis of the injected slave for increasing injected powers (amplification and saturation regimes) will give us a better understanding about the linewidth transfer between the master and slave laser under frequency locking conditions.

2.6 Transfer of purity using optical injection

In this section, we will present the frequency noise analysis of an optically injected slave laser using master lasers of different coherencies. The frequency noise analysis will help us to understand the evolution of low frequency noise and coherency of the injected slave from the initial free-running state of slave laser, when it is injected by a narrow linewidth master-laser with increasing injected powers.

2.6.1 Analysis of purity transfer using frequency noise in optical injection

The frequency noise measurement of the injected slave laser is presented in this section. Recall that the *Alcatel* slave laser is operated at 19.8 mA (1.1 times its threshold) and that it has an integrated linewidth of 39.8±3.9 MHz and an intrinsic linewidth of 32.73 MHz ($h_0 = 1.04 \times 10^7 Hz^2/Hz$). This slave laser is injected using a much narrower tunable master laser with an integrated linewidth of 332.8±33 kHz and 31.4 kHz intrinsic linewidth ($h_0 = 1 \times 10^4 Hz^2/Hz$). The integrated linewidths of slave and master lasers are measured using β-line method. The master source is a commercial tunable source™ (*Tunics PR*). The slave laser has an inbuilt optical isolator of 35 dB, that we have measured. The optical injected power is given, considering this optical isolation of the slave laser.

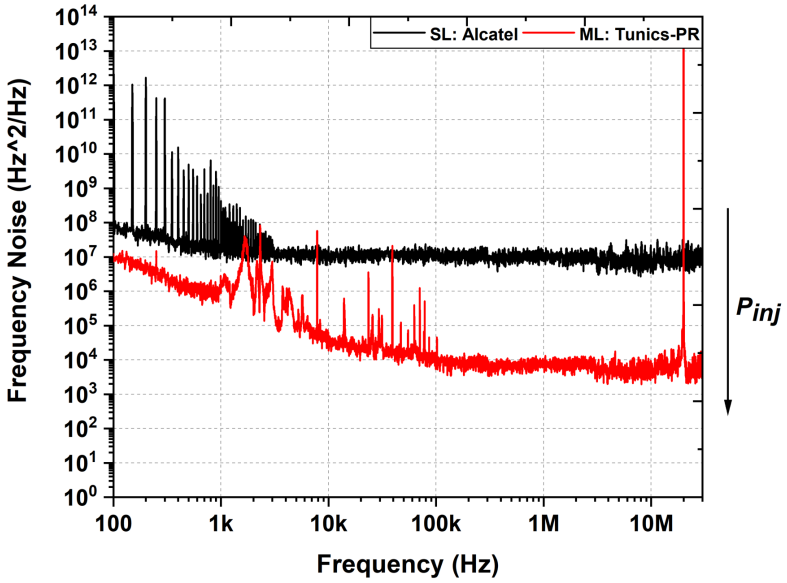

(a)

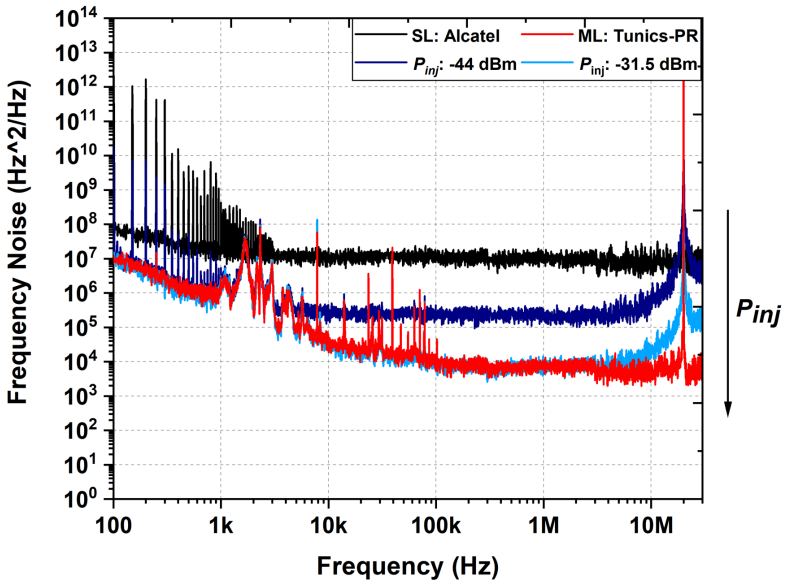

(b)

Figure 2. 9: (a) Frequency noise of the free-running *Alcatel* slave laser (SL) and of the Tunics-OM master laser (ML). (b) The frequency noise of the *Tunics-PR* is fully transferred to the *Alcatel* slave laser for an injected power of -31.5 dBm (blue spectrum). The navy spectrum shows the *Alcatel* injected slave at -44 dBm with a complete transfer of the low frequency components (of the stability) under 1 kHz and a partial transfer of the coherence.

The free-running *Alcatel* slave laser (black spectrum) frequency noise and *Tunics-PR* laser (red spectrum) frequency noise are displayed in the Figure 2. 9(a). SL and ML denote slave and master laser respectively. The spikes on the *Alcatel* slave laser spectrum as shown in Figure 2. 9(a) from 100 Hz to 3 kHz is arising from the *ILX* current source used to drive the slave laser. There is a difference of 30 dB in coherency between the Alcatel slave laser and Tunics-PR master laser. Hence, there will be a transfer of purity from the master laser to the slave laser upon increasing the injected power at null detuning. The resonance at 20 MHz (L_d = 10 m; τ_d = 50 ns) seen in Figure 2. 9 and Figure 2. 10 are arising from the Mach-Zehnder interferometer used for measuring frequency noise. Measurements are made with 10 meters length of delay fiber in the following.

The Figure 2. 10 shows the evolution of frequency noise spectrum of the injected slave upon increasing the injected power of the *Tunics-PR* master laser. The injected power varies from -51.5 dBm to -31.5 dBm. At an injected power of -51.5 dBm, we can see from the magenta spectrum that the frequency-noise level of injected slave is lower than the free-running slave laser. The integrated and intrinsic linewidths of the injected slave at this operating point are 28.45±0.28 MHz and 25.38 MHz ($h_0 = 8.08 \times 10^6\ Hz^2/Hz$). In this case, the injected slave laser just entered the amplification regime. By increasing the injected power, we can observe the continuous narrowing of the injected-slave spectrum from the Figure 2. 10 as the white noise and low frequency components are decreasing.

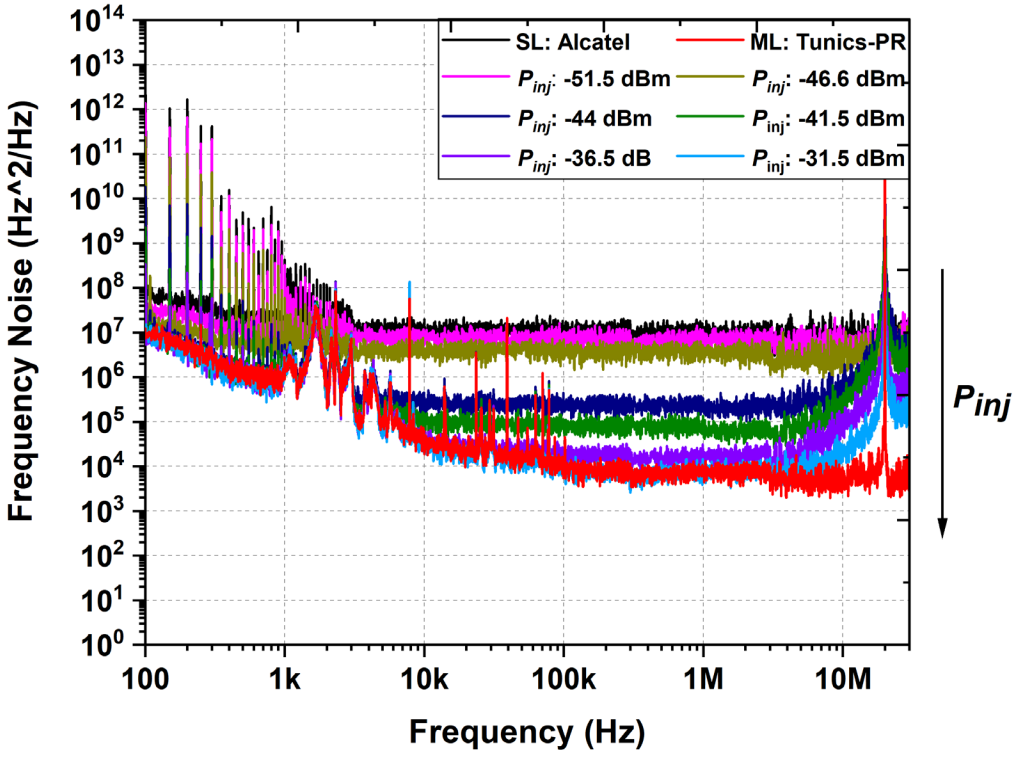

Figure 2. 10: Frequency noise of *Tunics-PR* master laser (ML) and of the *Alcatel* injected slave laser (SL) for different injected powers: -51.5 dBm, -46.6 dBm, -44 dBm, -41.5 dBm, -36.5 dBm and -31.5 dBm.

We can observe that, the low frequency flicker noise of *Tunics-PR* master is totally transferred for a power of -36.5 dBm while there is a partial transfer of the white noise ($h_0 = 1.75 \times 10^4 Hz^2/Hz$). This fact is simply due to noise power level, which are different for the noise contributions. In other words, the lower master-frequency-jitter at low frequencies (or the stability of the master laser) is first transferred when the injected power is increased. At a master injected power of -36.5 dBm (violet spectrum), the master laser completely transfers its low frequency noise to the injected *Alcatel* slave laser (in a

frequency band from 100 Hz up to 10 kHz). The frequency noise of the *Tunics-PR* is fully transferred to the *Alcatel* slave laser for an injected power of -31.5 dBm (blue spectrum) as seen from the Figure 2. 9(b) ($h_0 = 1 \times 10^4 Hz^2/Hz$). I have shown how the coherency is transferred in terms of PSD for the first time with a transfer rate, which is dependent on the noise PSD level or in other terms of the coherency and stability of the laser. We will study in the next section this transfer rate more precisely.

2.6.2 Optical injection with Tunics-OM master laser

In this section, frequency noise measurement will be performed with *Tunics-OM* master laser that has an integrated linewidth of 84.4 ± 8.44 kHz and an intrinsic linewidth of 3.16 kHz ($h_0 = 1 \times 10^3\ Hz^2/Hz$). The *Alcatel* slave laser has an integrated linewidth of 39.8 ± 3.9 MHz and an intrinsic linewidth of 32.73 MHz ($h_0 = 1.04 \times 10^7 Hz^2/Hz$). *Tunics-OM* is spectrally more coherent than *Tunics-PR*. The free-running *Alcatel* slave laser (black spectrum) and *Tunics-OM* master laser (red spectrum) is shown in the Figure 2. 11(a). As mentioned in the section 2.6.1, the spikes seen in the *Alcatel* slave laser spectrum in Figure 2. 11 is due to the *ILX* current driver source used. The *Tunics-OM* master laser is 40 dB narrower than the *Alcatel* slave laser.

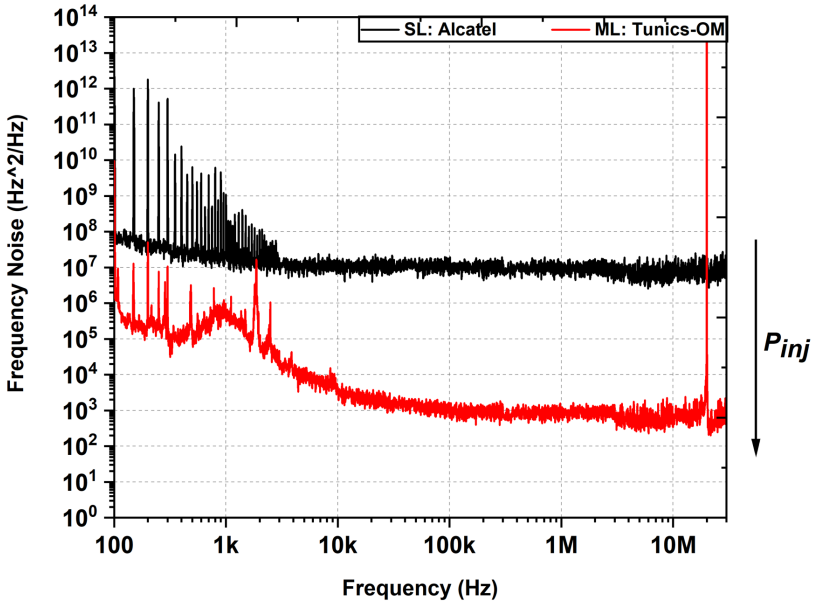

(a)

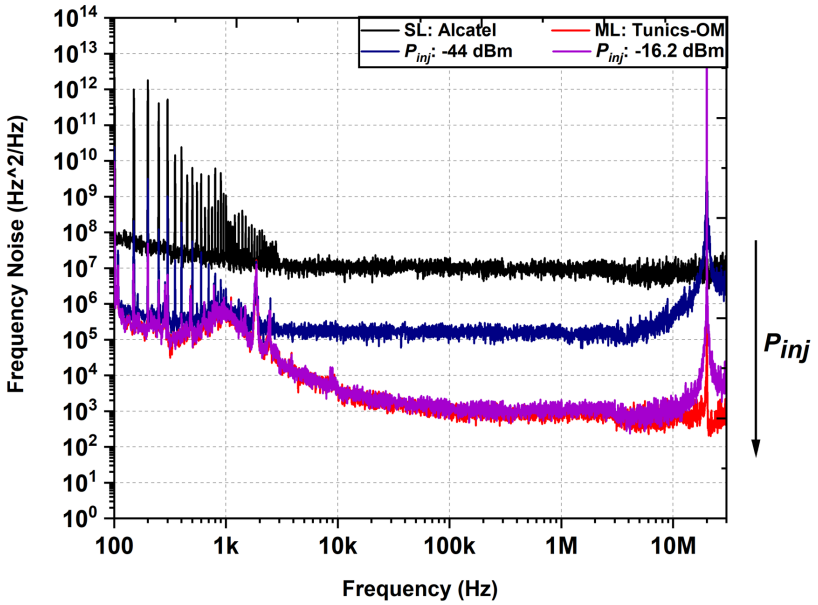

(b)

Figure 2. 11: (a) Frequency noise of the free-running *Alcatel* slave laser (SL) and of the *Tunics-OM* master laser (ML). (b) The frequency noise of the *Tunics-OM* is fully transferred to the *Alcatel* slave laser for an injected power of -16.2 dBm (violet spectrum).

At -51.5 dBm, we start to see the influence of the master field: the frequency noise level of the injected laser is lower than the one of the free-running slave laser level as observed from the Figure 2. 11(a) and Figure 2. 12. The integrated and intrinsic linewidths of the injected slave at this point is 34.4 ± 0.34 MHz and 27.93 MHz ($h_0 = 8.89 \times 10^6 Hz^2/Hz$). By increasing the injected power, the frequency noise level decreases so that the slave laser spectrum narrows (equations 1.14, 1.15).

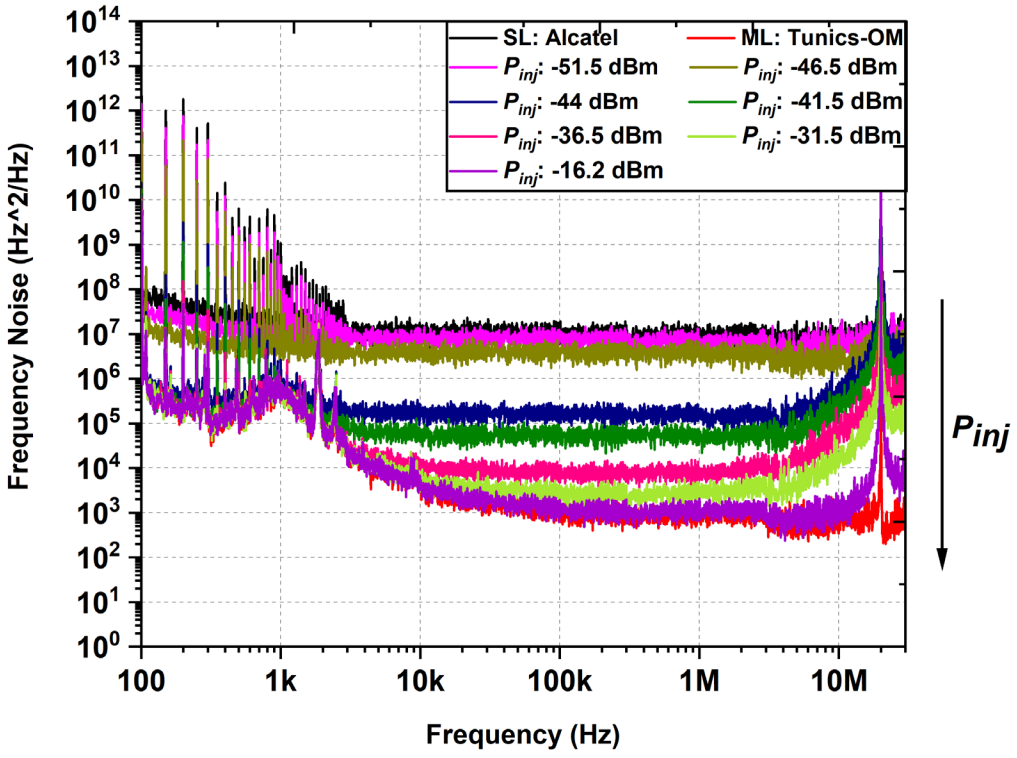

Figure 2. 12: Frequency noise of *Tunics-OM* master laser (ML) and of the *Alcatel* injected slave laser (SL) for different injected powers: -51.5 dBm, -46.5 dBm, - 44 dBm, -41.5 dBm, -36.5 dBm, -31.5 dBm, -16.2 dBm.

As already mentioned in the case of frequency noise measurement with the *Tunics-PR* master laser, the transfer of low-frequency noise occurs at a lower injected power level than for white noise because the contribution to frequency noise at low frequencies has at higher PSD. Thus, at an injected power of -31.5 dBm (light green spectrum), low frequency noise is completely transferred to the injected slave laser. The white noise at -31.5 dBm injected power is at the level $h_0 = 2.91 \times 10^3 Hz^2/Hz$. The *Tunics-OM* master laser completely transfers its spectral linewidth to the injected slave laser for an injected power of -16.2 dBm as depicted by the violet spectrum ($h_0 = 1 \times 10^3 Hz^2/Hz$). This value is much higher than for the Tunics PR (-31.5 dBm). The requirement of higher injected powers to reach a complete transfer is simply due to the fact that the *Tunics-OM* is more coherent (with a narrower line) than *Tunics-PR* laser.

2.6.3 Optical injection with Agilent master laser

The next master laser used for this study is an *Agilent* tunable laser, with an integrated linewidth of 2.15 ± 0.2 MHz and an intrinsic linewidth of 2.5 kHz ($h_0 = 7.96 \times 10^2 Hz^2/Hz$). *Agilent* and *Tunics-OM* master lasers have similar intrinsic linewidth. However, the low frequency noise of *Agilent* laser is higher than that of *Tunics-OM* master laser, which is an interesting point in order to draw a comparison when the low-frequency contribution is only varied. The frequency noise spectrum of *Agilent* tunable master laser and *Alcatel* slave laser is shown in the Figure 2. 13(a). Similar observations are made here as we can have already seen in the case of optical injection with *Tunics-PR* and *Tunics-OM* master lasers. When the *Agilent* master laser injected power is gradually increased from -60.6 dBm

(blue) with integrated and intrinsic linewidths of 39.09±0.39 MHz and 31.42 MHz ($h_0 = 1 \times 10^7 Hz^2/Hz$) to -51.7 dBm (sky blue) with integrated and intrinsic linewidths of 32.95 ± 0.33 MHz and 28.58 MHz ($h_0 = 9.1 \times 10^6 Hz^2/Hz$), and then to -44 dBm (maroon) with integrated and intrinsic linewidths 2.53 ± 0.25 MHz and 656.2 kHz ($h_0 = 2.08 \times 10^5 Hz^2/Hz$).

We witness the transfer of linewidth from the narrow master laser to the broader *Alcatel* slave laser from Figure 2. 14. Frequency noise in the low frequency region is transferred at a faster rate (for lower injected powers) than at high frequency regions, mainly, again for a question of higher power at these frequencies of fluctuations. At an injected power of -41.5 dBm, the *Agilent* master laser transfers its low frequency noise completely to the injected *Alcatel* slave laser. The intrinsic linewidth of injected slave at -41.5 dBm is 152.64 kHz ($h_0 = 4.86 \times 10^4 Hz^2/Hz$). Intrinsic linewidth of injected *Alcatel* slave laser decreases and approaches the intrinsic linewidth level of *Agilent* master laser on further increasing the injected power. The *Agilent* master laser completely transfers its coherency to the injected *Alcatel* slave laser for an injected power of -16.27 dBm (violet spectrum) ($h_0 = 7.96 \times 10^2 Hz^2/Hz$) as seen from the Figure 2. 13(b). *Tunics-OM* master laser with an intrinsic linewidth of 3.16 kHz transferred its coherency completely to the *Alcatel* slave laser for a similar injected power of -16.2 dBm. However, *Agilent* laser with an integrated linewidth of 2.1±0.2 MHz completely transferred its low frequency noise to the *Alcatel* slave laser at an injected power of -41.5 dBm. *Agilent* master laser with higher integrated linewidth than *Tunics-PR* (332.8±33 kHz) and *Tunics-OM* (84.4±8.44 kHz) master lasers required lower injected power to impose its low frequency noise to the injected *Alcatel* slave laser.

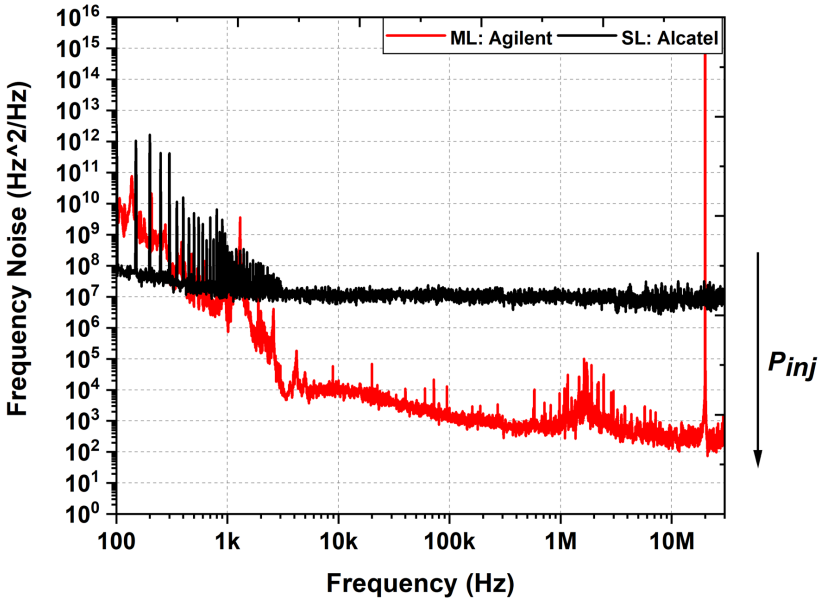

(a)

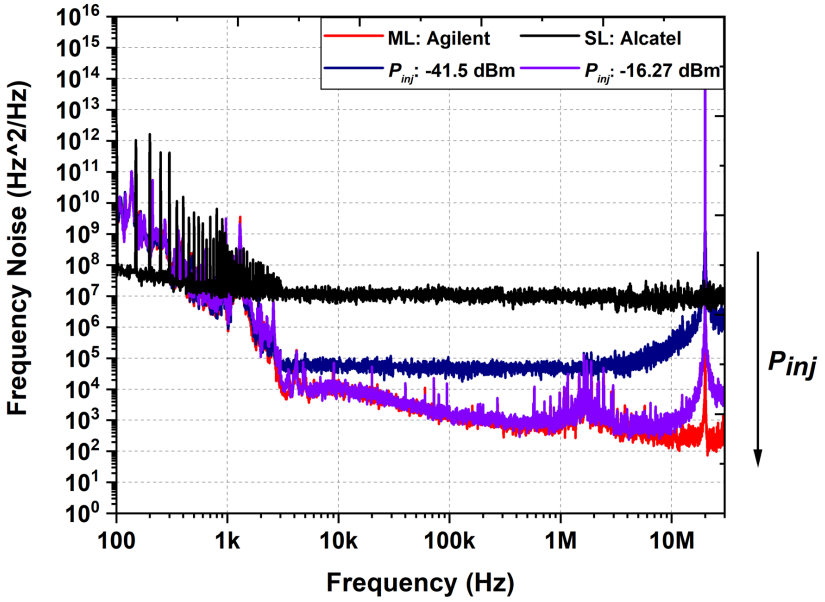

(b)

Figure 2. 13: (a) Frequency noise of the free-running *Alcatel* slave laser (SL) and of the *Agilent* master laser (ML). (b) The frequency noise of the *Agilent* is fully transferred to the *Alcatel* slave laser for an injected power of -16.27 dBm (violet spectrum).

Tunics-PR and *Tunics-OM* required -36.5 dBm and -35 dBm respectively to transfer its integrated linewidth to the *Alcatel* slave laser. The integrated and intrinsic linewidth is estimated from the frequency noise spectrum of the laser using β-line approximation method explained in the section 1.3.2.4.

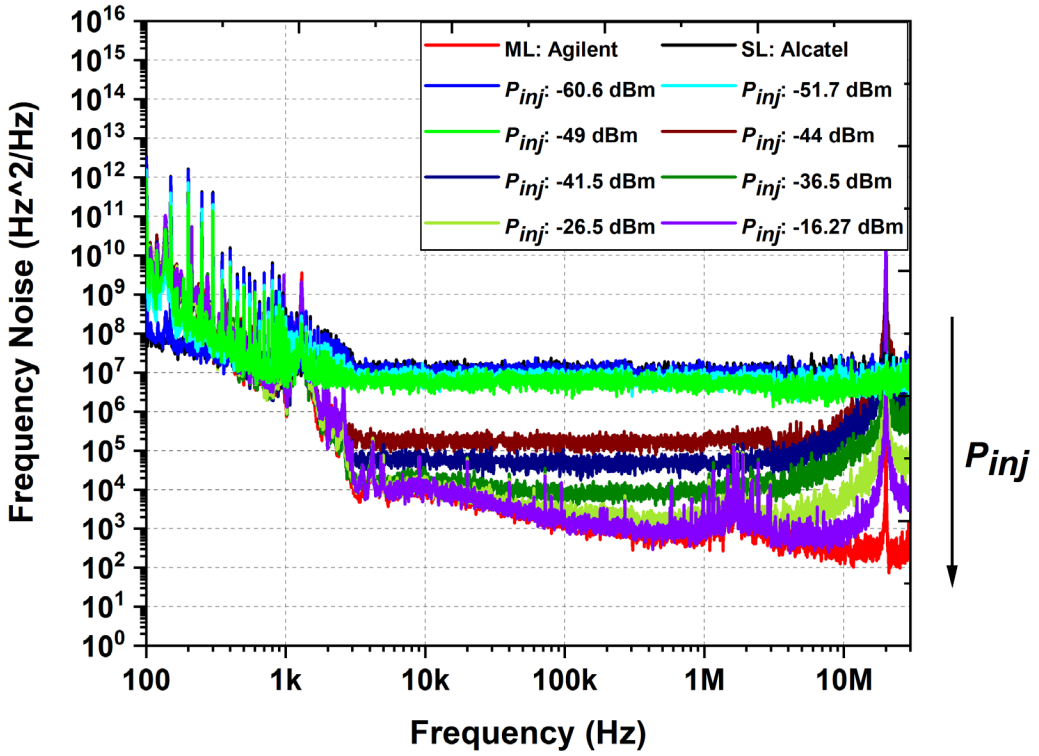

Figure 2. 14: Frequency noise of *Agilent* master laser (ML) and of the *Alcatel* injected slave laser (SL) for different injected powers: -60.6 dBm, -51.7 dBm, - 49 dBm, -44 dBm, -41.5 dBm, -36.5 dBm, -26.5 dBm, -16.27 dBm.

2.6.4 Optical injection with Tunics-OM BFL master laser

In this subsection, we use, as the master laser, a sub-kHz laser with a selectable wavelength in the C-band developed during my thesis. As the contribution of white noise and low-frequency noise can be distinguished, the transfer of coherency (white noise) and stability (low-frequency components) may be studied independently. As a matter of fact, we figure out that there is no need to stabilize the master laser through a servo-loop as mentioned previously.

The *Tunics-OM BFL* is the most coherent laser used as master laser to study the impact of coherency in optical injection for our experiment. It has an intrinsic linewidth of 1.17 Hz ($h_0 = 3.72 \times 10^{-1} Hz^2/Hz$) and an integrated linewidth of 5.11 ± 0.5 kHz. The free-running *Alcatel* slave laser (black spectrum) and *Tunics-OM BFL* (red spectrum) master is shown in the Figure 2. 15(a). *Tunics-OM BFL* master laser is 74 dB narrower than the *Alcatel* slave laser.

At -44 dBm injected power (navy blue), the intrinsic linewidth of the injected slave is between that of the free slave and *Tunics-OM BFL* master laser as seen from Figure 2. 15(b).

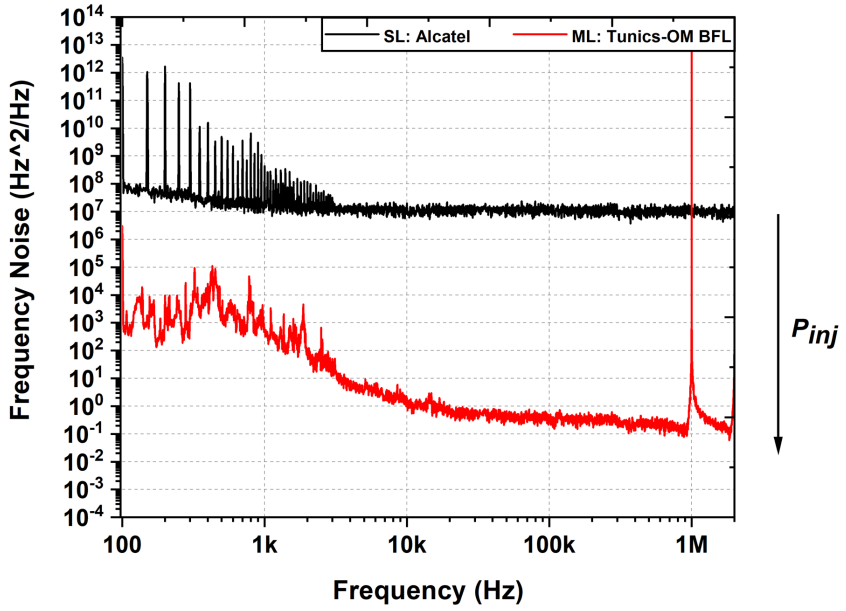

(a)

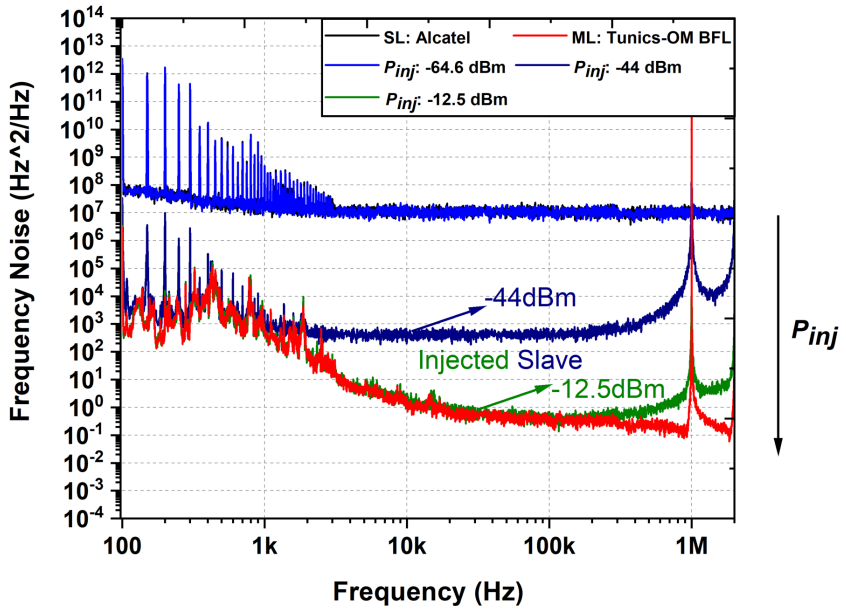

(b)

Figure 2. 15: (a)Free-running *Alcatel* slave laser (SL) and *Tunics-OM BFL* master laser (ML). (b)Frequency noise of SL, ML and injected slave at -64.6 dBm, -44 dBm and -12.5 dBm

The low frequency components of the injected slave are at the level of the master laser for an injected power of -41.5 dBm (magenta spectrum) shown by Figure 2. 16. At an injected power of -12.5 dBm (olive spectrum), *Tunics-OM BFL* transfers its coherency entirely to the injected *Alcatel* slave laser. For an intrinsic linewidth of 1.17 Hz, -12.5 dBm is necessary for a complete transfer while only -44 dBm for 1.72 kHz, implying a penalty of 31.5 dBm power. The difference in coherencies of the injected slave at -44 dBm and 12.5 dBm injected powers is 31.6 dB. The penalty in injected power and difference in coherencies at injected powers of -44 dBm and -12.5 dBm appears to coincide here. The injected *Alcatel* slave laser's linewidth is reduced to 1.17 Hz from its free-running linewidth of 32.73 MHz, which corresponds to a linewidth reduction of 74 dB.

We cannot go ahead without mentioning that we have used different delay lengths to measure the frequency noises of the injected slaves in our Mach-Zehnder interferometer setup. This can be understood by the fact that we have to characterize very different coherencies. The measurement of frequency noise was already introduced in section 1.3.3. We have used a delay length of 10 meters to measure the frequency noise of injected slave lasers using as master laser, *Tunics-PR*, *Tunics-OM* and *Agilent* sources. For the frequency noise measurement of optical injection with our most coherent laser *Tunics-OM BFL*, we have used delay length of 200 meters.

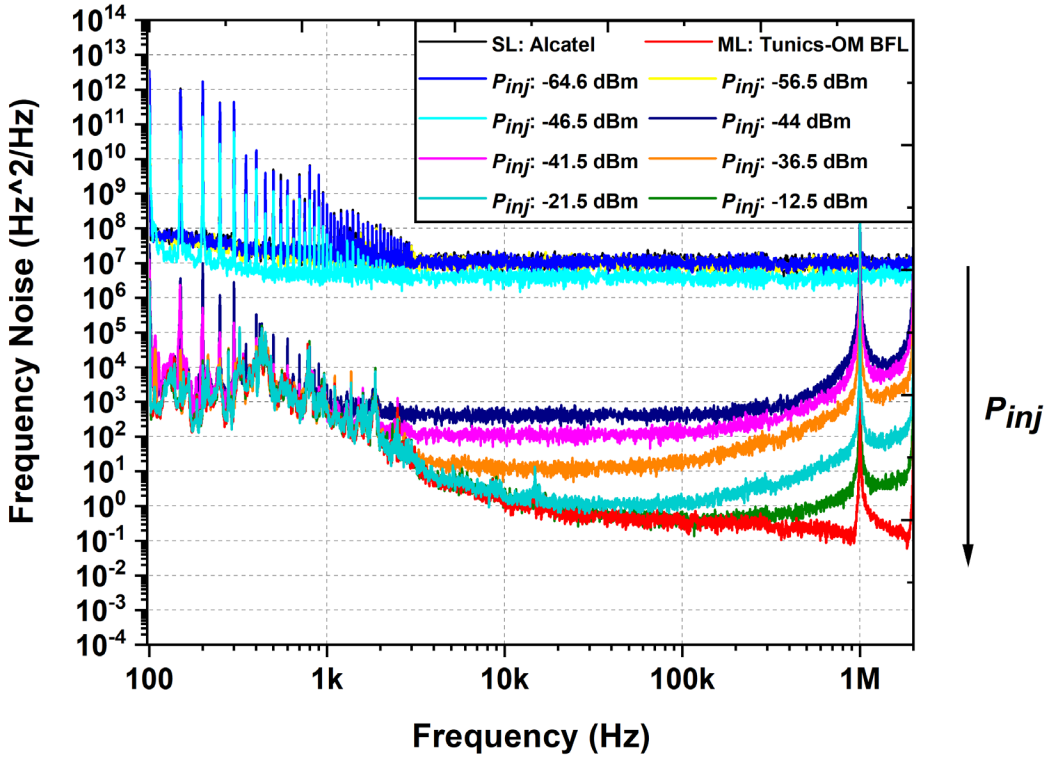

Figure 2. 16: The evolution of the frequency noise of the *Alcatel* injected slave laser when the injected power from *Tunics-OM BFL* is varied (from -64.5 dBm to -12.5 dBm).

The frequency noise spectrum of the *Alcatel* injected slave laser injected by a *Tunics-OM BFL* master laser is shown in the Figure 2. 17. The green spectrum represents the frequency noise of the injected slave, measured with a delay fiber length of 1.5 meter, in the Mach-Zehnder interferometer. The navy-blue spectrum shows the injected slave spectrum, measured with a fiber length of 200 meters. The green and navy-blue spectrum represents the Alcatel injected slave at the same injected power of -44 dBm. This shows the influence of delay length in measuring the frequency noise spectrum of an injected slave laser. The white noise level using a delay length of 1.5 meter is $h_0 = 1.876 \times 10^6 Hz^2/Hz$ while

with a delay length of 200 meters h_0 is equal to $4.203 \times 10^2 Hz^2/Hz$. The conversion gain ratio is $(200/1.5)^2 = 1.8 \times 10^4$ while the floor noise ratio is 4.46×10^3. This discrepancy (0.25) between the calculated conversion gain and the measured noise floor could be explained by the fact that a longer fiber delay spool will integrate more environmental noise.

This result in measurement of frequency noise may be surprising because the frequency-noise measurement is generally independent of the delay length. However, we have a very particular situation, for which we have to measure a signal (Figure 2. 7), which is the sum (relation 2.38) of two lines. One has a large bandwidth (the one of the solitary slave laser; integrated linewidth of 39.8±3.9 MHz and intrinsic linewidth of 32.73 MHz ($h_0 = 1.04 \times 10^7 Hz^2/Hz$)) and the other one a very narrow bandwidth (the one of the injected signal; integrated linewidth of 5.11±0.5 kHz and intrinsic linewidth of 1.17 Hz ($h_0 = 3.72 \times 10^{-1} Hz^2/Hz$)). The difficulty is then to measure two signals with very different coherencies. We have already explained the relation between measurement bandwidth and delay length in section 1.3.3. Figure 1.7(b) shows the gain conversion of the measurement bench as a function of delay length. The measurement with a delay fiber of 1.5 meter (FSR = 133 MHz; $\tau_d = 7.5$ ns) will have higher measurement bandwidth than with a delay length of 200 meters (FSR = 1 MHz; $\tau_d = 1$ μs) so that it will integrate more noise from the less coherent term of the injected signal (first term in the right expression of equation 2.40). In the case of 200 meters length, it is obviously not adapted to the measurement of the frequency noise of the slave laser. The laser line (40 MHz) is filtered out by the transmission function of the interferometer (FSR = 1 MHz). On the other hand, 1.5 meters is not adapted to the measurement of the frequency noise of the master signal ($h_0 =$

$3.72 \times 10^{-1} Hz^2/Hz$) as the noise floor ($h_0 = 1.876 \times 10^6 Hz^2/Hz$) is too high. The measurement bandwidth and gain conversion should be high enough to have access to the white noise (above the corner frequency) and also to have enough signal strength to measure the frequency noise of the master.

For optical injection with a very coherent master laser, which emits on a very thin line, the PSD maximum will be large with existing traces of pedestal. This small pedestal pollutes the frequency noise measurement of the injected slave as far as it contains a non-negligible power.

Nevertheless, we want to measure the optically injected power, above which the optically injected slave laser has taken all the spectral properties of the master, or in other words for which the optically injected laser line is the one of the master. It's why the measurement using a delay line of 200 meters is relevant and adapted in this case. Indeed, the measurement made with a signal containing a portion of the slave laser line will not be adapted even if it could give indications of the overall evolution.

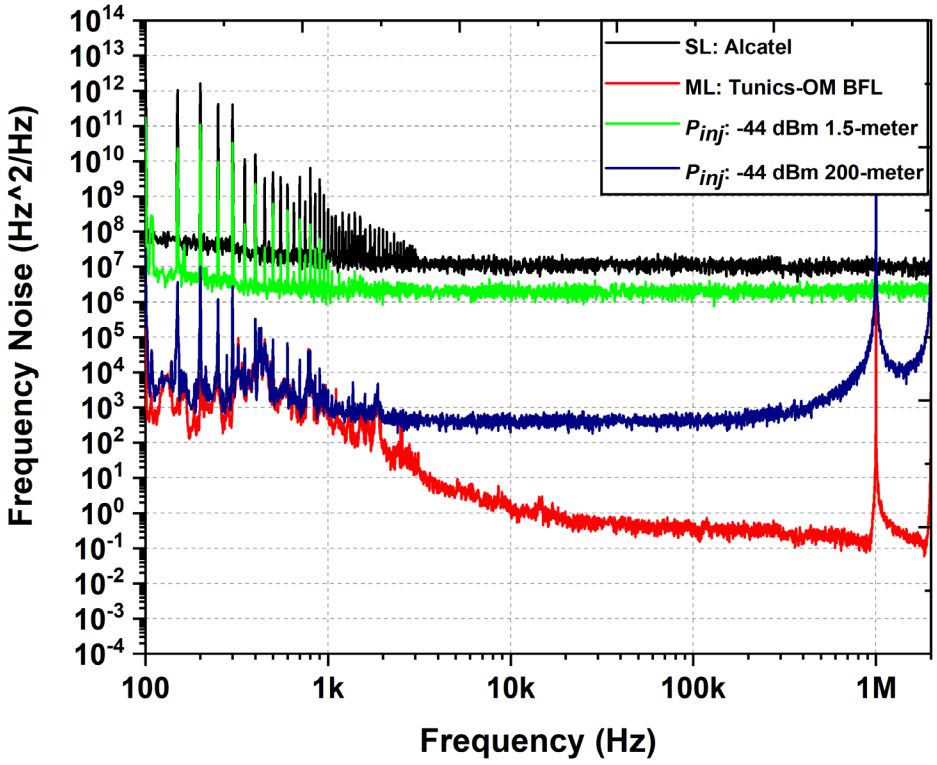

Figure 2. 17: Frequency noise spectrum of injected slave at an injected power of -44 dBm measured with 1.5-meter (green) and 200-meters (navy blue) fiber delay length in the Mach-Zehnder interferometer.

2.6.5 Evolution of spectral linewidth transfer with injected power

In this section, we will compare the results obtained from the frequency noise measurement of optical injection with master laser of different coherencies: *Tunics-PR*, *Tunics-OM*, *Agilent* and *Tunics-OM BFL* tunable master lasers.

Note that measuring the PSD maximum (Figure 2. 7(b)) will imply that the more coherent the master laser the less power is required to obtain a given signal to noise ratio. More coherency implies a higher amplified master peak as for the same number of photons, the

bandwidth containing them is decreased. Thus, the external beam will be amplified at the expense of the slave pedestal (Figure 2. 7(a)), which is a reminiscence of the free slave laser line as theoretically shown [116]. With higher coherency of the master, the lower is the injected optical power necessary to reach the regime of amplification. This method has been proposed to characterize highly coherent source [138]. Measuring the PSD maximum is therefore not a good indication of the noise properties of the injected slave, as we need to ensure that the pedestal is attenuated enough to have only the noise of the master laser on the detector. Close to the saturation regime, even a small pedestal will be enough to increase the frequency noise. When the master laser emits on a very thin line, the PSD maximum can be large with still an existing small pedestal that will pollute the frequency noise of the injected slave.

The evolution of intrinsic linewidth as a function of injected power is shown in the Figure 2. 18. It shows that the more coherent the master laser, the higher the injected power required to achieve full coherency transfer. *Tunics-OM BFL* master laser, being the most coherent among the four lasers, required injected power of -12.5 dBm to fully transfer its coherency to the *Alcatel* slave laser while *Tunics-PR* master laser with an intrinsic linewidth of 31.4 kHz required only -31.5 dBm of injected power.

Tunics-OM and *Agilent* master lasers have similar intrinsic linewidths. Hence, both these lasers transferred their coherency to the *Alcatel* slave laser at an almost equal injected power of -16.2 dBm and -16.27 dBm respectively. It is important to note that the frequency noise of injected slave with master lasers *Tunics-PR*, *Tunics-OM* and *Agilent* are measured using 10-meter delay fiber length in the Mach-Zehnder interferometer (FSR = 20 MHz; τ_d = 50 ns). *Tunics-OM BFL* being the most coherent master laser with an intrinsic linewidth

of 1.17 Hz, the frequency noise was measured using a delay fiber length of 200 meters (FSR = 1 MHz; τ_d = 1 µs).

Tunics-OM BFL master laser, which is 34 dB narrower than *Tunics-OM*, requires -12.5 dBm of injected power to transfer its frequency noise to the *Alcatel* slave laser, which means a slight increase of 3.7 dB.

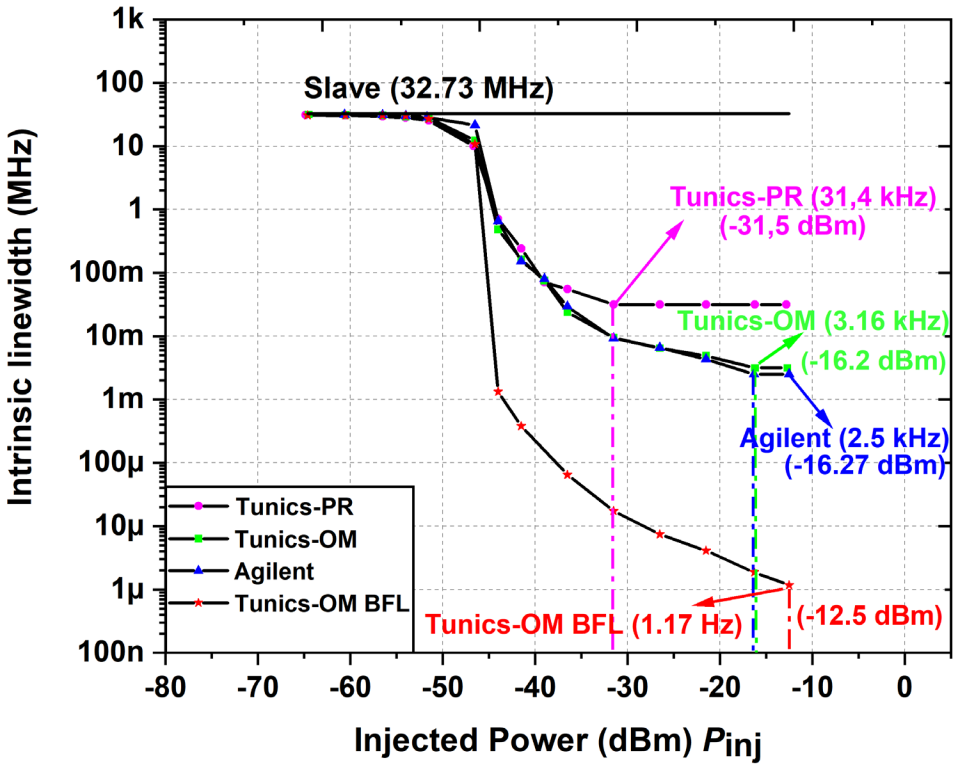

Figure 2. 18: The evolution of intrinsic linewidth as a function of injected power. *Tunics-PR*, *Tunics-OM*, *Agilent* and *Tunics-OM BFL* master lasers are used to inject the *Alcatel* slave laser.

From Figure 2.19, we can see that low frequency components of the master lasers are transferred to the slave laser for much lower injected powers than the intrinsic linewidths.

Table 2.1 briefs the injected powers required by the master lasers to transfer its frequency noise to the *Alcatel* slave laser. The difference in intrinsic linewidths between *Tunics-PR* and *Tunics-OM* is 10 dB, but the difference in injected powers to complete the coherence transfer to the SL is 15.3 dBm.

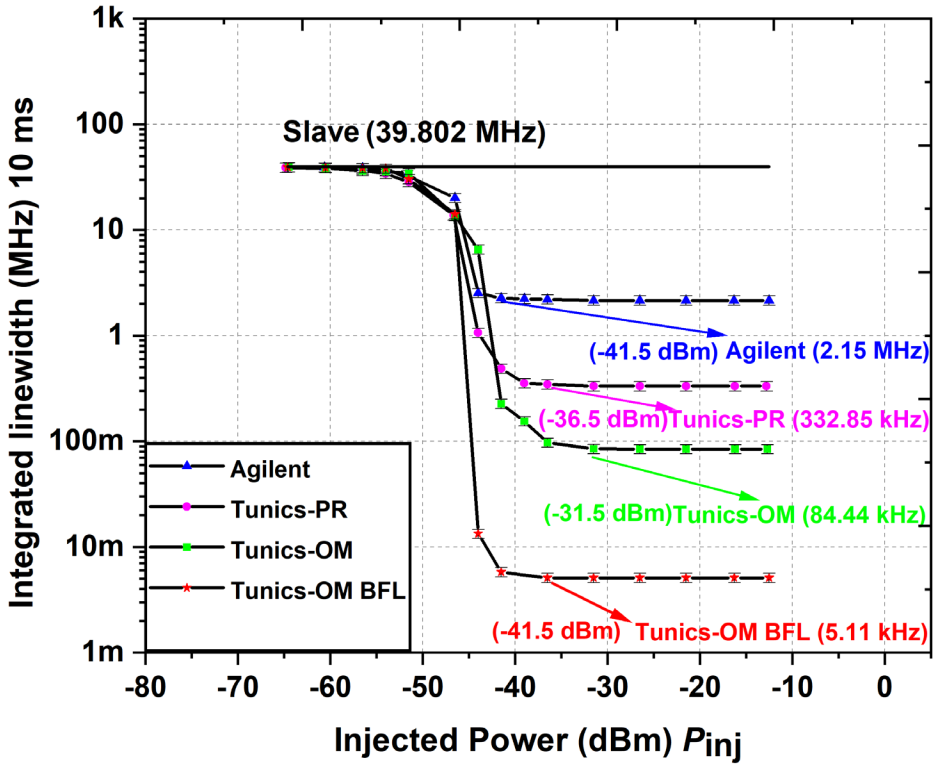

Figure 2. 19: The evolution of integrated linewidth as a function of injected power. *Tunics-PR*, *Tunics-OM*, *Agilent* and *Tunics-OM BFL* master lasers are used to inject the *Alcatel* slave laser.

Master laser	Integrated linewidth	h_0 (Hz^2/Hz)	Intrinsic linewidth	Delay fiber length for frequency noise measurement (in meters)	Injected power for intrinsic linewidth transfer (dBm)	Injected power for integrated linewidth transfer (dBm)
Tunics-PR	332.8±33 kHz	1×10^4	31.4 kHz	10	-31.5	-36.5
Tunics-OM	84.44±8.4 kHz	1×10^3	3.16 kHz	10	-16.2	-31.5
Agilent	2.15±0.21 MHz	7.96×10^2	2.5 kHz	10	-16.27	-41.5
Tunics-OM BFL	5.11±0.51 kHz	3.72×10^{-1}	1.17 Hz	200	-12.5	-41.5

Table 2.1: The master lasers and injected power required for the frequency noise transfer to *Alcatel* slave lasers.

The difference between the linewidth ratio and the ratio of the injected powers should be confirmed theoretically. However, we think that a change in detuning will increase the injected power required for a complete transfer. Recall that there is no stabilization, that the detuning is set to zero and that the locking bandwidth is very narrow at low injected rate (equation 2.1). We do observe an increase of frequency noise with detuning.

2.7 Frequency noise of the sum of two signals with different coherencies

In this section, the slave and master lasers are mixed (combined) using an optical coupler and the frequency noise of the output signal is measured to study the evolution of the linewidth upon increasing the power of the master laser. As previously described and explained, from a theoretical point of view, the optical injection is the addition of an extra term to the excitation field (equation 2.36), or the noise source, which will be multiplied

by the transfer function to give the output field. Thus, measuring the frequency noise of a signal resulting from the addition of two sources could give an insight in the evolution of the noise properties of an optically injected system.

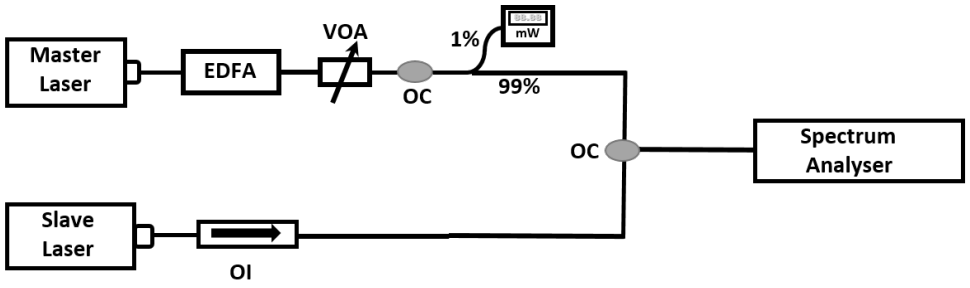

Figure 2. 20: Experimental setup to study the mixing of slave and master lasers.

The Alcatel slave laser is set to operate at 1.1 times its threshold. The experimental setup is shown in Figure 2. 20. The experimental setup for optical injection, described in section 2.5, is slightly tweaked to study the impact of mixing between the master and slave lasers. Alcatel laser was originally used as the slave laser, Agilent tunable laser as the master laser. The difference between this mixing experimental setup and optical injection setup is that, in the mixing setup the master and slave lasers are combined through an optical coupler as shown in the Figure 2. 20. In optical injection, the output of the master laser is directly seeded inside the cavity of the slave laser.

The mixing signal is collected from the output port of the optical coupler. It is analyzed in terms of frequency noise. The Alcatel laser operates at 1.1 times the threshold as in the previous experiments of optical injection. The power of the Agilent master laser is varied to analyze the frequency noise spectrum as for optical injection. The frequency noise

spectrum of the mixing of Alcatel slave laser and Agilent master laser is shown in the Figure 2. 21.

At -56.5 dBm (green) Agilent master laser power, we can observe the change in the frequency noise of the mixing spectrum. It is moving towards the low frequency noise region of the Agilent laser. Upon increasing the Agilent master laser power from -51.73 dBm to -46.5 dBm we can see changes in the low frequency region of the mixing spectrum. As observed in the transfer purity using optical injection section, we can see changes in the low frequency region for low powers of master laser. At -39 dBm (purple), the low frequency noise of the mixing signal is similar to the Agilent laser.

By further increasing the Agilent master laser power we can observe a complete transition of the mixing frequency noise spectrum to the frequency noise spectrum of Agilent master. At -16.22 dBm (orange), the mixing spectrum is fully transferred to the Agilent master laser frequency noise spectrum.

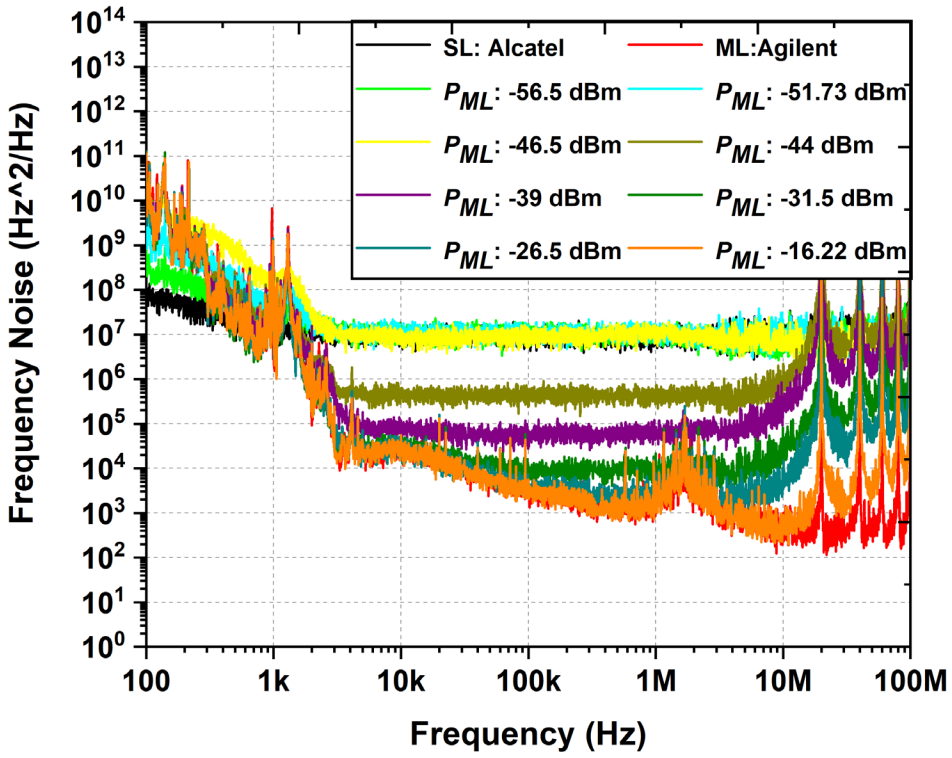

Figure 2. 21: Frequency noise of the mixing between the output signals from *Alcatel* and *Agilent* laser.

The evolution of the frequency of noise when two different coherencies are mixed is shown in the Figure 2. 22. The two lasers with different coherencies are Alcatel laser and Agilent laser. The frequency noise transfer curves shown in Figure 2. 22 looks like the frequency noise curves of optical injection with Alcatel slave laser and Agilent master laser as shown in Figure 2. 18 and Figure 2. 19.

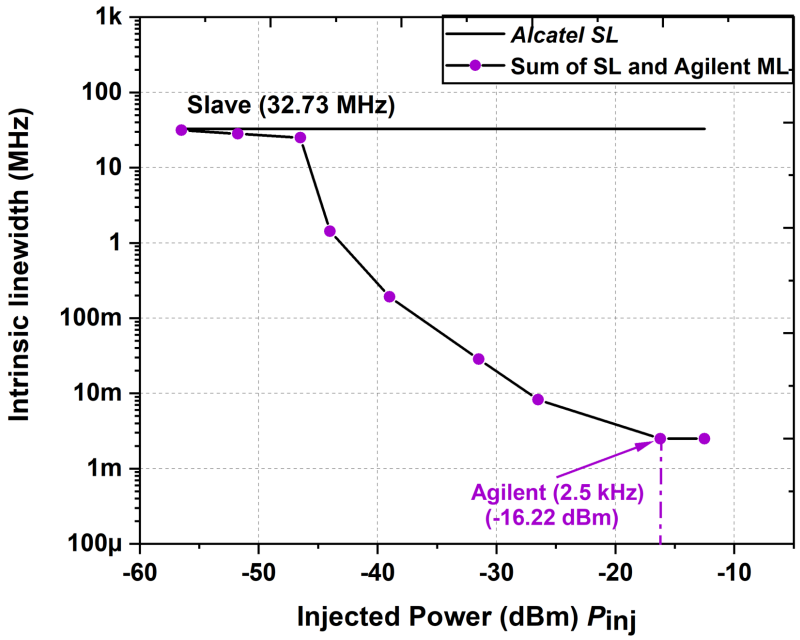

(a)

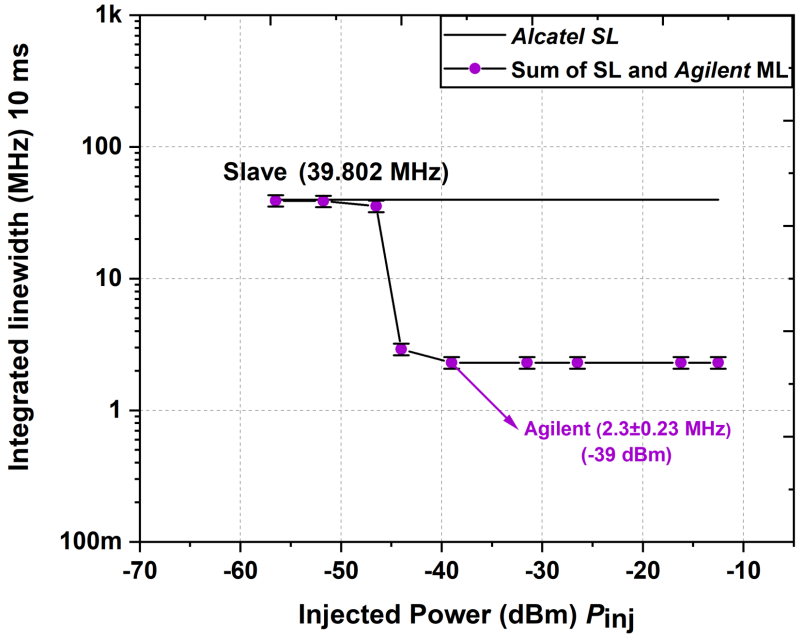

(b)

Figure 2. 22: The evolution of frequency noise of the mixing of 2 signals of different coherencies with injected powers. (a) Intrinsic linewidth (b) Integrated linewidth.

	Injected power for intrinsic linewidth transfer (dBm)	Injected power for integrated linewidth transfer (dBm)
Optical injection with SL: *Alcatel* & ML: *Agilent*	-16.27	-41.5
Addition of 2 coherencies: Alcatel & Agilent	-16.22	-39

Table 2.2: Comparison of the required optical power necessary to get the frequency noise of the master source (or of the more coherent source) when using optical injection or the mixing of two signals (one being more coherent than the other one).

The comparison between frequency noise transfer using optical injection and through the addition of 2 coherencies are shown in Table 2.2. For ease of understanding, the lasers used for both experiments are the same. The *Alcatel* laser has an integrated linewidth of 39.8 ± 3.9 MHz and an intrinsic linewidth of 32.73 MHz ($h_0 = 1.04 \times 10^7 Hz^2/Hz$) and *Agilent* tunable laser, with an integrated linewidth of 2.15 ± 0.2 MHz and an intrinsic linewidth of 2.5 kHz ($h_0 = 7.96 \times 10^2 Hz^2/Hz$). The injected power required for the transfer of intrinsic linewidth via optical injection is -16.27 dBm, and by taking the sum of the two lasers is -16.22 dBm. This value may be compared to the Slave (Alcatel) emission (-4 dBm) at 1.1 times its threshold current (19.8 mA) power so that the relative ratio "Agilent power / Alcatel power" ("coherent laser / less coherent laser" or "master power / slave power") is -12.3 dB corresponding in percentage to 5.9 % of the Slave power. Similarly, the power required to transfer the integrated linewidth in both cases is -41.5 dBm and -39 dBm. The results obtained by mixing the output signals of the Alcatel slave laser and the Agilent master laser is similar to the transfer of purity using optical injection with Agilent laser.

2.8 Conclusion

This chapter started with the basic introduction and general properties of optical injection. An overview about the work by previous work done in optical injection Institut Foton were also discussed. We then introduced the theory of the Airy function of a laser and Airy function of an optically injected laser. The architecture of optical injection experimental setup used in my thesis was presented.

We then evaluated the transfer of purity using optical injection with *Tunics-PR*, *Tunics-OM*, *Agilent* and homemade *Tunics-OM BFL* master lasers with different coherencies. *Tunics-OM BFL* master laser had an intrinsic linewidth of 1.1 Hz, *Tunics-PR* 31.4 kHz and *Tunics-OM* and *Agilent* had similar intrinsic linewidths of 3.1 kHz and 2.5 kHz. We experimentally proved that more the coherent the master laser, the higher the power required to achieve the full coherency transfer. However, *Tunics-OM BFL* master (1.1 Hz) achieved the complete coherency transfer for an injected power of -12.5 dBm, which is ~4 dB more than *Tunics-OM* (3.1 kHz*)* at -16.2 dBm, or *Agilent* (2.5 kHz*)* at -16.27 dBm. On the contrary, the increase of injected power to reach the locking threshold is much higher (15 dB) between these two last lasers and the *Tunics-PR* (31 kHz*)* at an injected power of -31.5 dBm.

The mixing of Alcatel slave and Agilent master signals showed similar performance to the optical injection experiment where the master signal is seeded into the slave laser cavity.

The transfer of frequency noise properties from a master laser to a slave laser is an old field of physics. This study reveals the role of the coherence of the master laser in triggering the locking for optical injection when the injected power is varied. The conclusion is that to use optical injection for the transfer of the coherency, the price to pay seems to be limited when going down to very narrow linewidth (1 Hz).

These results are encouraging to state that the transfer of coherency is possible for reasonable optical power.

CHAPTER 3. DISCUSSION, CONLUSION AND PERSPECTIVES

3.1 Discussions

3.1.1 General concepts

In the previous chapter, I have shown that when the injected power is varied, below the power-threshold of frequency locking, the frequency noise of the injected laser is quite similar to the one obtained by the simple mixing of the two signals, the one of the master and the other one of the slave. This similarity is directly linked to the expression of the power spectral density of the injected laser, given in equation 2.38, that could be summarized by:

$$y_{IS}(x) = y_{Modified\ Solitary\ Slave}(x) + y_{Master-Slave}(x) \qquad 3.1$$

The first term is exactly identical to the PSD of the solitary laser (equation 2.35), except that the operating point is affected by the optical injection. In other words, only Y is changed when compared to the solitary laser. The second term contains the effect of optical injection.

To fully understand this sum, one should recall basic properties of the transfer function generalized to a laser:

1. Increasing the term $S_S(x)$ broadens the laser line following the Schawlow-Townes formula (equation 2.33). The optical injection will have a minor effect on the total

optical intensity. Thus, we should be careful when reading 2.35 for which $S_S(x)$ appears in the numerator: $Y_S = \int y_S(x)dx$ is not proportional to $S_S(x)$.

2. Following this same formula, increasing Y will decrease the linewidth.
3. The total intensity Y is mainly fixed by the pump (or bias current the normalized pump parameter r): Y = r -1. It is given by a complex implicit equation 2.27 due to the fact that in 2.35, $y_S(x)$ is function of its own integral Y due to the saturated gain given by equation 2.11, $g = \frac{g_0}{1+Y}$.
4. The true solution $Y = Y_L + \delta Y$ has a standard deviation δY (see equation 2.30), which is typically 3 to 5 orders of magnitude lower than the Lamb solution, given by $equation\ 2.26$: $Y_L = r - 1$, so that it is negligible when considering the expression of the total intensity. However, this small quantity is very important to avoid that the transfer function (equations 2.20, 2.21) diverges at laser threshold; the condition gain equal losses (equation 2.24) leads to a divergence of the transfer function. δY in 2.30 is proportional to the spontaneous emission S, to $\frac{(1+Y_L)^2}{Y_L}$ and inversely proportional to g_0, so that the total intensity of a laser is very slightly dependent on the spontaneous emission.

3.1.2 Transfer of coherency

When the laser is submitted to optical injection, it consists to add to S_S (equation 2.37) an external term $\eta y_M(x)$, in which η is the coupling coefficient that gives the fraction of the external field (PSD of the external source) that it transmitted through the coupling face

with $\eta = \sqrt{1-r_2^2}\sqrt{f_c}$, considering equation A1 from Annex 1. If we consider a perfect stability, that means just the influence of spontaneous emission, equation 3.1 gives the way the internal spontaneous emission and the external source will compete.

It leads to the second term of equation 3.1 and one can state:

$$y_{IS}(x) = T_S(x)S_S + T_S(x)\eta y_M(x) \qquad 3.2$$

With the transfer function associated to the Slave

$$T_S(x) = \frac{1}{A_S^2 e^{-L_S+G_S}} \frac{1}{\mathbb{\Gamma}_S^2 + (x-x_S)^2}$$

The optical injection will not fundamentally change the total intensity of the injected slave, given by the more complex equation 2.40 as the number of the injected photons is of the order of the number of spontaneous photons or some orders of magnitude bigger, but much lower than the number of stimulated photons.

As a matter of fact, from equation 2.40, the master power spectral density that has to be considered added to the spontaneous emission S_S, is the master intensity filtered by both laser lines (master and slave): $\frac{\eta Y_M}{\pi(\mathbb{\Gamma}_S+\mathbb{\Gamma}_M)}$.

Then we can consider that the spontaneous emission is modified to $S_S + \frac{\eta Y_M}{\pi(\mathbb{\Gamma}_S+\mathbb{\Gamma}_M)}$ so that the total intensity of the injected slave will be slightly modified and can be considered to be $Y_{IS} = Y_L + \delta Y$ with $Y_L = r - 1$ and

$$\delta Y_{IS} = \frac{\pi(1+Y_L)^2}{A g_0 Y_L}\left(S_S + \frac{\eta Y_M}{\pi(\mathbb{\Gamma}_S+\mathbb{\Gamma}_M)}\right) \qquad 3.3$$

It follows that the first term in 3.2 (or 3.1) is basically the line of the slave laser. However, with optical injection, it is submitted to a slightly increased intensity for $\eta \neq 0$.

The spectral line of the first term remains almost the same with η but its linewidth may be slightly reduced (following Schawlow-Townes formula).

The second term in 3.2 (3.1) has a fixed line shape by the master source ($y_M(x)$) that does not depend on the slave parameters. It could be considered as a fixed filter that modifies the transfer function T_S of the slave.

When the injected power or η is increased from a null value, the transfer function will split the energy between the two lines by emptying the first term and filling up the second. Increasing η will favor the second term and its filtering effect so that the main effect for the injected laser is on its linewidth and not on its optical intensity. This is illustrated by the figures 3.1 (experiment) and 3.2 (theory).

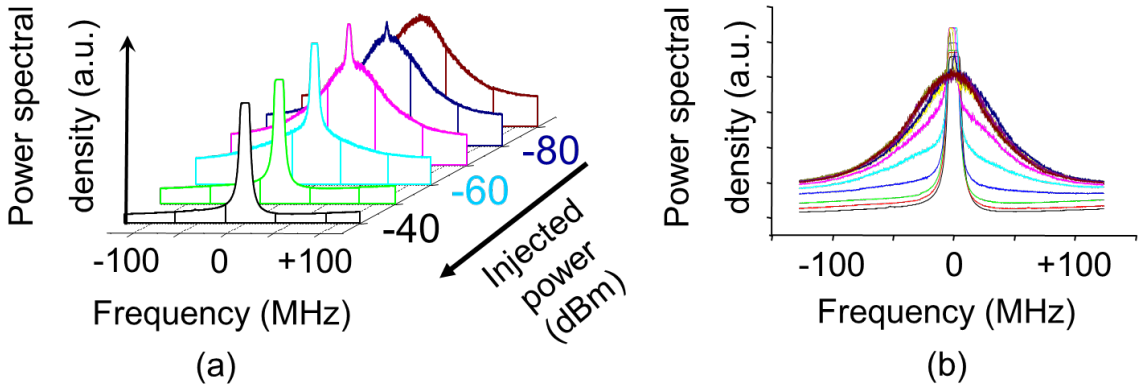

Figure 3.1: The experimental evolution of the optical spectra of a laser submitted to optical injection when the injected power is increased. (a) Waterfall representation of the injected laser lines; (b) Superposition of the different lines to reveal the progressive transfer of energy between the two lines.

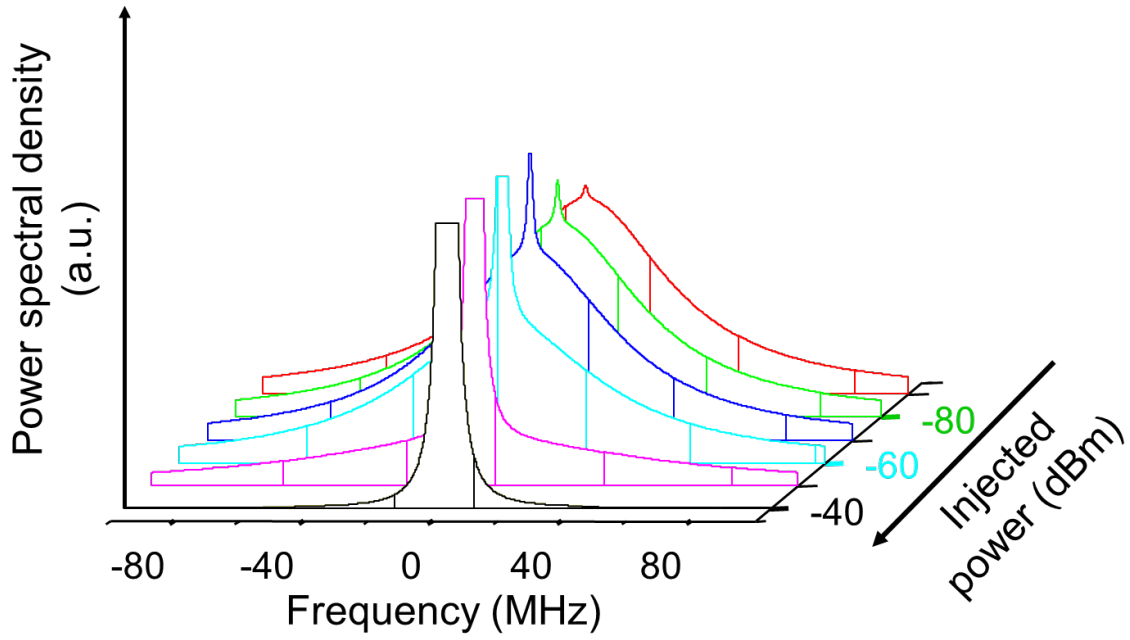

Figure 3.2: Typical optical spectra obtained by the generalized transfer function for an injected laser using the formalism given in section 2.4.

As η increases, the first term loses energy (or photons), while the second term is amplified with an increase of its total intensity. The bandwidth of the second term being fixed by the master, an increase of its energy will increase the peak power (or intensity).

We have then identified that the injected slave PSD is the sum of two terms with almost constant characteristics. Thus equations 3.1 and 3.2 may be written by introducing the laser Lorentzian line shape for the solitary slave ($\mathcal{L}_S(x)$) and for the master line ($\mathcal{L}_M(x)$):

$$y_{IS}(x) = coef_S(\eta)\mathcal{L}_S(x) + coef_M(\eta)\mathcal{L}_M(x) \qquad 3.4$$

With $\mathcal{L}_i(x) = \frac{1}{\mathbb{\Gamma}_i^2+(x-x_i)^2}$, I = M or S.

The coefficients $coef_S(\eta)$, $coef_M(\eta)$ are function of η and are giving through the calculation explained in section 2.4. $coef_S(\eta)$ is decreasing (towards 0) along with η and $coef_M(\eta)$ is increasing (starting from 0 for $\eta = 0$) while maintaining an almost constant intensity.

Note that here the second term, which is the product of the master line and of the solitary slave line, could be reduced to the master line as there is a null detuning and as the line of the solitary slave laser is quite broad (32.73 MHz).

The frequency noise could be deduced from relation 1.14. However, great care has to be taken in manipulating this formula. Thus, if two optical Lorentzian lines are mixed ($\mathcal{L}_a$ +$\mathcal{L}_b$), each line is characterized by a white noise (h_0^a, h_0^b). Note that applying formula 1.14 to the sum $h_0^a + h_0^b$ will generate a Lorentzian laser line with a linewidth $\pi\left(h_0^a + h_0^b\right)$, which is not at all the sum of two different Lorentzian lines. The formula 1.14 has to be applied to each term of the sum $h_0^a + h_0^b$, which corresponds to the mixing of uncorrelated fields. Then the sum of optical lines will correspond to a sum of two white noise each obtained by taking the inverse operator associated to 1.14. Thus, both terms can be associated to two white noise $h_{\text{modified slave}}$ and h_{master} that are added in the electrical domain corresponding to the linewidths $\pi\, h_{\text{modified slave}}$, $\pi\, h_{\text{master}}$.

The frequency noise is then given by:

$$h_0 = coef_S(\eta) h_{\text{modified slave}} + coef_M(\eta) h_{Master} \qquad 3.5$$

It shows that the frequency noise is the sum of two terms.

The transfer function has shown its ability to perfectly reproduce the optical spectra and thus the evolution in the electrical domain.

We can guess what will happen with an increase of coherency. Consider an operating point with a given η, with fixed master and slave characteristics (linewidth, pump current …), changing only the master linewidth will not modify the total intensity of the injected laser as explained earlier.

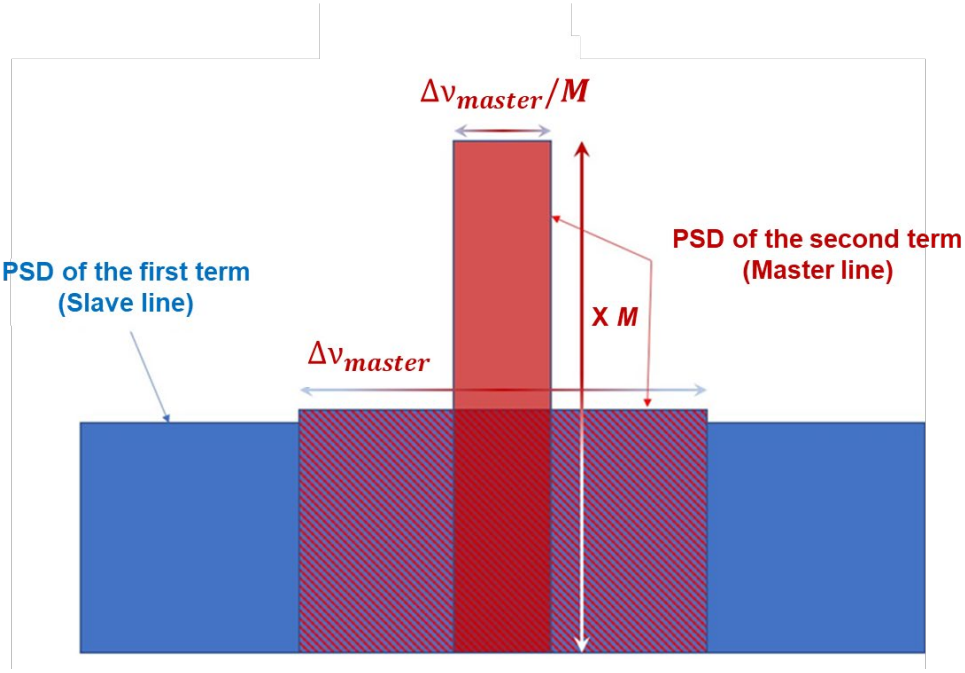

Figure 3.3: Schematic illustration of the variation of the master linewidth. When it is decreased, the contribution of the slave line increases.

Assume that the PSD $\eta y_M(x)$ of the external injected signal, instead of having a Lorentzian shape, has a rectangular shape $\left(with\ a\ PSD\ level\ of\ \frac{\eta Y_M}{\pi(\mathbb{\Gamma}_S+\mathbb{\Gamma}_M)}\right)$. As the slave line is broad

(32.73 MHz in our case), we can consider it as constant on the master band. This is illustrated in Figure 3.3 by the blue rectangular. If we consider that the coefficients in 3.5, which are obtained from the transfer function, are directly linked to the number of photons, then it can be clearly seen that decreasing the master linewidth by a factor M will increase the PSD level by the same factor M. If we assume that initially the master PSD (hatched rectangle) and the slave laser PSD $S_S(x)$ are at the same level, there will be a supplementary contribution of the slave line (first term in 3.1) of approximatively 1-1/M in percentage of the total injected master power. Then a decrease of 1/M of the linewidth will imply an increase of 1-1/M of the injected power to compensate for the supplementary photons in the first term. This leads to a contribution of 2-1/M. This reasoning tends to prove that to recover an equivalent frequency noise for the injected slave laser, η should be increased by a ratio that is not equivalent to the linewidth decrease but is at best 3 dB (which is not so far from the results of 4 dB with a master linewidth of 1.1 Hz). This reasoning fails to explain the increase in the frequency locking threshold when the laser linewidth is reduced from 30 kHz to 3 kHz.

Decreasing the master linewidth by a factor M, will decrease h_{Master} by the same factor and equation 3.5 is then written:

$$h_0 = coef_S(\eta)\mathrm{h}_{\text{modified slave}} + coef_M(\eta)\frac{h_{Master}}{M} \qquad 3.6$$

We have mentioned that the first term is mainly governed by the total intensity Y_{IS} of the injected slave. It turns out that looking at equation 2.40 that gives Y_{IS}, we can say if $\mathbb{\Gamma}_S \gg \mathbb{\Gamma}_M$ and if the only parameter that is changed is $\mathbb{\Gamma}_M$, Y_{IS} will remain the same so that the first term in equation 3.6 will remain identical. Thus, dividing the second term by M

(equations 3.5 and 3.6) and as we know from equation 3.2 that the second term is proportional to η $(T_S(x)\eta y_M(x))$, one has to increase η to recover the same h_0 in 3.5. To explain the experimental observation and get the exact value of $coef_M$ (η), it will be necessary to come back to the transfer function and its complexity (the mixing is through the amplifying medium and the experimental observation at 1 Hz tends to prove that the former deduction is not correct in that case).

Future work in the laboratory, following this thesis, will use this model to compare to my experimental results.

3.1.3 Transfer of the stability (Low Frequency components)

In itself, equation 3.1 (or 3.2) does not contain the slow components that reveals the stability of the central frequency. One has to add the statistical law of the central-frequency $(\nu_0 \; or \; x_0)$ fluctuations of the master and slave laser $(\nu_S \; or \; x_S, \nu_M \; or \; x_M)$, which is not realized in this Ph.D. work. Contrary to the assumption made in section 2.4 ($x_M = x_S = x_0$), one has to distinguish in this case the frequencies of the master x_M and of the slave x_S, as they suffer from different fluctuations. However, one can infer some properties from the generalized transfer function.

The first term in equation 3.1 (or 3.2) will only contain the low frequency fluctuations of the slave line. This term will cancel out with the increase of η.

The second term contains the fluctuations of the slave through T_S and of the master through y_M (equation 3.1). Nevertheless, one should keep in mind that the true function is the

multiplication found in the second term of 3.1. In our study, $T_S(x)$ is broad (linewidth superior to 32.73 MHz). As a matter of fact, $y_M(x)$ is almost a Dirac function when compared to $T_S(x)$ so that the second term in 3.2 can be written as $T_S(x_M)\eta y_M(x)$ with

$$T_S(x_M) = \frac{1}{A_S^2 e^{-L_S+G_S}} \frac{1}{\mathbb{\Gamma}_S^2+(x_M-x_S)^2} \quad 3.7$$

$T_S(x_M)$ is affected by both the fluctuations of the master frequency ν_M *or* x_M and of the slave frequency ν_S *or* x_S. This factor can bring noise to η. As T_S has a bandwidth greater than 32.73 MHz, fluctuations even in the range of 1 MHz has minor effects on the transmission given in 3.7.

The line shape of the second term is the one of $y_M(x)$ so that the stability of the second term is the one of the master.

Thus, in the low frequencies, the frequency noise of the optically injected laser will be that of the master, which imposes its stability with an increase of η.

It has been proved that this transfer can be made from a metrological reference signal [140].

A good picture is to consider the line of the solitary slave laser as noise with a given bandwidth over which the lasing frequency has to be fixed.

As mentioned formerly, the transfer function given in this manuscript does not consider the noise contribution in the low frequency band. It will require further development.

If the integrated linewidth is a good indicator, it does not describe finely the evolution of the PSD. For example, as seen by figure 2.9 b, 2.11 b, 2.13 b, 2.15 b, the complete transfer of frequency noise requires less power at low frequencies. The transfer is acquired below

1 kHz for less injected power than between 1 kHz and 10 kHz. That could be understood as the law for the noise frequency is of the form f^{α}: the PSD is more important at low frequencies. As a matter of fact, the coefficient α will continuously vary from the slave α to the master α when increasing the injected power. These observations are briefly described in Annex.4.

Finally, the power in one Hertz associated to the central-frequency fluctuations at a given (low) frequency is higher than the white noise associated to the spontaneous emission. It is why the master frequency drifts (flicker, random walk …) are first transferred to the injected laser. The required injected power to transfer the central frequency fluctuations is lower than the one required for the coherence transfer as shown in chapter 2.

3.2 Conclusion

In this manuscript, we have studied purity transfer using optical injection in the case of extremely coherent laser. Optical injection is the unidirectional coupling of two lasers, called slave and master. The main idea is to be able to distribute coherency among different sources. For this study, we have developed a highly coherent laser with selectable wavelength on the C-band by using Brillouin effect. We have obtained 3 mHz intrinsic linewidth. We can wonder what the lower limit of linewidth is when using a more coherent pump or having more Brillouin lasers in cascade. It could be difficult to compare this to the Schawlow-Townes limit, which applies to a different case (simulated emission and spontaneous emission from a collection of excited atoms). With a quality factor $Q = 5x10^8$, one can estimate, for an output P_{out} = 10 mW the Schawlow-Townes linewidth (full width

at half-maximum) to be below around 1 µHz (6 µHz if we take the Lax formula: $\Delta\nu_L = \frac{\pi h \nu_0 (\Delta\nu_{cav})^2}{Pout}$, with $\Delta\nu_{cav} = \frac{\nu_0}{Q}$). However, the community admits that the transfer function associated to the phase transfer from the pump to the Stokes component has a modulus lower than one (equations 1.1 and 1.2). So, the linewidth of the Brillouin laser spectra is decreased by a factor K < 1 (equation 1.4) when compared to that of the pump. Thus, the question of the limit for the lowest linewidth that could be obtained is an open question.

To study the transfer of purity, two methods were analyzed. One is to use the signal ratio between the maximum of the laser line of the injected signal corresponding to the master line and the solitary slave laser line. The other one is to use frequency noise, which fully characterizes the spectral properties of a laser. Such analysis was not performed in the past for optical injection. After having introduced the physical notions associated to such characterizations and discussing the stability and coherency of a laser, we use different tunable sources with very different linewidths to study the purity transfer when the spectral properties of the master laser is then varied. When looking for the minimum power necessary to observe frequency locking, we have shown that the analysis is very different when using the signal to noise ratio rather than the frequency noise.

In the first case, the minimum power required decreases when the master coherency increases. The price to pay is to have a sufficient narrow filter to observe the signal ratio.

In the second case, we have to distinguish two contributions: one from the spontaneous emission, which acts as a white noise; the other one, is due to fundamental and technical noises, which follows a $1/f^{\alpha}$ law in the low-frequency band of the electrical domain. In both cases, the transfer is progressive along with the injected power. We discuss the

experimental results, showing how a transfer function generalized to the laser gives insight to this nonlinear interaction. It turns out that in the amplification regime of the laser, which is in the range of injected optical power, characterizing the threshold of frequency locking (a few 100's nanowatts), the higher is the coherence, the more power is needed to get a complete transfer. This assumption is not verified when using laser with a thinner linewidth of 1 Hz as the additional optical injected power to reach the locking threshold is 4 dB above the one necessary for a linewidth of 3 kHz.

3.3 Perspectives

This work has enabled the laboratory to design coherent laser with selectable wavelength is the C-band. Obtaining ultra-coherent lasers only makes sense if the relative stability of the laser frequency is of the order of the coherence width for a given observation time. As already mentioned, an intrinsic linewidth of one Hz (mHz) is associated to a relative stability of 5×10^{-15} (5×10^{-18}), which requires metrological approach [68] or a metrological reference signal [80, 81]. This kind of signal will be provided to the Institut Foton by the Equipex T-Refimeve in a few years.

The actual results open the way to Schawlow-Townes linewidth limited laser (or at least to tackle the values given by the Schawlow-Townes limit). There is a challenge to characterizing and measuring very narrow intrinsic linewidth (nHz-µHz).

Highly coherent C-band laser with tunability will permit the study of the dynamics of lasers submitted to optical injection by highly coherent sources as it could have been done for optical feedback [141-143]. Such sources could also improve the coherency of frequency

comb through simple technique [140, 144]. The laboratory has shown the possibility to use the laser as a detector [136] by taking advantage of the coherency. With 100 kHz linewidth sources, detection of a femto-Watt CW optical signal at room temperature was demonstrated as well as the possibility to detect 100 photons.

ANNEXES

Annex.1 Calculation of the coupling coefficient in optical injection

The injected field is added to the differential equations (that can be found in [93]) by replacing the reflectivity of the coupling facet r_2 by an effective reflectivity r_{eff}:

$$r_{eff}E_{Slave}(t) = r_2E_{Slave}(t) + \sqrt{1-r_2^2}\sqrt{f_c}E_{Master}(t) \qquad \text{A. 1}$$

So that,

$$\frac{r_{eff}}{r_2} = 1 + \frac{\sqrt{1-r_2^2}}{r_2}\sqrt{f_c}\frac{E_{Master}(t)}{E_{Slave}(t)} \qquad A. 2$$

This last factor the usual losses by replacing the reflectivity r_2 of the coupling facet by r_{eff}. The photon lifetime τ_p (in s^{-1}) gives the losses (in m^{-1}). The photon lifetime τ_p and the losses are linked by a simple factor, the group velocity v_g:

$$\frac{1}{\tau_p} = v_g\left(\alpha_a + \frac{1}{2L}ln\left(\frac{1}{r_1r_2}\right)\right) \qquad \text{A. 3}$$

With $v_g = \frac{c}{n_g}$ (c being the velocity of light, n_g the group index); α_a are the losses mainly due to the materials (not to be confusing with the losses linked to the laser optical transition); r_1, r_2 are the field reflectivity of the first and the second facet of the cavity.

By replacing r_2 by r_{eff}, the global losses that includes the seeding light are written:

$$v_g\left(\alpha_a + \frac{1}{2L}ln\left(\frac{1}{r_1r_2} * \frac{r_2}{r_{eff}}\right)\right) = \frac{1}{\tau_p} + \frac{v_g}{2L}ln\left(\frac{r_2}{r_{eff}}\right) = \frac{1}{\tau_p} + \frac{1}{\tau_{cav}}ln\left(\frac{r_2}{r_{eff}}\right) \qquad \text{A. 4}$$

Actually, in the usual differential equation, the term $-\frac{E_{Slave}(t)}{\tau_p}$ is replaced by $-\frac{E_{Slave}(t)}{\tau_p}+\frac{E_{Slave}(t)}{\tau_{cav}} ln\left(\frac{r_{eff}}{r_2}\right)$. So that, to take into account optical injection, one has to add the following term to the expression of the derivative of the field $E_{Slave}(t)$:

$$\frac{E_{Slave}(t)}{\tau_{cav}} ln\left(\frac{r_{eff}}{r_2}\right) = \frac{E_{Slave}(t)}{\tau_{cav}} ln\left(1+\frac{\sqrt{1-r_2^2}}{r_2}\sqrt{f_c}\frac{E_{Master}(t)}{E_{Slave}(t)}\right) \quad \text{A. 5}$$

For low injected power, the development of the logarithm (ln(1+x) ~x) induces:

$$\frac{E_{Slave}(t)}{\tau_{cav}} ln\left(1+\frac{\sqrt{1-r_2^2}}{r_2}\sqrt{f_c}\frac{E_{Master}(t)}{E_{Slave}(t)}\right) \approx \frac{1}{\tau_{cav}}\frac{\sqrt{1-r_2^2}}{r_2}\sqrt{f_c}E_{Master}(t)$$

$$= +\kappa_{inj}E_{Master}(t) \quad \text{A.6}$$

The equation for the derivative of the Slave field is modified by adding to its expression:

$$+\kappa_{inj}E_{Master}(t)$$

$$\left(\kappa_{inj} = \frac{1}{\tau_{cav}}\frac{\sqrt{1-r_2^2}}{r_2}\sqrt{f_c}\right).$$

Annex.2 Some results from Institut Foton

Marc Bondiou's work[86] drew a view of the spectral properties of a DFB semiconductor laser at 1550 nm subjected to optical injection. He observed, as known, that for a slave laser operating far from threshold, the width of the locking range increases with the injected power of the master laser and that the locking area curves towards the negative detuning side at high powers in the optical injection mapping (the graph plotted in the phase space using injected power versus detuning). The observed width of the bistability domain also increases in the negative detuning side, along with the injected power. Non-linear regimes such as multi-wave mixing, period doubling and chaos were observed for moderate to high injected power, in agreement with different observations made for semiconductor lasers. When slave lasers are operating close to threshold the spectrum of the injected slave contained two frequencies, one at the master frequency and the other one at a frequency close to the one of the free-slave laser. Depending on the injected power, when the detuning decreases, the slave-laser frequency is pulled (at low injected power, the slave frequency seems to be attracted by the master frequency) or pushed (at moderate or high injected power; this property is linked to thermal effects, due to the injected power, which causes an index change). Spectral properties reveals the variations in the linewidth of the injected slave. It becomes the same as that of the master laser irrespective of the linewidth of the free-slave laser.

Renaud Gabet[87] continued the study started by Marc Bondiou. In his work he showed the modifications of the optical spectrum of the slave laser for a narrow linewidth master laser and very weak optical injected powers of the order of pico-watts to nano-watts. It was the first experimental demonstration of a laser used as an amplifier, subject, which was

discussed in the 70's. Above the microwatt regime, the energy distributed in the slave spectral line is totally transferred to the master line. Renaud Gabet did a rigorous measurement of the optical gain of the laser used as an amplifier (gains of order of 10^5 is achieved, which corresponds to the fact that one spontaneous photon or one seeded photon (opticall injected photon) generates 100 000 stimulated photons through the laser process). Renaud Gabet also performed the detection of low powerful signal using heterodyne technique[136]. Low power of the order of femtowatt was detected at room temperature for a CW laser and for seeded photons over a time slot of a few milliseconds, 1000 photons were detected. The best result was obtained for laser operating near the threshold. He performed a thorough study of optical injection when the slave laser is operating close to threshold at 1.2 (times the threshold) and he made also this study at 4 times threshold to check the validity of his results when compared to previous observations. When close to threshold, the slave laser behaves more like an amplifier with an optical spectra composed of the slave line and of the amplified master. However to to the nonlinear laser process, the picture could be more complex and he observed simple regime like locking and/or the presence of multi-wave mixing. Chaos was not found. For sufficient injected power, locking over the the whole frequency range was identified, showing that the injected laser is lasing on the master line. A bimode regime[94] may appear.

For laser operating far from threshold (typically 4 times), he observed more complicated regimes (relaxation, chaos, period doubling). He identified the presence of bistability, which was not identified in the literature.

The detailed study of optical injection using the semiconductor lasers from Institut Foton helped to lay the foundation of Stéphane Blin's Ph.D. thesis[123]. He identified four areas of optical injection according to the injected powers.

For very weak optical injected (injected powers less than about -60 dBm or the nanoWatt), the optical spectra (or laser line) of the injected slave laser is not modified and is the one of the solitary slave laser.

For weak optical injected power (injected powers above about -60 dBm and less than around -30 dBm or the μWatt), the slave laser behaves as an optical amplifier when the master laser is more coherent than the slave. The appearance of a linearly amplified component at master frequency in the lineshape of injected slave laser depicts the transition from very weak injection to weak injection. Stéphane Blin defines a locking frequency threshold, which correspond to the minimum injected optical power necessary to obtain frequency locking, which corresponds to a complete transfer of the spectral properties of the master laser to the ones ones of the injected laser.

Moderate optical injection (injected powers greater than -30 dBm and below about -10 dBm) is the range of the usual published results with the appearance of wave-mixing, relaxation, period doubling, chaotic regimes. The saturation of the amplification of the master component denotes the transition from weak to moderate optical injection.

High optical injection (high injected power) is characterized by bistability as observed by Gabet. Locking, chaos, single,double, quadruple, wave mixing and relaxation regimes were observed when injected power was increased from medium injected powers to high injected-power level. For low power injection, the slave laser is considered as an amplifier

for very weak coherent signals. The slave laser acquires the coherency of the master laser progressively when the injected power is increased. A theoretical study based on Airy function generalised to laser was developed. It was helpful in describing the spectral propeties of optically injected slave like the spectral shape of the injected slave laser. Thus, the progressive transfer of coherence from the master to the slave laser was predicted, as wall as the evolution of the gain of the slave laser, used as an optical amplifier for low-owerful coherent signal. The slave behavior when injected by weak signals was stuided for a non-zero detuning. He proposes a linewidth measurement method using these properties, by comparing the gain curves of a slave laser with different linewidths. He showed that coherent lasers (with linewidth less than a few kHz's) can be characterized.

The goal of Ph.D. thesis of Olivier Vaudel was to study the synchronisation of semiconductor lasers by realizing a cascade of injected lasers. It enables him to study chaos synchronization as well as continuous or time varying signal [93]. He measured and calculated the correlation between two injected lasers, in order to characterize the synchronization. He demonstrated the close link between synchronization and injection process through this correlated parameter. He also showed the possibility of transmitting relaxation, multi-excitability [139].

Céline Guignard in her Ph.D. thesis[124] performed the study and realisation of pulsed sources consisting of a semiconductor laser submitted to optical feedback by a non-linear mirror or fiber Bragg grating. Her numerical model based on the extension of Lang and Kobayashi model allowed to show that the frequency modal structure of a laser subjected to non-linear feedback depends on the characteristics of the mirror as well as of the injection current. She also analyzed semiconductor lasers submitted to optical feedback by

fiber Bragg grating and extended the study to the influence of optical injection on the dynamics of Fabry-Perot laser submitted to filtered feedback[127]. She observed a rich variety of dynamics for a semiconductor laser submitted to both optical injection and filtered feedback when the laser is biased close to its threshold.

Julien Poette contributes to the study of the amplitude noise of lasers dedicated to optical telecommunications [145]. He also studied the transfer of relative intensity noise [137] when a semi-conductor laser is optically injected.

Quoc Thai Nguyen [146] demonstrated the ability of optical injection to fix the wavelength of an achromatic laser component for a passive optical network (PON) for access, while respecting the normalizations imposed in international standards.

Jean-Francois Hayau [125] studied quantum dots and quantum dashes lasers in terms of intensity noise and optical injection. A theoretical study showed the major influence of the wetting layer in the noise properties of quantum dot lasers in agreement with the experimental study. He developed an analysis of the interaction between the modes of a multi-frequency laser based on noise measurements. Major differences are observed between a bulk (or DFB) laser and a quantum-dot (quantum dash) laser when measuring a correlation coefficient showing the interaction between longitudinal modes (,which is null for QD and equal to -1 for bulk showing an antiphase dynamics). A higher relaxation frequency and a higher damping rate in a quantum dot laser compared to a bulk laser are causing such a different behavior as well as a lower noise. The number of quantum dots planes is of fundamental importance. A smaller number leads to poorer noise characteristics while it also increases to the laser threshold.ptical injection in these

structures shows a behavior very close to that of single mode lasers. Few regimes are encountered in comparison to the injection in a massive multi-mode laser. Moreover he showed the observation of the multi-excitability regime in these structures.

Zhenyu Hao during his Ph.D. thesis made an extensive study of optical injection on quantum dashes DFB lasers [126]. The DFB structure for a quantum dash laser enables a single frequency operation and a closer comparison to a QW DFB laser. As Jean-François Hayau, he also observed, for quantum dash DFB laser, low relative intensity noise with high damping rate when compared to a bulk (or quantum well) DFB laser at 1550 nm. He showed a smaller locking range of 30 GHz compared to that of 100 GHz for a QW DFB laser. All regimes of optical injection like locking, wave mixing, relaxation and chaos are bonly observed close to threshold contrary to the usual observations made for bilk (or QW) DFB laser. A locking zone was present at positive detuning for low pumping rate and medium pumping rate on the mapping of the quantum dash DFB laser.

Annex.3 Comparison of different tunable sources

The tunable lasers in the C-band used for studying the transfer of purity through optical injection is presented here. Tunics-BFLPR, Tunics-OM, Agilent and Tunics-OM BFL was used as master lasers in this thesis. The frequency noise spectrum of the tunable lasers are shown in the Figure A.1. The integrated and intrinsic linewidth is given in the Table A.1.

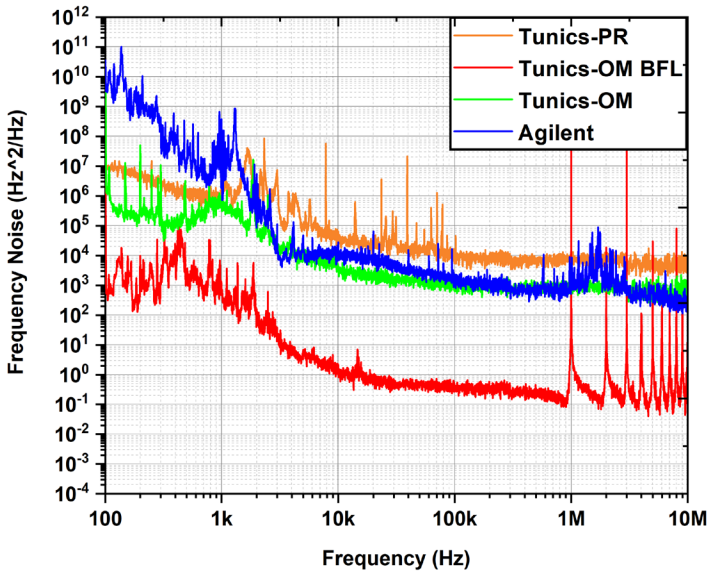

Figure A.1: Frequency noise of tunable lasers used as master lasers in optical injection.

Tunable laser	Integrated linewidth	Intrinsic linewidth
Tunics-PR	332.8±33kHz	31.4 kHz
Tunics-OM	85±8.5 kHz	3.16 kHz
Agilent	2.1±0.2 MHz	2.5 kHz
Tunics-OM BFL	5.1±0.5 kHz	1.17 Hz

Table A3.1: Integrated and Intrinsic linewidths of tunable master lasers.

Annex.4 Measurement of the transfer of low-frequency noise

In this work, the integrated linewidth is used to estimate the low frequency components. It is calculated from the β-line method and has the advantage to include all the technical noise. The parameters $h_{-\alpha}$ and α can be obtained from a simple linear regression. Figure A4.1 shows such kind of calculations. The drawback of this method is that this fitting is not always possible as for the Tunics-OM source, which has a bump around 1 kHz.

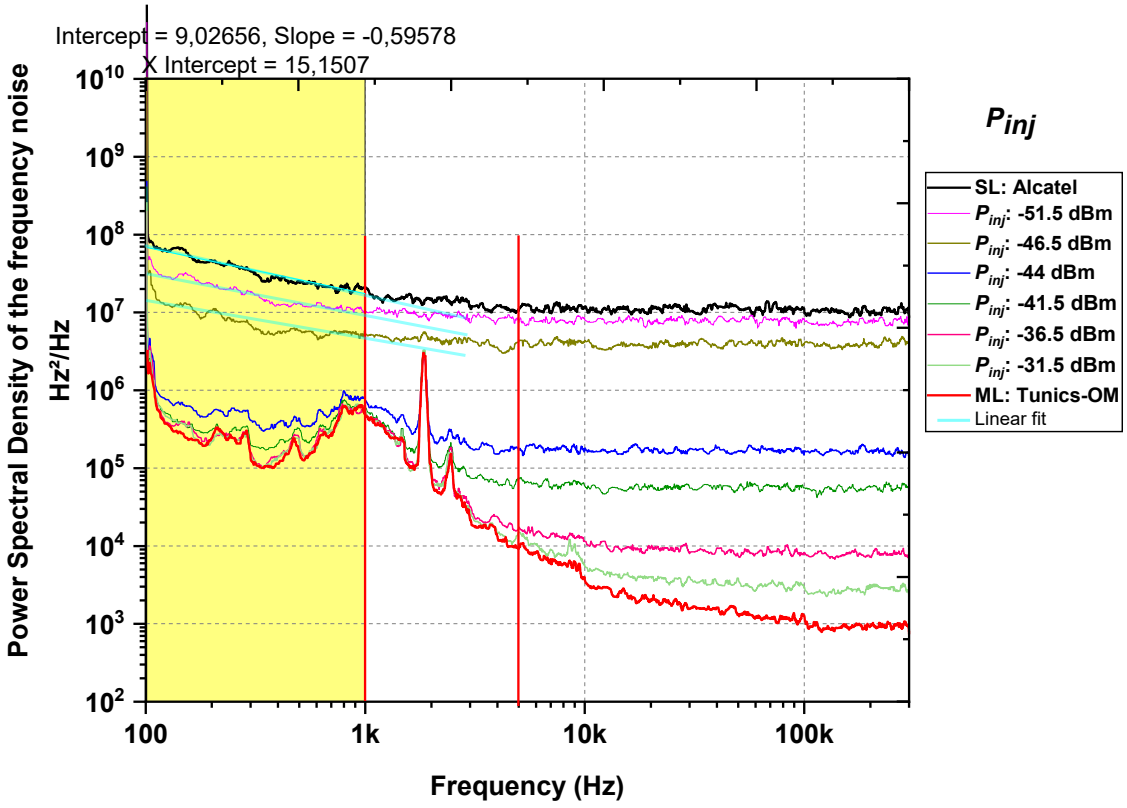

Figure A.2: Frequency noise measurements using Tunics OM and estimation of $h_{-\alpha}$ and α by linear regression.

This difficulty of measurements is noted by crosses (x) in tables A4.1 and A4.2. These two tables show that the calculation of $h_{-\alpha}$ and α will depend on the considered bandwidth (here 100 Hz-1 kHz and 100 Hz – 5 kHz).

Injected Power (dBm)	**α**	**$h_{-\alpha}$ (Hz^3/Hz)**
Alcatel (no injection)	0.59	10^9
-51.5	0.53	4.4×10^8
-46.5	0.46	1.1×10^8
-44	x	x
-41.5	x	x
-36.5	x	x
-31.5	x	x
Tunics-OM	x	x

Table A4.1: Estimation of $h_{-\alpha}$ and α using a bandwidth of 100 Hz – 1 kHz.

Injected Power (dBm)	α	$h_{-\alpha}$ (Hz^3/Hz)
Alcatel (no injection)	0.45	4.4×10^8
-51.5	0.32	1.1×10^8
-46.5	0.29	4×10^7
-44	x	x
-41.5	x	x
-36.5	x	x
-31.5	x	x
Tunics-OM	x	x

Table A4.2: Estimation of $h_{-\alpha}$ and α using a bandwidth of 100 Hz – 5 kHz.

These estimations show a continuous evolution of the parameters $h_{-\alpha}$ and α from the values of the slave towards those ones of the master.

Annex.5 Generalized Airy function for a semiconductor laser

For a semiconductor laser, the gain is expressed:

$$g(N,\nu,I_{tot}) = \frac{\tau_c}{2}\omega_{cv}\chi_i = \frac{\tau_c}{2}\left[\Gamma G_N(N-N_0)(1-\varepsilon I_{tot})\mathrm{sech}\left(\frac{\omega_{cv}(N)-\omega}{\gamma_\perp}\right) - \frac{1}{\tau_p}\right] \qquad A.7$$

Γ is the confinement factor, ε the compression gain, G_N the differential gain, N is the carrier density, N_0 the carrier density (per m^3) at transparency (carrier density for which the gain is equal to zero), τ_p is the photon lifetime, τ_c the cavity round-trip time, $\gamma_\perp$ is the gain linewidth, linked to the relaxation time of the coherence terms or the dipoles relaxation, $\omega_{cv}(N)$ is the angular laser frequency, I_{tot} is the total photon density (per m^3).

The evolution of the carrier density is given by:

$$\frac{dN}{dt} = J - \frac{N}{\tau_e} - \left(\Gamma G_N(1-\varepsilon I_{tot})(N-N_0)\mathrm{sech}\left(\frac{\omega_{cv}(N)-\omega}{\gamma_\perp}\right)\right) I_{tot} \qquad A.8$$

Where J is related to the bias current (J multiplied by the electron charge and the volume).

The stationary value N_{stat} is then:

$$\Gamma G_N(N_{stat}-N_0) = \Gamma G_N \tau_e \frac{J-\frac{N_0}{\tau_e}}{1+\Gamma G_N \tau_e \mathrm{sech}\left(\frac{\omega_{cv}(N)-\omega}{\gamma_\perp}\right)(1-\varepsilon I_{tot})I_{tot}} \qquad A.9$$

The phase could be expressed as:

$$\phi_\chi = (\omega-\omega_0)\tau_c + \phi(N,\nu,I_{tot}) \qquad A.10$$

With

$$\phi(N,\nu,I_{tot}) = \frac{\nu}{\nu_{cv}}\tau_c\frac{\alpha}{2}\left(\Gamma G_N(N-N_0)\mathrm{sech}\left(\frac{\omega_{cv}-\omega}{\gamma_\perp}\right) - \frac{1}{\tau_p}\right) \qquad A.11$$

Thus, the Airy function is expressed as:

$$I(\nu) = \frac{S(\nu)}{\left(1-e^{G(N,\nu,I_{tot})}\right)^2 + 4e^{G(N,\nu,I_{tot})}\sin^2\left(\frac{1}{2}\phi(N,\nu,I_{tot}) + \frac{1}{2}(\omega_0-\omega)\tau_c\right)} \quad \text{A. 12}$$

With

$$G(N,\nu,I_{tot}) = G_\chi - \frac{\tau_c}{2\tau_p} = \frac{1}{2}\frac{\tau_c}{\tau_p}\left[\frac{\Gamma G_N \tau_e\left(J-\frac{N_0}{\tau_e}\right)\mathrm{sech}\left(\frac{\omega_0-\omega}{\gamma_\perp}\right)}{1+\Gamma G_N \tau_e \mathrm{sech}\left(\frac{\omega_0-\omega}{\gamma_\perp}\right) I_{tot}} - 1\right] \quad \text{A. 13}$$

$$\phi(N,\nu,I_{tot}) \approx \left(1+\frac{\nu-\nu_0}{\nu_0}\right)\tau_c\frac{\alpha}{2}\left(\Gamma G_N(N-N_0)\mathrm{sech}\left(\frac{\omega_{c\nu}-\omega}{\gamma_\perp}\right) - \frac{1}{\tau_p}\right) \quad \text{A. 14}$$

By applying the following normalizations,

$\frac{N}{N_{\mathrm{th}}} \to N$ (normalized carrier density), $\frac{t}{\tau_p} \to t$ (normalized time), $y = \frac{\tau_e}{N_{th}\tau_p} I$ (normalized power spectral density), $Y = \frac{\tau_e}{N_{th}\tau_p} I_{tot}$ (normalized optical intensity), $i_b = \frac{J}{J_{th}}$ (normalized bias current), $J_{th} = \frac{N_{th}}{\tau_e}$ (J at threshold), $\xi_e = \frac{\tau_p}{\tau_e}$, $\xi_c = \frac{\tau_p}{\tau_c}$, $g_d = \Gamma G_N \tau_P N_{th} = n_{sp}$ (spontaneous emission rate), $\eta = 1 - \frac{1}{n_{sp}} = \frac{N_0}{N_{th}}$, $\delta_0 = \omega_0 \tau_P$ (normalized laser frequency), $\delta = (\omega_0 - \omega)\tau_P$ (normalized frequency offset), $\frac{1}{\gamma_n} = \frac{1}{\gamma_\perp \tau_p}$.

We obtain for the normalized gain:

$$y(\delta) = \frac{S(\delta)}{\left(1-e^{NetGain(i_b,\delta,Y)}\right)^2 + 4e^{NetGain(i_b,\delta,Y)}\sin^2\left(\frac{\phi(i_b,\delta,Y)}{2}\right)} \quad \text{A. 15}$$

With

$$NetGain(i_b,\delta,Y) = \frac{1}{2}\frac{1}{\xi_c}(Gain(i_b,\delta,Y)(1-\varepsilon Y) - 1) \quad A. 16$$

And $Gain(i_b, \delta, Y) = \frac{g(i_b-\eta)\mathrm{sech}\left(\frac{\delta}{\gamma_n}\right)}{1+g\ \mathrm{sech}\left(\frac{\delta}{\gamma_n}\right)(1-\varepsilon Y)Y}$ $A.17.$

For the phase:

$$\phi(i_b, \delta, Y) = \frac{1}{\xi_c}\left(\delta + \frac{1}{2}\alpha\left(1 + \frac{\delta}{\tau_p \nu_0}\right)(Gain(i_b, \delta, Y) - 1)\right) = \frac{1}{\xi_c}\left(\delta\left(1 + \frac{\psi}{\delta_0}\right) + \psi\right) \quad \text{A.18}$$

With $\psi = \frac{1}{2}\alpha(Gain(i_b, \delta, Y) - 1)$ A.19.

Finally, by considering a single frequency laser, we obtain:

$$y(\delta) = \frac{S(\delta)}{(1-e^g)^2 + e^g \frac{1}{\xi_c^2}\left(\delta\left(1+\frac{\psi}{\delta_0}\right)+\psi\right)^2} = \frac{\xi_c^2 S(\delta)}{e^g} \frac{1}{\Gamma_{1/2}^2 + \left(\delta\left(1+\frac{\psi}{\delta_0}\right)+\psi\right)^2} \qquad A.20$$

with $\Gamma_{1/2} = \xi_c \frac{(1-e^g)}{e^{\frac{g}{2}}}$ $A.21$

The normalized power spectral density y_{slave} of an injected laser is then related to master PSD $y_{master}(\delta)$:

$$y_{slave}(\delta) = \frac{S_s(\delta) + \eta y_{master}(\delta)}{(1-e^{g_{slave}})^2 + \frac{e^{g_{slave}}}{\xi_c^2}(\delta+\psi_s)^2} \qquad A.22$$

η is directly related to $\kappa_{inj} = \frac{1}{\tau_{cav}} \frac{\sqrt{1-r_2^2}}{r_2} \sqrt{f_c}$.

The total intensity is then obtained by solving:

$$Y_s = \xi_c \frac{\pi S_{total}(0, Y_s, i_{bs}) + \kappa\left(\frac{i_{bm}-1}{\Gamma_m + \Gamma_s(0, Y_s, i_{bs})}\right)}{(1-e^{g_{slave}})e^{\frac{g_{slave}}{2}}} \qquad A.23$$

The following values are taken for Alcatel DFB laser:

Active area: Length = 200 μm, width 3 μm, height = 0.15 μm, volume = 9×10^{-17} m^3.

Confinement factor Γ: 0.05.

Carrier lifetime τ_e: 181 ps (threshold bias current $I_{bias}^{threshold}$ 11 mA), 141 ps (25 mA).

Spontaneous emission rate n_{sp}: 1.1 ($I_{bias}^{threshold}$ 11 mA), 1 (25 mA).

Carrier density at transparency N_0: 1.8×10^{21} m^{-3} ($I_{bias}^{threshold}$ 11 mA), 1.1×10^{20} m^{-3} (25 mA).

Carrier density at threshold N_{th}: 1.5×10^{22} m^{-3} ($I_{bias}^{threshold}$ 11 mA), 5.1×10^{21} m^{-3} (25 mA).

Photon lifetime τ_p: 10 ps ($I_{bias}^{threshold}$ 11 mA), 5 ps (25 mA).

Gain G: 1.9 10^{-18} m^2 ($I_{bias}^{threshold}$ 11 mA), 1 10^{-17} m^2 (25 mA).

Differential Gain G_N: 1.5×10^{-10} $m^3 s^{-1}$ ($I_{bias}^{threshold}$ 11 mA), 8×10^{-10} $m^3 s^{-1}$ (25 mA).

Alpha parameter α_H: 5.

Annex.6 Résumé en Français

A.1 Résumé court

Cette thèse est consacrée à l'étude du transfert de pureté spectrale par injection optique avec la variation de la cohérence du signal injecté. L'idée principale est de distribuer cette forte cohérence à d'autres sources. L'injection optique peut-être défini comme le couplage unidirectionnel entre deux lasers : l'un, appelé maître, alimente en photons la cavité d'un second laser, appelé esclave. Cette technique de synchronisation en fréquence et en phase est couramment analysée à partir des spectres optiques, du comportement temporel ou du bruit d'intensité relatif du laser injecté. Notre analyse est faite grâce à la densité spectrale de puissance du bruit de fréquence, afin de comparer l'influence d'une source externe à la source spontanée interne.

Différents lasers accordables sont utilisés pour un contrôle de la cohérence. Un étage de laser à fibre Brillouin (BFL) est ajouté pour former une source plus cohérente (< kHz ou au Hz), avec une longueur d'onde sélectionnable sur la bande C. Un deuxième étage BFL permet d'atteindre 3 mHz.

Notre étude se concentre sur le seuil d'accrochage en fréquence, ou la puissance optique minimale requise pour un transfert total de pureté. Lorsque l'on diminue la largeur de raie (30 kHz) d'un facteur 10, le seuil augmente du même facteur ; mais seulement de +4 dB pour passer de 3 kHz à 1 Hz. Ceci ouvre la possibilité d'un transfert de grande pureté par injection optique sans pénalité sur la puissance optique.

A.2 Contexte, conclusion et perspectives

Contexte

L'objectif principal de cette thèse est d'étudier le transfert de pureté d'une source hautement cohérente par injection optique. Pour atteindre cet objectif, j'ai développé une source à largeur de raie intrinsèque sub-kHz avec une longueur d'onde sélectionnable en bande C. Elle nous permet d'étudier le rôle de la cohérence du laser maître dans le déclenchement du verrouillage de l'injection optique lorsque la puissance injectée est variée.

Le premier chapitre de ce manuscrit se concentre sur le développement et la caractérisation des performances d'une source à longueur d'onde sélectionnable en bande C sub-kHz utilisant une cavité Brillouin non-résonnante. Les propriétés du laser Brillouin et ses différentes architectures sont présentées ainsi que les phénomènes de rétrécissement de la largeur de ligne dans un laser à fibre Brillouin. Ensuite, j'explique le processus de mesure de la cohérence d'un laser en utilisant la technique de mesure du bruit de fréquence. La stabilisation de la fréquence du laser et certaines techniques expérimentales associées pour y parvenir sont également présentées. La dernière partie de ce chapitre est consacrée au développement d'un laser sélectionnable en longueur d'onde en bande C avec une largeur de raie intrinsèque de l'ordre du mHz, en cascadant deux cavités Brillouin non résonnantes, établissant, à notre connaissance, un record. A noter qu'en utilisant un laser de pompe plus cohérent (KoherasTM Adjustik), la largeur de raie ne peut être mesurée et se situe en dessous de notre limite de détection (700 μHz).

L'objectif principal du deuxième chapitre est d'examiner le rôle de la cohérence du laser maître dans le déclenchement du verrouillage de l'injection optique lorsque la puissance

injectée varie. Après une brève introduction sur les propriétés générales de l'injection optique, le cadre théorique est décrit pour cette étude. Il s'agit d'une fonction de transfert généralisée (Airy) pour un laser et de sa variante pour un laser à injection optique. Ensuite, le dispositif expérimental de l'injection optique est décrit. Des lasers maîtres de différentes cohérences nous permettent de montrer que des conclusions opposées dans l'estimation du seuil de verrouillage de fréquence sont tirées lorsque l'on utilise le rapport signal sur bruit ou le bruit de fréquence. Pour schématiser, lorsque la cohérence du laser maître est augmentée, la puissance minimale injectée nécessaire pour obtenir un verrouillage de l'injection (que l'on peut appeler seuil de verrouillage) diminue si le paramètre d'estimation est le rapport signal/bruit, alors qu'elle augmente si le paramètre d'estimation est le bruit de fréquence.

Le dernier chapitre de cette thèse est consacré aux discussions, conclusions et perspectives. En particulier, nous montrons à partir de l'expérience et de la théorie que l'injection optique dans un régime d'amplification peut être comparée au mélange de deux signaux ayant des cohérences différentes. Cette étude donne une perception simple des propriétés de bruit d'un système optiquement injecté. Elle ouvre la voie à la réalisation de sources fonctionnant dans la limite quantique de Schalow-Townes et à leur utilisation dans diverses applications allant de l'optique quantique à des capteurs très sensibles.

Conclusion

Dans ce manuscrit, nous avons étudié le transfert de pureté en utilisant l'injection optique dans le cas d'un laser extrêmement cohérent. L'injection optique est le couplage unidirectionnel de deux lasers, appelés esclave et maître. L'idée principale est de pouvoir distribuer la cohérence entre différentes sources. Pour cette étude, nous avons développé

un laser hautement cohérent avec une longueur d'onde sélectionnable sur la bande C en utilisant l'effet Brillouin. Nous avons obtenu une largeur de ligne intrinsèque de 3 mHz. La limite de la plus petite largeur de raie atteignable, si l'on utilise une pompe plus cohérente ou si l'on a plus de lasers Brillouin dans la cascade, reste une question ouverte car il n'est pas certain que la comparaison à la limite de Schawlow-Townes soit pertinente, car elle s'applique à un cas différent (émission simulée et émission spontanée issus de même atomes excités). Avec un facteur de qualité Q = 5 10^8, on peut estimer, pour une puissance laser Brillouin P_{out} = 10 mW, que la largeur de raie de Schawlow-Townes (largeur totale à mi-maximum) est inférieure à environ 1 µHz (6 µHz si l'on utilise la formule de Lax : $\Delta\nu_L = \frac{\pi h \nu_0 (\Delta\nu_{cav})^2}{Pout}$, avec $\Delta\nu_{cav} = \frac{\nu_0}{Q}$). Cependant, la communauté admet que la fonction de transfert associée au transfert de phase de la pompe vers la composante de Stokes a un module inférieur à un. Ainsi, la largeur de raie des spectres du laser Brillouin est diminuée d'un facteur K < 1 par rapport à celle de la pompe. La question de la limite de la plus petite largeur de raie pouvant être obtenue reste donc ouverte.

Pour étudier le transfert de pureté, deux méthodes ont été analysées. L'une utilise le rapport de signal entre la raie du laser maitre (signal injecté) et la raie du laser esclave isolé. L'autre se propose d'utiliser le bruit de fréquence, qui caractérise pleinement les propriétés spectrales d'un laser. Une telle analyse n'a pas été réalisée dans le passé pour l'injection optique. Après l'introduction des notions physiques associées à ces caractérisations et discuté de la stabilité et de la cohérence d'un laser, nous utilisons différentes sources accordables avec des largeurs de raie très différentes pour étudier le transfert de pureté spectrale lorsque les propriétés spectrales du laser maître sont modifiées. En recherchant la puissance minimale nécessaire pour observer un verrouillage de fréquence, nous avons

montré que l'analyse est très différente si l'on utilise le rapport signal/bruit plutôt que le bruit de fréquence.

Dans le premier cas, la puissance minimale requise diminue lorsque la cohérence du maître augmente. Le prix à payer est d'avoir un filtre suffisamment étroit pour observer le rapport des signaux.

Dans le second cas, il faut distinguer deux contributions : l'une provenant de l'émission spontanée, qui agit comme un bruit blanc ; l'autre, due aux bruits fondamentaux et techniques, qui suit une loi $1/f^{\alpha}$ dans la bande de basse fréquence du domaine électrique. Dans les deux cas, le transfert est progressif avec la puissance injectée. Nous discutons les résultats expérimentaux, en montrant comment la fonction de transfert généralisée au laser donne un aperçu de cette interaction non linéaire. Il s'avère que dans le régime d'amplification du laser, qui se situe dans la gamme de puissance optique injectée caractérisant le seuil de verrouillage de fréquence (quelques centaines de nanowatts), plus la cohérence est élevée, plus il faut de puissance pour obtenir un transfert complet. Cette hypothèse n'est pas vérifiée lors de l'utilisation d'un laser avec une largeur de raie plus fine de 1 Hz, car la puissance optique supplémentaire à injecter pour atteindre le seuil de verrouillage est supérieure de 4 dB à celle nécessaire pour une largeur de raie de 3 kHz.

Perspectives

Ce travail a permis au laboratoire de concevoir un laser cohérent dont la longueur d'onde est sélectionnable dans la bande C. L'obtention de lasers ultra-cohérents n'a de sens que si la stabilité relative de la fréquence du laser est de l'ordre de la largeur de cohérence pour un temps d'observation donné. Comme nous l'avons déjà mentionné, une largeur de raie

intrinsèque d'un Hz (mHz) est associée à une stabilité relative de 5 x 10^{-15} (5 x 10^{-18}), ce qui nécessite une approche métrologique [68] ou un signal de référence métrologique [80, 81]. Ce type de signal sera fourni à l'Institut Foton par l'Equipex T-Refimeve dans quelques années.

Les résultats actuels ouvrent la voie à des lasers ayant une largeur de raie en limite de Schawlow-Townes. La caractérisation et la mesure d'une largeur de raie intrinsèque très étroite (nHz-µHz) constituent un défi.

Un laser en bande C hautement cohérent et accordable permettrait d'étudier la dynamique de lasers soumis à une injection optique par des sources hautement cohérentes, comme cela a pu être fait pour la rétroaction optique [141-143]. De telles sources pourraient également améliorer la cohérence du peigne de fréquences grâce à une technique simple [140, 144]. Le laboratoire a montré la possibilité d'utiliser le laser comme détecteur [136] en tirant parti de la cohérence. Avec des sources de largeur de raie de 100 kHz, la détection d'un signal optique en régime continu à température ambiante a été démontrée au femto-Watt ainsi que la possibilité de détecter 100 photons.

REFERENCES

1. K. Hey. Tow, Y. Leguillon, S. Fresnel, P. Besnard, L. Brilland, D. Méchin, P. Toupin, and J. Troles, “Toward more coherent sources using a micro structured chalcogenide Brillouin fiber laser,” IEEE Journal of Photonics Technology Letters, 25(3), 238–241 (2013).

2. W. Loh, J. Becker, D. Cole, A. Coillet, F. Baynes, S. Papp, and S. Diddams, “A microrod-resonator Brillouin laser with 240 Hz absolute linewidth,” New Journal of Physics. 18 (2016).

3. W. Loh, S. Yegnanarayanan, F. O’Donnell, and P. W. Juodawlkis, “Ultra-narrow linewidth Brillouin laser with nanokelvin temperature self-referencing,” Optica Vol. 6, Issue 2, pp. 152-159 (2019).

4. Y. Qin, S. Ding, M. Zhang, Y. Wang, Q. Shi, Z. Li, J. Wen, M. Xiao, and X. Jiang, “High-power, low-noise Brillouin laser on a silicon chip,” Opt. Letters Vol. 47, Issue 7, pp. 1638-1641 (2022).

5. K. Liu, N. Jin, H. Cheng, N. Chauhan, M. W. Puckett, K. D. Nelson, R. O. Behunin, P. T. Rakich, and D. J. Blumenthal, “Ultralow 0.034 dB/m loss wafer-scale integrated photonics realizing 720 million Q and 380 μW threshold Brillouin lasing,” Opt. Letters Vol. 47, issue 7, 1855-1858 (2022).

6. G. Danion, M. Vallet, L. Frein, P. Szriftgiser, and M. Alouini, “Brillouin Assisted Optoelectronic Self-Narrowing of Laser Linewidth,” IEEE Photonics Technology Letters. PP (99). 1-1, (2019).

7. L. Dang, L. Huang, L. Shi, F. Li, G. Yin, L. Gao, T. Lan, Y.Li, L. Jiang, and T. Zhu, "Ultra-high spectral purity laser derived from weak external distributed perturbation," Opto-Electron Adv 6, 210149 (2023).

8. Y. Kotaki, S. Ogita, M. Matsuda, Y. Kuwahara, and H. Ishikawa, "Tunable, Narrow-Linewidth and High-Power γ/4-Shifted DFB Laser," Electron Lett **25**(15), 990–992 (1989).

9. M. Okai, "Spectral characteristics of distributed feedback semiconductor lasers and their improvements by corrugation-pitch-modulated structure," Journal of Appl. Physics **75**(1), 1–29 (1994).

10. G. W. Yoffe, S. Y. Zou, S. A. Rishton, R. W. Olson, M. A. Emanuel, and B. Pezeshki, "Widely-tunable 30mW laser source with sub-500kHz linewidth using DFB array," Conference Proceedings - Lasers and Electro-Optics Society Annual Meeting-LEOS 892–893 (2008).

11. H. Ishii, K. Kasaya, and H. Oohashi, "Spectral linewidth reduction in widely wavelength tunable DFB laser array," IEEE Journal on Selected Topics in Quantum Electronics **15**(3), 514–520 (2009).

12. K. Nemoto, T. Kita, and H. Yamada, "Narrow-spectral-linewidth wavelength-tunable laser diode with si wire waveguide ring resonators," Appl. Physics Express **5**(8), 2–5 (2012).

13. M. Faugeron, M. Tran, O. Parillaud, M. Chtioui, Y. Robert, E. Vinet, A. Enard, J. Jacquet, and F. van Dijk, "High-power tunable dilute mode DFB laser with low RIN and narrow linewidth," IEEE Journal of Photonics Technology Letters **25**(1), 7–10 (2013).

14. J. C. Hulme, J. K. Doylend, and J. E. Bowers, “Widely tunable Vernier ring laser on hybrid silicon,” Opt. Express **21**(17), 19718 (2013).

15. S. Keyvaninia, G. Roelkens, D. van Thourhout, C. Jany, M. Lamponi, A. le Liepvre, F. Lelarge, D. Make, G.-H. Duan, D. Bordel, and J.-M. Fedeli, “Demonstration of a heterogeneously integrated III-V/SOI single wavelength tunable laser,” Opt. Express **21**(3), 3784 (2013).

16. M. C. Larson, Y. Feng, P. C. Koh, X. Huang, M. Moewe, A. Semakov, A. Patwardhan, E. Chiu, A. Bhardwaj, K. Chan, J. Lu, S. Bajwa, and K. Duncan, “Narrow linewidth high power thermally tuned sampled grating distributed Bragg reflector laser,” Optical Fiber Communication Conference, OFC 2013 31–33 (2013).

17. E. Marchena, T. Creazzo, S. B. Krasulick, P. K. L. Yu, D. van Orden, J. Y. Spann, C. C. Blivin, J. M. Dallesasse, P. Varangis, R. J. Stone, and A. Mizrahi, “Integrated Tunable CMOS Laser for Si Photonics Elton,” (Mmi), 7–9 (2013).

18. Y. Sasahata, K. Matsumoto, T. Nagira, H. Sakuma, K. Kishimoto, M. Suzuki, D. Suzuki, Y. Horiguchi, M. Takabayashi, K. Mochizuki, M. Gotoda, H. Aruga, and E. Ishimura, “Tunable 16 DFB laser array with unequally spaced passive waveguides for backside wavelength monitor,” Optical Fiber Communication Conference, OFC 2014 **2**, 1–3 (2014).

19. T. Komljenovic, M. Davenport, S. Srinivasan, J. Hulme, and J. E. Bowers, “Narrow linewidth tunable laser using coupled resonator mirrors,” Optical Fiber Communication Conference, OFC 2015 5–7 (2015).

20. T. Komljenovic, S. Srinivasan, E. Norberg, M. Davenport, G. Fish, and J. E. Bowers, "Widely Tunable Narrow-Linewidth Monolithically Integrated External-Cavity Semiconductor Lasers," IEEE Journal of Selected Topics in Quantum Electronics **21**(6), 214–222 (2015).

21. N. Kobayashi, K. Sato, M. Namiwaka, K. Yamamoto, S. Watanabe, T. Kita, H. Yamada, and H. Yamazaki, "Silicon photonic hybrid ring-filter external cavity wavelength tunable lasers," IEEE Journal of Lightwave Technology **33**(6), 1241–1246 (2015).

22. B. Stern et al, "Compact narrow-linewidth integrated laser based on a low-loss silicon nitride ring resonator," Opt. Lett **42**, 4541 (2017).

23. Y. Fan, R. M. Oldenbeuving, C. G. H. Roeloffzen, M. Hoekman, D. Geskus, R. G. Heideman, and K. J. Boller, "290 Hz intrinsic linewidth from an integrated optical chip-based widely tunable InP-Si3N4 hybrid laser," 2017 Conference on Lasers and Electro-Optics, CLEO 2017 - Proceedings **2017-January**, 1–2 (2017).

24. P. A. Morton, C. Xiang, J. B. Khurgin, C. Morton, M. Tran, J. Peters, J. Guo, M. Morton, and J. E. Bowers, "Integrated Coherent Tunable Laser (ICTL) with 118 nm tuning range and sub-100 Hz Lorentzian Linewidth," Optics InfoBase Conference Papers 18–20 (2021).

25. T. Kessler, C. Hagemann, C. Grebing, T. Legero, U. Sterr, F. Riehle, M. J. Martin, L. Chen, and J. Ye, "A sub-40-mHz-linewidth laser based on a silicon single-crystal optical cavity," Nature Photonics **6**(10), 687–692 (2012).

26. J. Dong, Y. Hu, J. Huang, M. Ye, Q. Qu, T. Li, and L. Liu, "Sub hertz linewidth laser by locking to a fiber delay line," Appl. Optics, 54, 1152-1156 (2015).

27. T. Day, E. K. Gustafson, and R. L. Byer, “Sub-Hertz Relative Frequency Stabilization of Two-Diode Laser-Pumped Nd: YAG Lasers Locked to a Fabry-Perot Interferometer,” IEEE Journal of Quantum Electron **28**(4), 1106–1117 (1992).

28. F. Kéfélian, H. Jiang, P. Lemonde, and G. Santarelli, “Ultralow-frequency-noise stabilization of a laser by locking to an optical fiber-delay line,” Opt. Letters. 34, 914-916 (2009).

29. T. Steshchenko, K. Manamanni, H. Mouhamad, V. Roncin, and F. Burck, “Limitations of the frequency stability transfer in the near infrared using a fiber-based ring cavity,” Opt. Letters. 47. 10.1364 (2022).

30. S. P. Smith, F. Zarinetchi, and S. Ezekiel, “Narrow-linewidth stimulated Brillouin fiber laser and applications,” Opt. Letters. **16**(6), 393 (1991).

31. A. Debut, S. Randoux, and J. Zemmouri, “Linewidth narrowing in Brillouin lasers: Theoretical analysis,” Phys Rev A **62**(2), 1–4 (2000).

32. A. Debut, S. Randoux, and J. Zemmouri, “Experimental and theoretical study of linewidth narrowing in Brillouin fiber ring lasers,” Journal of the Optical Society of America B **18**(4), 556 (2001).

33. J. Geng, S. Staines, Z. Wang, J. Zong, M. Blake, and S. Jiang, “Highly stable low-noise Brillouin fiber laser with ultranarrow spectral linewidth,” IEEE Journal of Photonics Technology Letters **18**(17), 1813–1815 (2006).

34. G. J. Cowle and D. Yu. Stepanov, “Hybrid Brillouin/erbium fiber laser,” Opt. Lett **21**(16), 1250 (1996).

35. V. Lecoeuche, P. Niay, M. Douay, P. Bernage, S. Randoux, and J. Zemmouri, “Bragg grating based Brillouin fiber laser,” Opt. Communications **177**(1), 303–306 (2000).

36. J. C. Yong, L. Thévenaz, and B. Y. Kim, “Brillouin fiber laser pumped by a DFB laser diode,” IEEE Journal of Lightwave Technology **21**(2), 546–554 (2003).

37. H. Lee, T. Chen, J. Li, K. Y. Yang, S. Jeon, O. Painter, and K. J. Vahala, “Chemically etched ultrahigh-Q wedge-resonator on a silicon chip,” Nature Photonics **6**(6), 369–373 (2012).

38. J. Lee et al., “Microwave synthesizer using an on-chip Brillouin oscillator,” Nature Communications vol. 4, 2097 (2013)

39. J. Li, H. Lee, T. Chen, and K. J. Vahala, “Characterization of a high coherence, Brillouin microcavity laser on silicon,” Opt. Express **20**(18), 20170 (2012).

40. J. Li, H. Lee, and K. J. Vahala, “Low-noise Brillouin laser on a chip at 1064 nm,” Opt. Letters **39**(2), 287 (2014).

41. I. V. Kabakova et al., “Narrow linewidth Brillouin laser based on chalcogenide photonic chip,” Opt. Letters **38**, pp. 3208-3211 (2013).

42. S. Gundavarapu, G. M. Brodnik, M. Puckett, T. Huffman, D. Bose, R. Behunin, J. Wu, T. Qiu, C. Pinho, N. Chauhan, J. Nohava, P. T. Rakich, K. D. Nelson, M. Salit, and D. J.

Blumenthal, “Sub-hertz fundamental linewidth photonic integrated Brillouin laser,” Nature Photonics **13**(1), 60–67 (2019).

43. W. Loh, S. Yegnanarayanan, F. O’Donnell, and P. W. Juodawlkis, “Ultra-narrow linewidth Brillouin laser with nanokelvin temperature self-referencing,” Optica **6**(2), 152 (2019).

44. K. Hey Tow, « Laser Brillouin à fibre microstructurée en verre de chalcogénure, » thèse de l’Université de Rennes 1 (2013).

45. K. Hey Tow, Y. Léguillon, P. Besnard, L. Brilland and J. Troles, P. Toupin, D. Mechin, D. Tregoat, “Relative intensity noise and frequency noise of a compact Brillouin laser made of AsSe suspended-core chalcogenide fiber,” Opt. Letters **37**, 1157–1159 (2012).

46. K. Hey Tow, Y. Léguillon, S. Fresnel, P. Besnard, L. Brilland, D. Méchin, D. Trégoat, J. Troles, “Linewidth narrowing and intensity noise reduction of the 2nd order Stokes component of a low threshold Brillouin laser made of GeAsSe chalcogenide fiber,” Opt. Express **20**(26), B104–B109 (2012).

47. S. Fresnel, « Lasers à fibre Brillouin multi-stokes : cohérence et caractérisation en bruit, » thèse de l’Université de Rennes 1 et de l’Université Laval (Québec, Ca) (2018).

48. A. Sebastian, “Noise dynamics in multi-Stokes Brillouin laser,” thèse de l’Université de Rennes 1 (2020).

49. A. Sebastian, S. Trebaol, and P. Besnard, “Intracavity Brillouin gain characterization based on cavity ringdown spectroscopy,” OSA Contin **2**(12), 3539 (2019).

50. A. Sebastian, I. V. Balakireva, S. Fresnel, S. Trebaol, and P. Besnard, “Relative intensity noise in a multi-Stokes Brillouin laser,” Opt. Express **26**(26), 33700 (2018).

51. E. P. Ippen and R. H. Stolen, “Stimulated Brillouin scattering in optical fibers,” Appl. Phys Letters **21**(11), 539–541 (1972).

52. G. G. Stokes, “On the change of refrangibility of light,” Phil. Trans. R. Soc **142**, 463–562 (1852).

53. V. Sundar and R. E. Newnham, “Electrostriction,” The Electrical Engineering Handbook 2nd Edition., 1193–1200 (1997).

54. K. O. Hill, D. C. Johnson, and B. S. Kawasaki, “CW generation of multiple Stokes and anti-Stokes Brillouin-shifted frequencies,” Appl. Phys Letters **29**(3), 185–187 (1976).

55. L. F. Stokes, M. Chodorow, and H. J. Shaw, “All-fiber stimulated Brillouin ring laser with sub milliwatt pump threshold,” Opt. Letters **7**(10), 509 (1982).

56. J. L. Hall, F.V. Kowalski, J. Hough, G.M. Ford, A.J. Munley and H. Ward, “Laser phase and frequency stabilization using an optical resonator,” Appl. Physics B (31(2)), 97–105 (1983).

57. V. V. Spirin, P. Mégret, and A. A. Fotiadi, “Passively Stabilized Doubly-Resonant Brillouin Fiber Lasers,” in Fiber Laser. London, United Kingdom: IntechOpen (2016).

58. F. Mihelic, « Diffusion Brillouin Stimulée dans les fibres optiques : Amplification Brillouin large bande et laser Brillouin, » thèse de l’Université des Sciences et Technologies de Lille (2008).

59. A. L. Schawlow and C. H. Townes, “Infrared and optical masers,” Physical Review **112**(6), 1940–1949 (1958).

60. J. A. Barnes, “Models for the Interpretation of Frequency Stability Measurements,” Final Report National Bureau of Standards, Boulder, CO. Time and Frequency Div. **13**, (1976).

61. G. M. Stephan, T. T. Tam, S. Blin, P. Besnard, and M. Tetu, “Laser line shape and spectral density of frequency noise,” Phys Rev A **71**, 43809 (2005).

62. G. di Domenico, S. Schilt, and P. Thomann, “Simple approach to the relation between laser frequency noise and laser line shape,” Appl. Opt **49**(25), 4801–4807 (2010).

63. D. S. Elliott, R. Roy, and S. J. Smith, “Extracavity laser band-shape,” Phys Rev A 26(1), 12–18 (1982).

64. S. Camatel and V. Ferrero, “Narrow linewidth CW laser phase noise characterization methods for coherent transmission system applications,” IEEE Journal of Lightwave Technology **26**(17), 3048–3055 (2008).

65. F. Du Burck, G. Tetchewo, A. N. Goncharov, O. Lopez, “Narrow band noise rejection technique for laser frequency and length standards: application to frequency stabilization to I2 lines near dissociation limit at 501.7 nm,” Metrologia 46(5), 599-606, (2009).

66. V. Ahtee, M. Merimaa, and K. Nyholm, “Fiber-based acetylene stabilized laser,” IEEE Trans. Instrum. Meas. 58, 1211–1216 (2009).

67. K. Manamanni, T. Steshchenko, F. Wiotte, R. Le Targat, M. Abgrall, O. Lopez, E. Cantin, P-E. Pottie, A. Amy-Klein, V. Roncin and F. Du-Burck, “Limitations due to residual

interferences in fiber-based optical frequency reference at 1.55 μm," Journal of the Optical Society of America B 39(2) 438-443, (2022).

68. T. Steshchenko, K. Manamanni, H. Mouhamad, V. Roncin, and F. Burck, "Limitations of the frequency stability transfer in the near infrared using a fiber-based ring cavity," Opt. Letters. 47. 10.1364 (2022).

69. W. Nagourney, "Quantum electronics for atomic physics and telecommunication," Second edition., Oxford University Press (2014).

70. M. de Labachelerie, K. Nakagawa, Y. Awaji, and M. Ohtsu, "High-frequency-stability laser at 15 μm using Doppler-free molecular lines," Opt. Letters **20**(6), 572 (1995).

71. S. S. and T. I. Yoshihisa Sakai, "Frequency stabilization of laser diodes using 1.51-1.55 mu m absorption lines of/sup 12/c/sub-2/h/sub 2/and/sup 13/c/sub 2," IEEE Journal of Quantum Electron **28(1)**, 75–81 (1992).

72. A. A. S. and L. M. Vladimir S Ilchenko, Andrey B Matsko, "Kilohertz optical resonances in dielectric crystal cavities," Phys Rev A (Coll Park) (70 (5)), 051804 (2004).

73. P.H. M. and G. C. Olivier Llopis, "Laser stabilization on a fiber ring resonator and application to rf filtering," IEEE Journal of Photonics Technology Letters (20(16)), 1399–1401 (2008).

74. J. L. Hall, F.V. Kowalski, J. Hough, G.M. Ford, A.J. Munley and H. Ward, "Laser phase and frequency stabilization using an optical resonator," Appl. Physics B (31(2)), 97–105 (1983).

75. R. W. Fox, C. W. Oates, L. W. Hollberg, “Stabilizing diode lasers to high-finesse cavities,” Experimental methods in the Physical Sciences, Academic Press, Vol **40**, 1–46 (2003).

76. W. Lewoczko-Adamczyk, C. Pyrlik, J. Häger, S. Schwertfeger, A. Wicht, A. Peters, G. Erbert, “Ultra-narrow linewidth DFB-laser with optical feedback from a monolithic confocal Fabry-Perot cavity,” Opt. Express (23(8)), 9705–9 (2015).

77. G. X. Fang Wei, Fei Yang, Xi Zhang, Dan Xu, Meng Ding, Li Zhang, Dijun Chen, Haiwen Cai, Zujie Fang, “Sub kilohertz linewidth reduction of a DFB diode laser using self-injection locking with a fiber Bragg grating Fabry-Perot cavity,” Opt. Express (24(15)), 17406–15 (2016).

78. K. J. Åström and R. M Murray, “Feedback Systems: An Introduction for Scientists and Engineers*”* (Princeton university press, 2010).

79. G. Danion, L. Frein, D. Bacquet, G. Pillet, S. Molin, L. Morvan, G. Ducournau, M. Vallet, P. Szriftgiser and M. Alouini, “Mode-hopping suppression in long Brillouin fiber laser with non-resonant pumping,” Opt. letters, *41*(10), 2362–2365 (2016).80.M. Schioppo, J. Kronjäger, A. Silva, R. Ilieva, J. W. Paterson, C. F. A. Baynham, W. Bowden, I. R. Hill, R. Hobson, A. Vianello , M. Dovale-Álvarez, R. A. Williams, G. Marra, H.S.Margolis, A. Amy-Klein, O. Lopez , E. Cantin, H. Álvarez-Martínez, R. Le Targat, P. E.Pottie, N. Quintin, T. Legero, S. Häfner, U. Sterr, R. Schwarz, S. Dörscher, C. Lisdat, S. Koke, A. Kuhl, T. Waterholter, E. Benkler and G. Grosche"Comparing ultrastable lasers at $7 \times 10{-}17$ fractional frequency instability through a 2220 km optical fibre network." Nature Communications 13(1): 212 (2022).

81. C. Clivati, M. Pizzocaro, E.K. Bertacco, S. Condio, G.A. Costanzo, S. Donadello, I. Goti, M. Gozzelino, F. Levi, A. Mura, M. Risaro, D. Calonico, M. Tønnes, B. Pointard, M. Mazouth-Laurol, R. Le Targat, M. Abgrall, M. Lours, H. Le Goff, L. Lorini, P.-E. Pottie, E. Cantin, O. Lopez, C. Chardonnet, and A. Amy-Klein, "Coherent Optical-Fiber Link Across Italy and France," Phys. Rev. Applied 18, 054009 2022.

82. L. Wu, Y. Jiang, C. Ma, W. Qi, H. Yu, Z. Bi, and L. Ma "0.26-Hz-linewidth ultrastable lasers at 1557 nm." Scientific Reports 6(1): 24969 (2016).

83. A. E. Siegman, "*Lasers*," University Sciences Books, Mill Valley, CA (1986).

84. L. E. Erickson and A. Szabo, "Spectral narrowing of dye laser output by injection of monochromatic radiation into the laser cavity," Appl. Phys Lett **18**(10), 433–435 (1971).

85. G. M. Stéphan, "Spectral properties of an injected laser," Phys Rev A **58**(3), 2467–2471 (1998).

86. M. Bondiou, « Étude des propriétés spectrales d'un laser semi-conducteur soumis à injection optique, » thèse de l'Université de Rennes 1 (1999).

87. R. Gabet, « Etude expérimentale et théorique de l'injection optique dans un laser à semi-conducteur : Application à la détection de signaux à faible cohérence à 1,55 µm, » thèse de l'Université de Rennes 1 (2000).

88. Z. Liu and R. Slavík, "Optical Injection Locking: From Principle to Applications," Journal of Lightwave Technology, 38, 43-59 (2020).

89. J. Ohtsubo, "Semiconductor Lasers*"* Springer Series in Optical Sciences 111, 3rd Edition (2013).

90. C. Henry, "Theory of the linewidth of semiconductor lasers," IEEE Journal of Quantum Electron **18(2)**, 259–264 (1982).

91. Giuliani, G. Donati, S. Villafranca, A. Lasobras, J. Garces, I. Chacinski, M. Schatz, R. Kouloumentas, C. Klonidis, D. Tomkos, I. Landais, P. Escorihuela, R. Rorison, J. Pozo, J. Fiore, A. Moreno, P. Rossetti, M. Elsasser, W. Von Staden, J. Huyet, G. Saarinen, M. Pessa, M. Leinonen, P. Vilokkinen, V. Sciamanna, M. Danckaert, J. Panajotov, K. Fordell, T. Lindberg, A. Hayau, J.-F. Poette, J. Besnard, P. Grillot, F. Pereira, M. Nelander, R. Wacker, A. Tredicucci, A. Green, R. "Round-Robin Measurements of Linewidth Enhancement Factor of Semiconductor Lasers in COST 288 Action" CLEO-IQEC Munich (2007).

92. F. Mogensen, H. Olesen, and G. Jacobsen, "Locking Conditions and Stability Properties for a Semiconductor Laser with External Light Injection," IEEE Journal of Quantum Electron **QE-21**(7), 784–793 (1985).

93. O. Vaudel, « Étude de synchronisation de chaos par simple injection optique, » thèse de l'Université de Rennes 1 (2009).

94. S. Blin, O. Vaudel, P. Besnard, and R. Gabet, "Power- or frequency-driven hysteresis for continuous-wave optically injected distributed-feedback semiconductor lasers," Opt. Express **17**(11), 9288 (2009).

95. S. Wieczorek, B. Krauskopf, T.B. Simpson, D. Lenstra, “The dynamical complexity of optically injected semiconductor lasers,” Physics Reports, Volume 416, Issues 1–2, (2005).

96. E. Lau, L. Wong, and M. Wu, “Enhanced Modulation Characteristics of Optical Injection-Locked Lasers: A Tutorial,” Selected Topics in IEEE Journal of Quantum Electronics, **15**, 618–633 (2009).

97. Y. Doumbia, T. Malica, D. Wolfersberger, K. Panajotov, M. Sciamanna, “Nonlinear dynamics of a laser diode with an injection of an optical frequency comb,” Opt. Express. 28. 30379-30390. 10.1364 (2020).

98. S. K. Hwang and J. M. Liu, “Dynamical characteristics of an optically injected semiconductor laser,” Opt. Commun **183** (1), 195–205 (2000).

99. C. Huygens, “Oeuvres complètes. Tome VIII.” The Tests of Time, (2019) 167–179 (1684).

100. J. H. Vincent, “On some experiments in which two neighboring maintained oscillatory circuits affect a resonating circuit,” Proceedings of the Physical Society of London **32**(1), 84–91 (1919).

101. R. Adler, “A study of Locking Phenomena in Oscillators,” IEEE Proceedings: Science, Measurement and Technology **61**(10), 351–357 (1946).

102. L Paciorek, “Injection Locking of Oscillators,” IEEE Proceedings: Science, Measurement and Technology **53**(11), (1965).

103. T. H. Maiman, “Stimulated Optical Radiation in Ruby” (L. Allen, 1969), **87**(1959).

104. H. L. Stover and W. H. Steier, “Locking of laser oscillators by light injection,” Appl Phys Lett **8**(4), 91–93 (1966).

105. S. Kobayashi and T. Kimura, “Injection Locking Characteristics of an AlGaAs Semiconductor Laser,” IEEE Journal of Quantum Electron **16**(9), 915–917 (1980).

106. R. Lang, “Injection locking properties of DFB semiconductor lasers,” IEEE Journal of Quantum Electron **18**(6), 976–982 (1982).

107. I. Petitbon, P. Gallion, G. Debarge, and C. Chabran, “Locking Bandwidth and Relaxation Oscillations of an Injection-Locked Semiconductor Laser,” IEEE Journal of Quantum Electron **24**(2), 148–154 (1988).

108. Q.T. Nguyen, P. Besnard, L. Bramerie, J.-C. Simon, A. Shen, G.H. Duan, and C. Kazmierski, “30 Gbit/s downstream capacity of cost-effective colourless WDM-PON based on injection-locked Fabry-Perot lasers” Electronics Letters 27 Volume 45, Issue 18, p.948–949, (2009).

109. G. Yabre, “Effect of relatively strong light injection on the chirp-to-power ratio and the 3 dB bandwidth of directly modulated semiconductor lasers,” IEEE Journal of Lightwave Technology **14**(10), 2367–2373 (1996).

110. A. C. Bordonalli, C. Walton, and A. J. Seeds, “High-Performance Phase Locking of Wide Line width Semiconductor Lasers by Combined Use of Optical Injection Locking and Optical Phase-Lock Loop,” IEEE Journal of Lightwave Technology **17**(2), 328–342 (1999).

111. E. K. Lau, X. Zhao, H.-K. Sung, D. Parekh, C. Chang-Hasnain, and M. C. Wu, “Strong optical injection-locked semiconductor lasers demonstrating > 100-GHz resonance frequencies and 80-GHz intrinsic bandwidths,” Opt. Express **16**(9), 6609 (2008).

112. L. Chrostowski, “Optical Injection Locking of Vertical Cavity Surface Emitting Lasers,” McGill University (2004).

113. Y. Doumbia, D. Wolfersberger, K. Panajotov and M. Sciamanna, “Two Polarization Comb Dynamics in VCSELs Subject to Optical Injection,” Photonics. 9. 115. 10.3390 (2022).

114. D. S. Wu, D. J. Richardson, and R. Slavík, “Optical Fourier synthesis of high-repetition-rate pulses,” Optica **2**(1), 18 (2015).

115. Q. T. Nguyen, P. Besnard, L. Bramerie, A. Shen, C. Kazmierski, P. Chanlou, G.-H. Duan, and J.C. Simon, “Bidirectional 2.5-Gb/s WDM-PON Using FP-LDs Wavelength-Locked by a Multiple-Wavelength Seeding Source Based on a Mode-Locked Laser” IEEE Photonics Technology Letters vol.22 n°11 p 733-735 (2010).

116. S. Blin, G. M. Stéphan, R. Gabet, P. Besnard, and D. Kilper, “Amplification process in a laser injected by a narrow band weak signal,” Europhys Lett **52**(1), 60–65 (2000).

117. J. Kim, G. Marra, D. S. Wu, D. J. Richardson, and R. Slavík, “Wavelength conversion technique for optical frequency dissemination applications,” Opt. Letters **41**(8), 1716 (2016).

118. Z. Liu, J. Y. Kim, D. S. Wu, D. J. Richardson, and R. Slavik, “Homodyne OFDM with optical injection locking for carrier recovery,” IEEE Journal of Lightwave Technology **33**(1), 34–41 (2015).

119. J. Jignesh, B. Corcoran, J. Schröder, and A. Lowery, “Polarization independent optical injection locking for carrier recovery in optical communication systems,” Opt. Express **25**(18), 21216 (2017).

120. S. T. Cundiff and A. M. Weiner, “Optical arbitrary waveform generation,” Nature Photonics **4**(11), 760–766 (2010).

121. A. J. Seeds, M. J. Fice, K. Balakier, M. Natrella, O. Mitrofanov, M. Lamponi, M. Chtioui, F. van Dijk, M. Pepper, G. Aeppli, A. G. Davies, P. Dean, E. Linfield, and C. C. Renaud, “Coherent terahertz photonics,” Opt. Express **21** (19), 22988 (2013).

122. G. J. Schneider, J. A. Murakowski, C. A. Schuetz, S. Shi, and D. W. Prather, “Radiofrequency signal-generation system with over seven octaves of continuous tuning,” Nature Photonics **7**(2), 118–122 (2013).

123. S. Blin, « Réalisation de lasers à fibre à contre-réaction répartie pour l’étude de l’injection optique : comparaison à l’injection avec des lasers à semi-conducteurs, » thèse de l’Université de Rennes 1 (2003).

124. C. Guignard, « Réalisation de sources impulsionnelles pour les télécommunications, » thèse de l’Université de Rennes 1 (2005).

125. J.-F. Hayau, « Caractérisation de composants photoniques à base d'îlots quantiques à semi-conducteurs InAs / InP : bruit et injection optique, » thèse de l'Université de Rennes 1 (2009).

126. Z. Hao, « Caractérisations de structures à base d'îlots et bâtonnets quantiques en termes de bruit, de non-linéarité et d'injection optique, » thèse de l'Université de Rennes 1 (2014).

127. C. Guignard and P. Besnard, "Experimental injection map of semiconductor laser submitted to filtered feedback," Opt. Quantum Electron **38** (4–6), 411–428 (2006).

128. S. Blin, C. Guignard, P. Besnard, R. Gabet, G. M. Stéphan, and M. Bondiou, "Phase and spectral properties of optically injected semiconductor lasers," C R Phys **4**(6), 687–699 (2003).

129. M. Bondiou, R. Gabet, G. M. Stéphan, and P. Besnard, "Linewidth of an optically injected semiconductor laser," Journal of Optics B: Quantum and Semiclassical Optics **2**(1), 41–46 (2000).

130. B. Van der Pol, "VII. Forced oscillations in a circuit with non-linear resistance. (Reception with reactive triode)," The London, Edinburgh, and Dublin Philosophical Magazine and Journal of Science **3**(13), 65–80 (1927).

131. R. H. Pantell, "The laser oscillator with an external signal," Proceedings of the IEEE **53**(5), 474–477 (1965).

132. M. E. Hines, J.-C. R. Collinet, and J. G. Ondria, “FM Noise Suppression of an Injection Phase-Locked Oscillator,” IEEE Transactions on Microwave Theory and Tech **16**(9), 738–742 (1968).

133. M. Born and E. Wolf, “Principles of Optics,” 6th Edition, **45**(353), (1961).

134. W. T. Silfvast, “Laser Fundamentals,” Cambridge University Press, 2nd Edition (2004).

135. R. Boyd, “Nonlinear Optics,” Academic press, 4th edition (2020).

136. R. Gabet, G. M. Stéphan, M. Bondiou, P. Besnard, and D. Kilper, “Ultrahigh sensitivity detector for coherent light: The laser,” Opt. Commun **185**(1–3), 109–114 (2000).

137. J. Poette, O. Vaudel, and P. Besnard, “Relative Intensity Noise of an injected semiconductor laser,” proceedings of SPIE **6054**, 605407-605407–10 (2005).

138. S. Blin, O. Vaudel, G. M. Stéphan, P. Besnard, T. T. Tam, and S. LaRochelle, “Measuring spectral linewidth of highly-coherent laser using optical injection,” Conference on Lasers and Electro-Optics (CLEO), (2004).

139. O. Vaudel, J. F. Hayau, and P. Besnard, “Synchronization between optically injected semiconductor lasers on undamped relaxation oscillations,” Opt. Quantum Electron **40**(2–4), 109–118 (2008).

140. K. Manamanni, T. Steshchenko, F. Wiotte, A. Chaouche-Ramdane, M. O. Sahni, V. Roncin, F. Du-Burck, “Frequency Stability Transfer in Passive Mode-Locked Quantum-dash Laser Diode using Optical Injection Locking,” in IEEE Journal of Quantum Electron., 58(4), 1, (2022).

141. A. Naumenko, P. Besnard, N. Loiko, G. Ughetto and J.C. Bertreux “Characteristics of a semiconductor laser coupled with a fiber Bragg grating with arbitrary amount of feedback” IEEE Journal of Quantum Electronics, vol. 39 N° 10 pp. 1216-1228 (2003).

142. H. Erzgräber, B. Krauskopf, D. Lenstra, A.P.A. Fischer, and G. Vemuri, “Frequency versus relaxation oscillations in a semiconductor laser with coherent filtered optical feedback,” Physical Review E: Statistical, Nonlinear, and Soft Matter Physics. 73(5), p. 1 - 4 4 p., 055201(R) (2005).

143. H. Erzgraber, B. Krauskopf, D. Lenstra, “Bifurcation analysis of a semiconductor laser with filtered optical feedback,” SIAM Journal on Applied Dynamical Systems, Vol. 6, No. 1 p. 1-28 (2007).

144. M. Sahni, S. Trebaol, L. Bramerie, M. Joindot, S. Ó Dúill, S. Murdoch, L. Barry, and P. Besnard, “Frequency noise reduction performance of a feed-forward heterodyne technique: application to an actively mode-locked laser diode”, Opt. Letters. 42, 4000-4003 (2017).

145. J. Poette, “contributions à l’étude du bruit d’amplitudes de lasers dédiés aux télécommunications,” thèse de l’université de Rennes 1, (2005).

146. Q. T. Nguyen, “Émetteurs achromatiques pour le réseau d'accès optique haut débit multiplexé en longueurs d'onde,” thèse de l’université de Rennes 1, (2011).

147. Olivier Llopis, Zeina Abdallah, Vincent Auroux, and Arnaud Fernandez, “High spectral purity laser characterization with a self-heterodyne frequency discriminator”, 2015 Joint Conference of the IEEE International Frequency Control Symposium & the European Frequency and Time Forum, pages 602–605. IEEE, 2015.

148. P. Gallion, F.J. Mendieta and R. Leconte, “Single-frequency laser phase-noise limitation in single-mode optical-fiber coherent-detection systems with correlated fields”, JOSA B, Vol.72, N° 9, 1982.